

Karin Hedman

**Statistical Fusion
of Multi-aspect Synthetic Aperture Radar Data
for Automatic Road Extraction**

München 2010

**Verlag der Bayerischen Akademie der Wissenschaften
in Kommission beim Verlag C. H. Beck**



**Statistical Fusion
of Multi-aspect Synthetic Aperture Radar Data
for Automatic Road Extraction**

Vollständiger Abdruck
der von der Fakultät für Bauingenieur-, Geo- und Umweltwissenschaften
des Karlsruher Instituts für Technologie
zur Erlangung des akademischen Grades eines
Doktor-Ingenieurs (Dr.-Ing.)
genehmigten Dissertation
von
M.Sc. Karin Hedman

München 2010

Verlag der Bayerischen Akademie der Wissenschaften
in Kommission beim Verlag C. H. Beck

Adresse der Deutschen Geodätischen Kommission:



Deutsche Geodätische Kommission

Alfons-Goppel-Straße 11 • D – 80 539 München

Telefon +49 – 89 – 23 031 1113 • Telefax +49 – 89 – 23 031 - 1283/ - 1100

e-mail hornik@dgfi.badw.de • <http://www.dgk.badw.de>

Vorsitzender: Univ. Prof. Dr.-Ing. Dr. h.c. mult. Franz Nestmann

Prüfer der Dissertation: 1. Univ.-Prof. Dr.-Ing. Stefan Hinz, Karlsruher Institut für Technologie

2. Univ.-Prof. Dr.-Ing. Uwe Stilla, Technische Universität München

3. Univ.-Prof. Dr.-Ing. Hans-Peter Bähr, Karlsruher Institut für Technologie

Tag der mündlichen Prüfung: 15.07.2010

© 2010 Deutsche Geodätische Kommission, München

Alle Rechte vorbehalten. Ohne Genehmigung der Herausgeber ist es auch nicht gestattet,
die Veröffentlichung oder Teile daraus auf photomechanischem Wege (Photokopie, Mikrokopie) zu vervielfältigen

ISSN 0065-5325

ISBN 978-3-7696-5066-2

Summary

In this dissertation, we have presented a new statistical fusion for automatic road extraction from SAR images taken from different looking angles (i.e. multi-aspect SAR data). The main input to the fusion are extracted line features. The fusion is carried out on decision-level and is based on Bayesian network theory.

The developed fusion fully exploits the capabilities of multi-aspect SAR data. By means of Bayesian network theory a reasoning step could be modeled which describes the relation between the extracted road, neighboring high objects and the sensor geometry. For instance an extracted road oriented in the looking angle of the sensor (range) is considered more reliable than other detections closer to azimuth. Furthermore information about neighboring high objects (local context information) could be integrated since these objects could be detected by a bright line extraction. Examples of neighboring high objects are trees and buildings. By incorporating this into the reasoning step, contradicting hypotheses (e.g. detection of a road in the first image, detection of parallel shadow and layover regions caused by neighboring high objects in the second image) could be solved. Furthermore integrating local context information enables the fusion to distinguish between different pre-defined types of road (e.g. highways, roads with vegetation nearby, open roads, etc.)

Information about the scene context (global context information) was obtained by a textural classification of large image regions. In this work the image was classified into built-up areas, forest and fields. This information is incorporated as prior knowledge into the fusion.

The development of the fusion contains the following steps; defining a road and local context model in multi-aspect SAR data, analyzing the feature extraction (i.e. dark and bright line extraction and textural classification), setting up a Bayesian network structure, learning the fusion, and implementing an association step. Some network structures of varying complexity are presented and discussed. The learning is carried out by estimations of conditional probability functions and conditional probability tables based on manually collected training data. Each step is described in detail in this work.

Two different fusions were developed and tested; one developed for extracted dark linear features only and one designed for both dark and bright linear features. Both fusions consider the sensor geometry, while the last one is based on a more complex road and local context model. The performance of these two fusions was compared by evaluating the results from a data set of multi-aspect SAR data. In addition the transferability of the fusion concept was also tested on data acquired from a second SAR sensor. A discussion on the behavior of the two fusions follows. The advantages and disadvantages of using Bayesian network theory for this application are also discussed. Finally, some ideas for improving the fusion are presented.

Zusammenfassung

In dieser Dissertation wird ein Ansatz zur Datenfusion für die automatische Extraktion von Straßen aus mehreren SAR-Szenen desselben Gebiets vorgestellt, die aus verschiedenen Einfalls- und Aspektwinkeln aufgenommen wurden (sog. Multi-Aspekt SAR-Daten). Die wichtigste Eingangsinformation bilden aus dem Bild extrahierte Merkmale (Linien). Die Datenfusion findet auf einer symbolischen Ebene (*Decision-level fusion*) statt und basiert auf der Theorie der Bayes'schen Netze.

Die entwickelte Fusion nutzt das Potenzial der Multi-Aspekt SAR-Daten optimal aus. Die Theorie der Bayes'schen Netze ermöglicht statistische Rückschlüsse, die auf den Beziehungen zwischen der extrahierten Straße, benachbarten Objekten und der Sensorgeometrie beruhen. Beispielsweise wird eine extrahierte Straße, die entlang der Entfernungsrichtung des Sensors orientiert ist, als zuverlässiger bewertet als eine extrahierte Straße in Azimutrichtung.

Informationen über benachbarte Objekte (lokales Kontextwissen) können eingebunden werden, indem deren helle Rückstreuung über eine Linienextraktion detektiert wird. Die Berücksichtigung von lokalem Kontextwissen in der Fusion kann widersprüchliche Annahmen auflösen (z.B. wenn eine Straße in einem Bild sichtbar, in einem zweiten aber so verdeckt ist, so dass nur die parallelen Schatten- und Layoverregionen detektiert werden). Darüber hinaus bietet die Einbindung von lokalem Kontextwissen die Möglichkeit, verschiedene Straßenklassen voneinander zu trennen (z.B. Autobahnen, offene Straßen, Straßen mit benachbarter hoher Vegetation, usw.).

Informationen über den Kontext der Aufnahme (globales Kontextwissen) werden über eine Texturklassifikation großräumiger Gebiete extrahiert. In dieser Arbeit wird das Bild in die drei Kategorien Siedlungsgebiete, offene Landschaft und Wald klassifiziert, die als Vorwissen in die Fusion eingeführt werden.

Die Entwicklung der neuen Fusion beinhaltet folgende Schritte: Die Definition eines Straßenmodells und seines lokalen Kontexts, die Analyse der Linienextraktion, den Aufbau der Bayes'schen Netze, den Lernprozess der Fusion und die Zuordnung von extrahierten Merkmalen, die zu derselben Beobachtung gehören (*Association*). Mehrere Netzwerke unterschiedlicher Komplexität werden vorgestellt und diskutiert. Im Lernprozess werden bedingte Wahrscheinlichkeitsdichtefunktionen und Wahrscheinlichkeitstabellen aus Trainingsdaten ermittelt. Alle Schritte werden in der Arbeit ausführlich beschrieben.

Zwei verschiedene Fusionen, eine für dunkle extrahierte Linien und eine für dunkle und helle Linien, wurden entwickelt und getestet. Anhand des Vergleichs der Ergebnisse für Multi-Aspekt SAR-Daten wurde die Effizienz der beiden Fusionen analysiert. Darüber hinaus wurde die Übertragbarkeit des Konzepts auf Daten eines zweiten SAR-Sensors getestet. Am Ende der Arbeit werden die Leistungsfähigkeit der beiden Fusionen sowie die Vor- und Nachteile des Einsatzes der Theorie der Bayes'schen-Netze für diese Anwendung diskutiert und einige Ideen für eine Verbesserung der Fusion präsentiert.

Contents

1	Introduction	7
1.1	Motivation	7
1.2	Aim of this work	8
1.3	Structure of the thesis	8
2	Previous work	9
2.1	Automatic road extraction from SAR data	9
2.1.1	<i>Automatic road extraction from SAR data - previous work</i>	9
2.1.2	<i>Description, analysis and discussion of the automatic road extraction approach TUM-LOREX</i>	11
2.2	Data fusion for automatic object extraction from SAR	13
2.2.1	<i>What is data fusion?</i>	13
2.2.2	<i>Data fusion for man-made object extraction from SAR data - previous work</i>	15
3	SAR principles and image characteristics	19
3.1	SAR principles	19
3.2	SAR image characteristics	20
3.2.1	<i>Geometrical effects</i>	20
3.2.2	<i>SAR radiometry</i>	21
3.2.3	<i>SAR systems and their data</i>	23
4	Bayes probability and network theory	25
4.1	Plausible reasoning and Bayesian probability theory	25
4.2	Bayesian networks	26
4.2.1	<i>Belief propagation in Bayesian networks</i>	28
5	A Bayesian fusion approach for road extraction from SAR	30
5.1	Modeling of roads and their context for SAR data	30
5.1.1	<i>Modeling of roads</i>	30
5.1.2	<i>Modeling of context</i>	31
5.2	Feature extraction	36
5.2.1	<i>Extraction and analysis of dark and bright linear features</i>	36
5.2.2	<i>Classification of global areas</i>	39
5.3	Setting up a Bayesian network for fusion of multi-aspect SAR data for automatic road extraction	41
5.4	Estimating continuous conditional probability density functions	46
5.4.1	<i>Independency criteria</i>	47
5.4.2	<i>Histogram fitting</i>	48
5.4.3	<i>Results: probability density functions</i>	49
5.4.4	<i>Evaluating and testing the classification</i>	56
5.5	Conditional probability tables	60
5.5.1	<i>Definition of conditional probability table - without local context</i>	60
5.5.2	<i>Definition of conditional probability table - including local context</i>	63
5.6	Incorporating global context information	68
5.7	Association	70
6	Results and analysis	73
7	Conclusion and discussion	84
	References	87
	Acknowledgements	92

1 Introduction

1.1 Motivation

Remote sensing data acquired from air- or satellite-borne sensors has rapidly increased during the last years. New sensors with improved spatial, spectral and temporal resolution have been launched. The availability of remote sensing data has increased enormously. At the same time geographic information systems (GIS) have taken a prominent role in our daily life. While GIS data bases are in general up-to-date in industrial countries, the developing countries are still working on the digitizing of cartographic information. The work is often done manually which is time-consuming, but could be speeded up by automatic or semi-automatic road extraction approaches.

Compared to optical sensors, the advantages of synthetic aperture radar (SAR) are its weather-independency and the ability to operate during both day and night. Especially in case of a natural catastrophe real time acquisitions might be hard to obtain with other remote sensing systems due to bad weather conditions. As also new high resolution SAR systems are being developed, SAR has become a compliment to optical data in terms of urban remote sensing (STILLA, 2007). However, the improved resolution does not automatically make automatic object extraction easier, yet automatic object extraction from SAR data is a difficult task. Due to the side-looking geometry of the SAR sensor occlusions (shadow and layover effects) still appear frequently (STILLA et al., 2003). Compared to optical data where layover does not occur, the extent of the occlusions is in general higher. Simulations of one SAR image of a city has shown that less than 20% of the roads remained undisturbed from occlusions (SOERGEL et al., 2003). By adding three more simulated images acquired from different directions, the visible road area could be increased as much as three times. Preliminary work has also stated that the usage of SAR images illuminated from different directions (i.e. multi-aspect images) improves the road extraction result. This has been tested both for building recognition and reconstruction (BOLTER, 2001)(THIELE et al., 2007) and for road extraction (TUPIN et al., 2002)(DELL'ACQUA et al., 2003). If the road is occluded in one image, it might be detectable from an other image acquired from a more favourable direction (see Fig. 1).

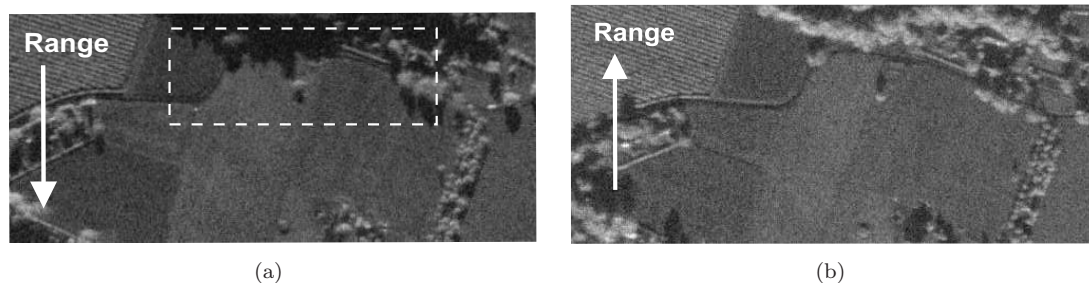


Fig. 1. Occlusions due to nearby high trees occur frequently in SAR imagery (Sensor: MEMPHIS (FGAN-FHR), 35 GHz). Due to the large incidence angle of the SAR sensor long shadow regions occur in the image. The road within the white dashed box is occluded by a shadow in the first image (a), but is visible when it is acquired from a more favorable direction (b) (STILLA et al., 2007).

Roads oriented in the looking angle of the sensor (i.e. in range direction) are in general less affected by shadow- and layover caused by neighboring high objects such as trees or buildings. Hence the detection of these roads can be considered as more reliable than other detections. If a road with high trees nearby approaches azimuth (perpendicular to range) the road can most probably no longer be seen. Instead only the parallel layover and shadow regions occur. Here the integration of information about nearby objects (i.e. local context) can support and give weight to the detection. However the extent of the occlusions is also dependent on the incidence angle and the position of the high object. A correct fusion of multi-aspect SAR data shall therefore include the sensor geometry and the relation between extracted objects.

Fusion techniques can be divided into low- and high-level fusion techniques. Low-level fusion techniques are applied when the fusion takes place on pixel-level as high-level fusion is used when features, relations and decisions shall be fused. In the next few years, it is expected that the development as well as the application of high-level fusion techniques will rise (GAMBA et al., 2005)(ZHANG, 2010). It will be used not only for map updating but also for many other purposes such as for instance Earth system applications. Hence, there is a demand for high-level fusion approaches also in the future. The development of a new fusion approach for object extraction from SAR data would certainly be an important contribution to future high-level fusions for object extraction.

1.2 Aim of this work

The aim of this work is to design and implement a new fusion module for multi-aspect SAR data in an already existing road extraction approach named TUM-LOREX. TUM-LOREX was originally developed for optical images (WIEDEMANN, 2002) and was later modified for SAR data (WESSEL, 2006). The approach contains a fusion module already, but it was designed for a fusion of different optical channels and neither for SAR nor from data acquired from different directions (WIEDEMANN, 2002). Further the fusion was based on the fuzzy-theory. One disadvantage of this approach was that the user defined fuzzy parameters manually. More or less the parameter setting was not only done on an ad hoc basis but was also time-consuming. The new fusion module shall be based on probability theory and shall be designed specifically for multi-aspect SAR data. As was shown by the example in Fig. 1 the sensor geometry has an high impact on how objects appear in the SAR image. Hence a reasoning step which is based on the sensor geometry and its influence on the relations between the extracted features and its context information shall be included. Both information about the scene context and neighboring objects shall be involved in the approach. Last but not least the possibilities and limits of using multi-aspect SAR data for road extraction shall be exploited.

1.3 Structure of the thesis

The thesis is organized as follows:

Sect. 2 is dedicated to previous work. The first part deals with road extraction approaches from SAR data and presents the existing road extraction approach TUM-LOREX. The second part is concentrated on data fusion, starting with an explanation of what data fusion really is, followed by a summary of some data fusion approaches applied to remote sensing and in particular object extraction from SAR data.

The following two sections, Sect. 3 and 4, contain the theory needed for this work. First an introduction to SAR is given. The emphasis is on the radiometric and geometric characteristics of SAR imagery. Later the main concept of Bayesian probability theory and the theory behind Bayesian networks are presented.

The design and implementation of the fusion approach is described in Sect. 5. First the underlying geometric and radiometric modeling of roads and their context for SAR data is presented. The sensor geometry and its impact on the road and the local context plays an important role here. Second, an analysis of the behavior of the feature extraction is presented. The analysis is important since the feature extraction is the input to the fusion module. The modeling and the analysis underlie the structure and the set-up of the Bayesian network (Sect. 5.3). Included is also a description of the information flow in the network. Next step is the learning, where the conditional probabilities between the network variables are estimated (Sect. 5.4 and 5.5). Both continuous probability density functions and discrete conditional probability tables are defined. Also there is a discussion on how to incorporate scene context information, later defined as global context information (Sect. 5.6). In the end it is described how the fusion is implemented. Here there is a focus on how to associate the extracted information, i.e. how to decide which extracted information belongs to the same object.

The results obtained by testing the fusion on a couple of SAR images are presented in Sect. 6. The analysis of these results underlie the final conclusion and discussion (Sect. 7). In this part we discuss the relevance of the fusion and the conclusions that we can draw from the work. Some ideas about the future work are presented at the end of this thesis.

2 Previous work

2.1 Automatic road extraction from SAR data

2.1.1 Automatic road extraction from SAR data - previous work

Compared with road extraction from optical images, rather few approaches have concentrated on road extraction from SAR images. Even though qualitative research has been going on for more than ten years no more than a few approaches have been presented. The complexity of the SAR data seems to be the reason. Especially in urban areas, the complexity arises through dominant scattering caused by building structures, traffic signs and metallic objects in cities. Furthermore one has to deal with the imaging characteristics of SAR, such as speckle-affected images, foreshortening, layover, and shadow. Since the image characteristics are so different compared to optical data, most approaches have put much effort into the first step, the line detection. Some line- and edge detectors were therefore especially developed for SAR data (TOUZI et al., 1988)(HELLWICH, 1996)(TUPIN et al., 1998)(DELL'ACQUA and GAMBA, 2001).

Good literature reviews of road extraction from optical and from SAR data were presented in WESSEL (2006). In this section the most prominent works in terms of road extraction from SAR are selected.

One of the most comprehensive road extraction approaches was presented by a French group at Ecole Nationale Supérieure des Telecommunications (ENST) (TUPIN et al., 1998). The approach consists of two parts, a line detector and a graph search based on Markov random field (MRF). The line detector was especially developed for SAR data and considers the SAR speckle distribution. The detector is often applied to SAR data, not only for road extraction but also for other purposes such as bright linear detection for building extraction (TUPIN, 2010) (CHAABOUNI CHOUAYAK and DATCU, 2010). The detection of line structures is based on two line detectors, D1 and D2. The first one consists of a coupling of two ratio edge detectors (TOUZI et al., 1988) on both sides of a region. Lines are extracted depending on the ratio of radiometric averages of the regions. The second detector D2 applies a cross-correlation between two regions, resulting in a line detector which considers both homogeneity as well as the contrast of the regions. Afterward the responses from these two are fused by a fusion operator (BLOCH, 1996), followed by a cleaning step. Road networks are constructed by a grouping based on a MRF-model for roads of the extracted segments. A graph is first built from the detected segments. Connections according to rules are generated. In the end the best road network is found by a an "optimal binary labeling" of the nodes (1 for road, 0 for other). The optimal labeling is based on the radiometrical and geometric properties. Here a-priori knowledge about the shape of a road is introduced. The approach was also applied for a joint identification of roads and global context areas (TUPIN et al., 1999) and was further developed for the use of multi-aspect SAR data (TUPIN, 2000) (TUPIN et al., 2002). In this work the network generation is modified for dense urban areas. The problem with a fixed line width of five pixels is solved by carrying out the line extraction twice, once using an image with its original resolution and once with a degraded resolution. This work showed the potential in using multi-aspect data. A combination of multi-aspect data delivered better results compared to the results from one image alone.

At the Dipartimento di Elettronica, Universita di Pavia an approach based on a fuzzy clustering and street tracking was developed (DELL'ACQUA and GAMBA, 2001). The procedure starts with an initial fuzzy clustering which classifies the data into some land use classes; vegetation, road/parking lots and built-up areas. Here two fuzzy membership functions, fuzzy C Means (FCM) and possibilistic C means (PCM), are applied. The output is a fuzzy partitioned scene, which is further processed by a street tracking. The tracking consists of three algorithms, (1) a connectivity weighted Hough transform (CWHT), (2) a rotation Hough transform and (3) a shortest path search by dynamic programming. The first two are useful for detecting vertical and horizontal lines, while the third one is aimed to detect curvilinear roads. In order to detect both larger and smaller roads, the CWHT algorithm is applied several times with linearly decreasing parameter. During the following years the approach was further developed. After a first further development the approach was tested on simulated multi-aspect SAR data (DELL'ACQUA et al., 2003). Although the results are poor in terms of correctness and completeness values (due to the complexity of the scene), the test showed that more streets can be detected and extracted using multi-aspect data. Furthermore additional line extractors were incorporated and the approach was also extended with a slight modified version of the above mentioned MRF road network optimization (LISINI et al., 2006)(NEGRI et al., 2006)(HEDMAN et al., 2010). The approach is also part of a rapid mapping approach of urban areas as described in (DELL'ACQUA et al., 2009). The significance of this approach is the performance for detecting urban regular networks. Especially street grid patterns similar to

those extracted from optical data by PRICE (1999) were well detected.

A Hough-transform based line extraction was also applied by AMBERG et al. (2005a). In this work urban areas are identified by a classification. Road tracking is carried out by dynamic programming. Contextual information such as bright scattering from buildings and non-moving vehicles are detected by bright line extraction and blob detection (AMBERG et al., 2005b). The idea was to fill gaps of the tracking result with the contextual information. However the integration of the context information into the road tracking was yet not implemented.

JEON et al. (2002) developed a road extraction approach which starts with a line extraction using Steger's differential geometry approach (STEGER, 1998a), followed by a grouping method based on a genetic algorithm. Unlike the previous two approaches, this one is developed for rural areas in low resolution SAR data (ERS-1, SIR-C/X-SAR). Some pre-processing steps such as speckle reduction and a selection of dark areas are required before the line extraction. The grouping consists of two steps, a connection of nearby segments by an initial grouping and a region growing based on a genetic algorithm. In the end the results are cleaned by an active contour model.

BENTABET et al. (2003) proposed an approach for updating road data bases by means of SAR data, which originates from an approach designed for update by using optical data (AUCLAIR FORTIER et al., 1999). In order to adopt the approach to SAR data much effort was put into the speckle filtering. The old line extractor was replaced by line extractor based on Canny's criteria (ZIOU, 2000). Line structures were preserved by modifying the Standard Frost Filter into a Directional Modified Frost Filter. Potential roads are initialized by the road data base, followed by the line detector. The update of the road data base is then carried out by using active contours.

At the Technische Universität München a road extraction approach named TUM-LOREX was adopted to SAR data by WESSEL and WIEDEMANN (2005) WESSEL (2006). The TUM-LOREX approach was originally designed for optical images with a ground pixel resolution of about 2m (WIEDEMANN and HINZ, 1999) and (WIEDEMANN, 2002). Also this work applies Steger's differential geometry for detecting line structures. TUM-LOREX is based on explicit modeling of roads. That means that the model includes both local (radiometric), regional (geometrical) and global (functional and topological) typical characteristics of roads. The network grouping is carried out by a shortest-path search between automatically selected seed points in a weighted graph. The weighting is based on the local and regional characteristics of the extracted lines and is essential for the selection of the seed points. Line extractions from multiple spectral channels can be combined by a fusion step, which is implemented before the graph search. Later the network grouping was refined with further link hypotheses which are derived from the global network characteristics (WIEDEMANN and EBNER, 2000). New measures such as detour factor and connection factor were introduced. TUM-LOREX performs well in rural or in sub-urban areas. That was confirmed by a road extraction test in 2006 (MAYER et al., 2006). TUM-LOREX delivered among the best results for some of the rural scenes acquired by the optical satellite-borne sensor Ikonos. A modified version of TUM-LOREX is part of a semi-automatic approach for updating and qualifying GIS data by means of optical data (GERKE et al., 2004).

The adaption to SAR data required some SAR pre-processing steps. It was corrected for near far range loss and speckle was reduced by a speckle filter or by the use of multi-look data (WESSEL and WIEDEMANN, 2005). Forest and built-up areas were masked out. In these areas the frequency of false alarms is especially high. The idea that information about neighboring objects could support the road extraction process was further investigated by WESSEL (2004) and WESSEL and HINZ (2004). Here a separate extraction strategy for highways is presented. The model assumes that the highway is characterized by two parallel dark lines separated by a thin bright line which is the central crash barrier. Context objects such as vehicles, trees and junctions are manually extracted and are included as additional seed points. The research presented by WESSEL (2006) showed indeed that an optical approach could be successfully adapted to SAR data, if appropriate pre-processing was carried out before.

2.1.2 Description, analysis and discussion of the automatic road extraction approach TUM-LOREX

The automatic road extraction approach TUM-LOREX developed at Technische Universität München is very well documented in previous works (WIEDEMANN, 2002)(WESSEL, 2006)(STILLA et al., 2007). Here a summarized version of the approach is first presented, followed by an analysis and a critical discussion. Based on this the specific improvements carried out in this doctoral work are derived.

The structure of TUM-LOREX is illustrated in Fig. 2.

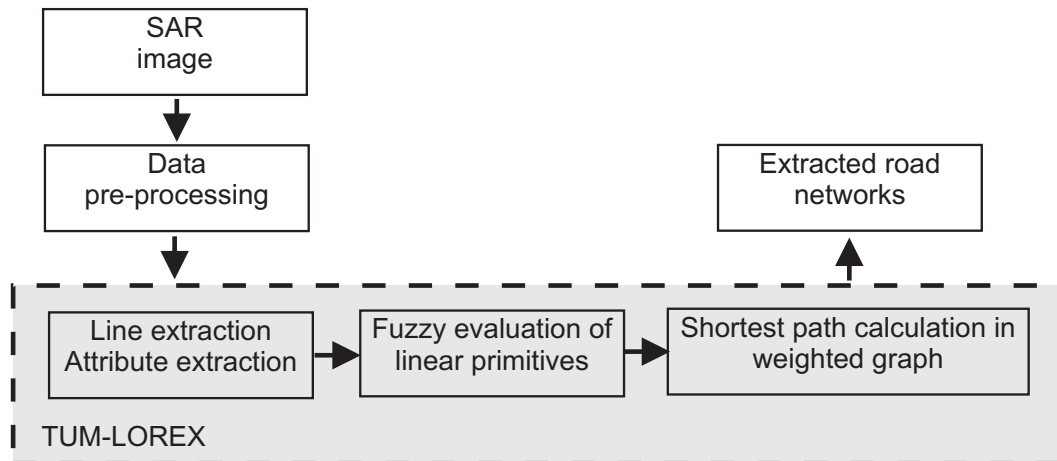


Fig. 2. A condensed version of the TUM-LOREX approach.

Data pre-processing First of all, the SAR data is prepared for TUM-LOREX. Depending on which SAR product is used a correction of the near-far range intensity loss, speckle reduction and data scaling may be required (WESSEL, 2006).

Line and attribute extraction Next step consists of line extraction using Steger’s differential geometry approach (STEGER, 1998a)(STEGER, 1998b). This powerful line extractor is based on differential geometry and can optionally extract bright or dark lines. Since roads appear dark in SAR images, only dark lines are extracted. A description of the approach can be found in Sect. 5.2.1. Additional outputs to the extracted line primitives are line attributes such as width, direction and contrast. The line extraction is followed by a smoothening and split operation.

Fuzzy evaluation of attributes The line extraction detects not only linear primitives belonging to roads but also a large number of *false alarms*. In order to differentiate between the worst false alarms and the correct extractions, each linear primitive is evaluated due to its attributes (*internal evaluation*). The selection of attributes of the line primitives is based on the knowledge about roads. These are both radiometrically and geometrically attributes such as:

- (1) Length of the linear primitive
- (2) Straightness - the standard deviation of the local orientation
- (3) Mean width of the linear primitive
- (4) Constant width - standard deviation of the local width
- (5) Constant intensity (standard deviation)
- (6) Mean Intensity

The evaluation is carried out by means of the Fuzzy theory. Each attribute is evaluated individually, while the final score is calculated by the “fuzzy-and” operator. In the end each line primitive has obtained a weight ranging from 0 to 1. The user can define the Fuzzy-functions based on the specific scene that should be processed.

Extracted line primitives from different image channels can be fused using a “best-first” strategy. All overlapping line primitives within a certain buffer width and with a certain collinearity are assumed to be redundant. After the fusion the lines are prepared for the generation of junctions. Lines are split at points close to where other line ends. Hence also so called “T-intersections” can be extracted.

Shortest path-calculation in weighted graph The linear primitives and their Fuzzy-values are the input to the following step, a shortest-path search (STEGER et al., 1997). A weighted graph of the evaluated road

primitives is constructed. In this graph edges correspond to linear primitives and vertices correspond to the starting and ending points of the linear primitives. The edges become each a final weight (e.g. cost) which is defined as its length divided by its Fuzzy value. Since the Fuzzy values range from 0 to 1, the final weight of the highest rated segments (Fuzzy value = 1) will be equal to its length. As the evaluation get closer to 0, the final weight approaches ∞ .

In general there is a gap between the road segments. In order to fill the gaps, new hypothetic connecting segments are introduced. The gap length between vertices of not already connected edges are calculated. If certain criteria are fulfilled a connecting segment is introduced. These are:

- (1) The absolute gap length
- (2) The relative gap length (compared with the adjacent road segments)
- (3) The direction differences between the gap and the adjacent road segments, whereby collinearity (within a road) and orthogonality (e.g., at junctions) are preferred
- (4) An additional clipping threshold, which ensures that the weight of a gap cannot become higher than that of the adjacent road segments

The result of introducing connection hypotheses is an highly oversegmented network which is “cleaned” by selecting the most significant parts of the network. The selection is based on criteria derived from the functional properties of roads, i.e. that different places or roads are connected in the scene. This is algorithmically implemented as a shortest-path-search in a weighted graph. Here best-valued road segments are selected as seed points and these are connected by the shortest-path-search through the graph. If road networks eventually have to cross the image border, road segments next to the image border can be selected manually by a user (STEGER et al., 1997). This heuristic approach is both simple and effective and is especially important for small sub-urban scenes. The path search is based on the Dijkstra algorithm. An optimal path is selected as part of the road network if the total length of the path exceeds a certain threshold. This favors a connection between two seed points placed far away from each other.

External evaluation At Technische Universität München an external evaluation method for comparing the automatically extracted road networks with reference data was also evolved (HEIPKE et al., 1997) (WIEDEMANN, 2002). The evaluation consists of two steps; (1) the extracted network is matched to the reference data and (2) three quality measures, *correctness*, *completeness*, and *root mean square error* are calculated.

The matching is carried out by first re-sampling both the reference and the extracted results. The distance between each point of a line primitive is then equal for both data sets. Extraction points and reference points are matched to each other given that the points are close and within a certain distance (“buffer”) and that the local direction difference between the two is not bigger than a certain threshold. Redundant matching is avoided by making sure that each point is only matched once.

Completeness gives us an indication of how much of the reference network was actually extracted. It is defined as the percentage of the reference data which is matched with the extracted network data.

$$completeness = \frac{length\ of\ matched\ reference}{length\ of\ reference} \quad (1)$$

Correctness tells us how correct the extracted network is and is the percentage of the extracted network which is matched with the reference data.

$$correctness = \frac{length\ of\ matched\ reference}{length\ of\ extracted\ network} \quad (2)$$

RMS tells us the geometrical accuracy of the extracted road data. In general the value varies with the buffer width.

$$RMS - error = \sqrt{\frac{\sum_{i=1}^n d_i^2}{n}} \quad (3)$$

where d_i is the distance between the each pair i of matched extraction and reference points.

Analysis and discussion important for this work

The advantage of TUM-LOREX is its well modeled network characteristics (STILLA et al., 2007). Any line extraction applied to any image data can be the input to the network generation. Therefore the modifications made for SAR data were mainly concentrated to pre-processing steps. TUM-LOREX has already shown promising results in terms of road extraction from SAR data, but was still neither adapted nor tested thoroughly for

multi-aspect data. As common for most approaches the line extraction from TUM-LOREX often delivers partly fragmented and erroneous results. Especially in forest and in urban areas over-segmentation occurs frequently. Furthermore occlusions due to surrounding objects may cause gaps, which are hard to compensate. One step to a solution is the use of multi-aspect SAR images. If line extraction fails to detect a road in one SAR view, it might succeed in another view illuminated from a more favorable direction. Therefore multi-aspect images supply the interpreter with both complementary and redundant information. But due to the over-segmented line extraction, the information is often contradicting as well. A correct fusion step has the ability to combine information from different sensors, which in the end is more accurate and better than the information acquired from one sensor alone.

Context does not give us direct information about the object of interest but additional information which has influence and/or stand in relation to the object of interest (BAUMGARTNER et al., 1997a). Local context means information about nearby objects such as buildings, trees, traffic signs, which stands in a relation to the appearance of the road (BAUMGARTNER et al., 1997b). Global context information (e.g. forest, residential, industrial and rural areas) gives us information about larger image regions where roads have different typical characteristics. Hence global context provides us with a-priori information. As already stated previous work has shown that local and global context can improve the results obtained by TUM-LOREX. For multi-aspect SAR data the integration of this information is even more important. Due to the different aspect angle the occlusions appear very differently. In order to exploit multi-aspect SAR data optimally these occlusions should not only be detected but also included in the fusion. Naturally the sensor geometry must be included as well.

Hence a fusion module shall be developed which makes use of both sensor geometry information as well as context information. The following goals should be achieved:

- ◊ To exploit the possibilities of multi-aspect SAR imagery for automatic road extraction.
- ◊ To develop a fusion module for multi-aspect SAR data. The fusion shall be implemented in TUM-LOREX.
- ◊ To extend the integration of local and global context as well as the sensor geometry.

2.2 Data fusion for automatic object extraction from SAR

2.2.1 What is data fusion?

Data fusion techniques are beneficial as soon as data from multiple sensors are combined for making a decision that is not possible from one sensor alone. Data fusion was in the beginning a research topic for military purposes and has been practiced for ocean surveillance, air-to-air defense, battlefield intelligence, and target acquisition (HALL and LLINAS, 2001). Most systems were designed for detection, tracking, and identification of targets. In recent years, data fusion has been utilized for non-military applications addressing problems such as implementation of robotics, automated control of industrial manufacturing systems, and medical applications. In the field of remote sensing data fusion has been a current topic for many years. This is due to the extensive availability of satellite data of the Earth acquired from different sensors. Utilizing the data fusion concept within remote sensing is hardly something new. However the exact meaning of the term data fusion applied to remote sensing was in the beginning vague and could vary from one researcher to another (WALD, 1999).

Data fusion gives the user a tool for formalizing the approach and for estimating the quality of information during the fusion process. Furthermore well-known definitions are applied and data fusion scientists working in different fields are able to cooperate. In fact, data fusion is a multi-disciplinary topic and combines a large number of methods and mathematic tools, including signal processing, pattern recognition and artificial intelligence. Even though data fusion has existed for some years, the terminology is not always consistent. For military applications, the Joint Directors of Laboratories (JDL) Data Fusion Working Group has defined a unifying terminology for data fusion. Their short and concise definition on data fusion is (STEINBERG et al., 1998)

“Data fusion is the process of combining data or information to estimate or predict entity states.”

WALD (1998) and WALD (1999) suggested a common formalism for data fusion applied to remote sensing. He has also written a book entirely about data fusion and remote sensing (WALD, 2002),

Data fusion is a formal framework in which are expressed means and tools for the alliance of data originating from different sources. It aims at obtaining information of greater quality will depend upon the application.

In remote sensing, data fusion deals with problems such as (WALD, 2002):

- ◊ Image data from multiple sensors with different signal properties, such as optical and radar data
- ◊ Image data with different spatial and/or temporal resolution
- ◊ Image data combined with numerical models representing geophysical/biological processes

The aim of this section is to shortly explain some definitions used in this work, and not to give an introduction to data fusion. The topic is extensive and there are many good textbooks available (WALD, 2002) (HALL, 1992).

Data fusion definitions

- ◊ *Measurements* represent the output coming from the sensor, in general signals or pixel values. These are the observations.
- ◊ *Attributes* are properties of the object of interest. That can be a color, geometrical measures, or statistical values such as mean or standard deviation. These are also sometimes called *features*. However the definition attributes is better used when fusion is applied to remote sensing, since features is also the definition of extracted information such as edges, lines, points, etc. Attributes are often gathered in state vectors.
- ◊ *Associations* link observations and make sure that these observations belong to the same entity.
- ◊ *Rules* define relationships between objects and their state vectors. Rules may be mathematical operations, methods or reasoning
- ◊ *Decisions* or with other words, *identity declaration* result from the application of rules.

According to WALD (2002) there are three common *data fusion architectures*; 1) *centralized*, 2) *decentralized* and 3) *hybrid*. Centralized means that the original sensor data is fused directly without approximations. In the decentralized fusion architecture, each information source enters a fusion cell and the obtained result from each fusion cell is fused in a final process. The output of this fusion cell includes a quality parameter, which will afterward help to decide the weight of a source in the final fusion process. Decentralized architecture is recommended, when the quality of the collected information is highly variable. The disadvantage of the decentralized fusion is that the resulting input to the final fusion has rather low information content. The hybrid architecture is a combination by the centralized and decentralized architecture.

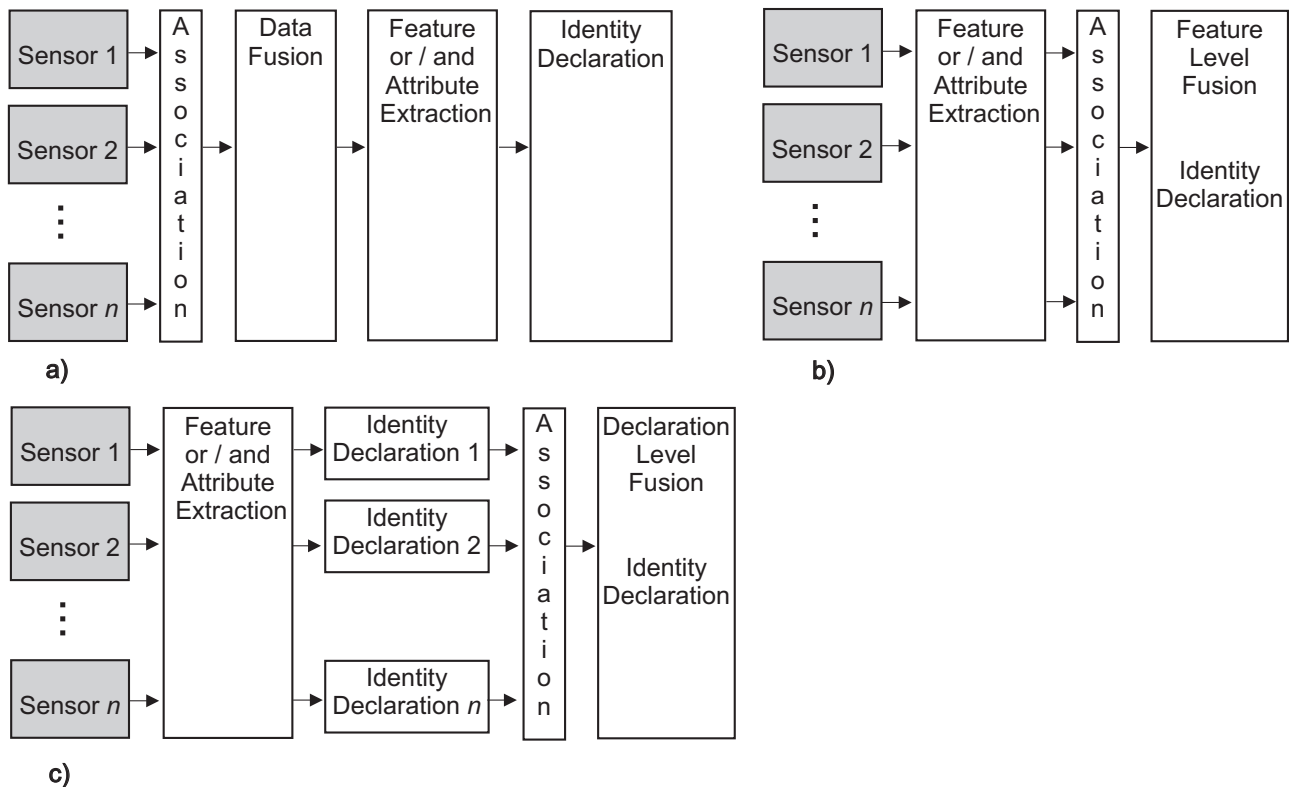


Fig. 3. Common fusion architectures: (a) Direct fusion of sensor data. (b) Representation of sensor data via feature vectors and subsequent fusion of the feature vectors. (c) Processing of each sensor to achieve high-level inferences or decisions that are subsequently combined. - adapted from HALL and LLINAS (2001)

HALL and LLINAS (2001) suggests three architectures, whose definitions are more “easy-to-grasp” than those proposed by Wald. These are 1) *direct fusion of data*, 2) *representation of sensor data via state vector, or feature vectors* and 3) *processing of each sensor to achieve high-level inferences or decisions, which are subsequently combined* (see Fig. 3). The first one is very similar to Wald’s definition of centralized architecture, while the third one has similarities with the definition of the decentralized fusion.

It is also common within remote sensing fusion to divide the fusion approaches into different levels instead of architectures. Remote sensing fusion approaches are then classified into three levels; pixel level, feature level and decision level (POHL and VAN GENDEREN, 1998) (ZHANG, 2010). Pixel-level fusion is regarded as low-level fusion while feature-level and decision-level are often called high-level fusion. Pixel-level fusion means that the data is fused at the lowest processing level. Here a centralized (direct fusion) architecture is applied. Feature-level fusion is used when different features such as edges, corners, lines or different texture parameters are first extracted from each single image. Based on the fused features the following processing takes place. One can say that the features create a common feature space for the subsequent object classification (WALTZ, 2001). Decision level fusions represent the decentralized architecture. Each image is first processed by a certain algorithm. The output of these algorithms are expressed as decisions or confidences, which are combined in a following fusion. Decision-level fusion can be applied both to processed pixel information or to processed extracted features. However important is that the fused pixels or features have obtained decisions or confidences before the subsequent fusion. Sometimes the discrimination between the different fusion levels is diffuse.

2.2.2 Data fusion for man-made object extraction from SAR data - previous work

At first glance better accuracy is obtained by direct fusion of data since the fusing information is closer to the source and the fusion works on signal level (pixel-level). However, direct fusion on signal level is only recommendable if the data is commensurate (i.e. the sensors measure the same physical phenomena). Also if an information source has a large error rate, it might (depending on the fusion process) damage the outputs of the fusion. In contrary to multi-spectral optical images, a direct fusion of multi-aspect SAR data on pixel-level must be handled with much more care. Preferably the statistical and phenomenological properties of SAR image data shall be taken into consideration.

In this section different fusion approaches carried out on pixel-, feature- and decision-level are discussed. We have mainly concentrated on approaches developed for object extraction from SAR data.

Pixel-level fusion Pixel-level fusion has been applied widely to optical images when multi-spectral and panchromatic data shall be fused. The aim is to obtain a better spatial resolution, get enhanced structural and textural details but also to keep the original multi-spectral information, so called pan-sharpening (ZHANG, 2010), (WEIDNER and CENTENO, 2009). But pixel-level fusion has also been applied to SAR data, mainly for land use classification. An interesting approach uses pixel-level fusion on SAR and optical data (LOMBARDO et al., 2003). First the data is fused on pixel-level, hence resulting in a vector for each pixel with signal response from each image. A classification is then carried out by assuming that the data follows a multivariate log-normal distribution. Pixel-level fusion was also applied to land use classification of RADARSAT images (ASILO et al., 2007). A fusion on pixel-level using different pixel-level fusion techniques delivered good results, also thanks to the low resolution and the temporal data obtained by same sensor geometry.

Feature-level fusion Feature-level fusion is often applied to urban SAR remote sensing. For instance it has been applied to urban area interpretation of TerraSAR-X data (CHAABOUNI CHOUAYAK and DATCU, 2010). A combination of extracted bright and dark linear features using the line detector as proposed in TUPIN et al. (1998) are fused. Areas are labeled by using geometrical properties as well as contextual properties (i.e. the combination of high or low frequency of bright and dark linear features). An other interesting topic is building detection and building height estimation from multi-aspect SAR data. For the grouping of extracted features a production system based on perceptual grouping was applied (SOERGEL et al., 2009). Also for this topic the viewing geometry of the SAR sensor plays an important role. That is considered for building recognition and building signature analysis from multi-aspect InSAR data (THIELE et al., 2007)(THIELE et al., 2010). Feature-level fusion is also utilized as soon as several line detectors are combined (HEDMAN et al., 2008)(HEDMAN et al., 2010). The two line extractors used in HEDMAN et al. (2010) performs differently. One is powerful in rural areas as the other one performs better in urban areas. Hence urban and rural areas were extracted before the line detectors were applied. The fusion of the line detectors were carried out by a logical AND operation.

Decision-level fusion Techniques often applied to decision-level fusion are rule-based systems (knowledge-based methods), fuzzy-theory, Dempster-Shafer’s method and Bayesian theory. An early work dedicated to

Fuzzy-fusion of linear features extracted from SAR data was presented by CHANUSSOT et al. (1999). The aim of this work was to improve the first step of road extraction, the results from a morphological line extractor, by using multitemporal images. The ability to suppress false alarms and at the same time improve the detection was tested for different fusion operators, mostly fuzzy operators. Fuzzy-fusion was also applied for building detection (LEVITT and AGHDASI, 2000).

LISINI et al. (2006) presents an approach which combines both Markovian and fuzzy-theory. Here the line segments were assigned a likelihood value (based on a Markovian and fuzzy ARTMAP classifier) before the fusion. Based on an associative symmetrical sum, also applied in TUPIN (2000), the response from each line detector is merged.

A decision-level fusion for land cover classification of SAR and optical data has been developed. Each single source is classified by means of support vector machines. The outcome of the support vector machine classification is fused testing different fusion techniques such as maximum likelihood, decision trees, boosted decision trees, support vector machines, and random forest. Here support vector machines (WASKE and BENEDIKTSSON, 2007) and random forest (WASKE and VAN DER LINDEN, 2008) showed promising results.

TUPIN et al. (1999) proposed a Dempster-Shafer fusion process of several structure detectors. This work is interesting since it aims to give an overall interpretation of low resolution SAR images. Many cartographic elements such as roads, rivers, urban areas, forest areas, etc. are detected. For this reason different linear features and larger objects are extracted from the scene. The output of each detector is assigned with a confidence value that the object belong to certain classes. The reason why Dempster-Shafer is applied in this case is while Dempster-Shafer is able to deal with union of classes. Furthermore some detectors only detect one or only a few classes. Classical Bayesian theory would require that the operators were able to distinguish all classes. Anyway Bayesian network theory should be able to deal with a fusion of this kind of information and could have been an option.

Bayesian network theory has been successfully tested for feature fusion for 3D building description (KIM and NEVATIA, 2003)(KIM and NEVATIA, 2004). Line features are extracted from optical data and grouped in rectangles. Hypothesis that the groupings are correct or not are verified by a Bayesian network. Since the number of images varies an expandable Bayesian network (EBN) is applied. An EBN contains repeatable nodes for various number of image data. Knowledge about semantic relationships among the nodes is included since the EBN has a causal structure. Hidden nodes are introduced for handling correlation between the nodes. Data fusion based on Bayesian network theory has been applied in numerous other applications such as vehicle classification (JUNGHANS and JENTSCHER, 2007), acoustic signals (LARKIN, 1998) and land mine detection (FERRARI and VAGHI, 2006).

Fusion applied to road extraction from multi-aspect data An interesting work that has shown the usefulness of multi-aspect data was presented by TUPIN (2000) and TUPIN et al. (2002). Here the fusion is carried out twice on different levels; road networks (i.e. final results) in the end and line segments (i.e. intermediate results) inside the extraction process. Extracted road networks are merged by using a simple superimposition, while the fusion of the line segments is more complicated. An initial graph of the line segments detected from both images is built. The connection step uses an energy minimization procedure as summarized in Sect. 2.1.1.1. The measure from two merged line segments is computed by using a disjunctive operator. The disjunctive operator is characterized by an indulgent behavior (BLOCH, 1996). The results from fusing the intermediate results are not clearly better than the results from the fusion of the end results. The reason could be that the displacement caused by layover and shadow regions due to high buildings between two possible line segments is not considered. The difficulty of correctly including this displacement is pointed out (TUPIN, 2000).

Merging extracted TUM-LOREX road networks at the end was also investigated by HEDMAN et al. (2005a). A simple fuzzy-fusion strategy which favors roads which are closer to the range direction of the sensor or which were detected in more than one image was introduced. Each image was first processed by TUM-LOREX, meaning that the extracted result also underwent the shortest-path calculation, before the fuzzy-fusion was applied. The fusion strategy was tested on road networks extracted from three multi-aspect images of a small sub-scene (see Fig. 4(a)-(c). The result after fusion can be seen in Fig. 4(d). Those roads close to range direction are marked by an "R". Falsely extracted roads are marked by an "F". The usefulness of multi-aspect data is here exemplified by the road in the middle marked "R" in Fig. 4(c). On the upper side of the road there is a row of trees. In the first two images the road is occluded by shadow and layover but is well detectable in the last one. Since the road is in this case close to range direction, it obtained a higher rating meaning that it was kept after the fusion. This test shows that the strategy works well for small uncomplicated scenes. But one should keep in mind that the

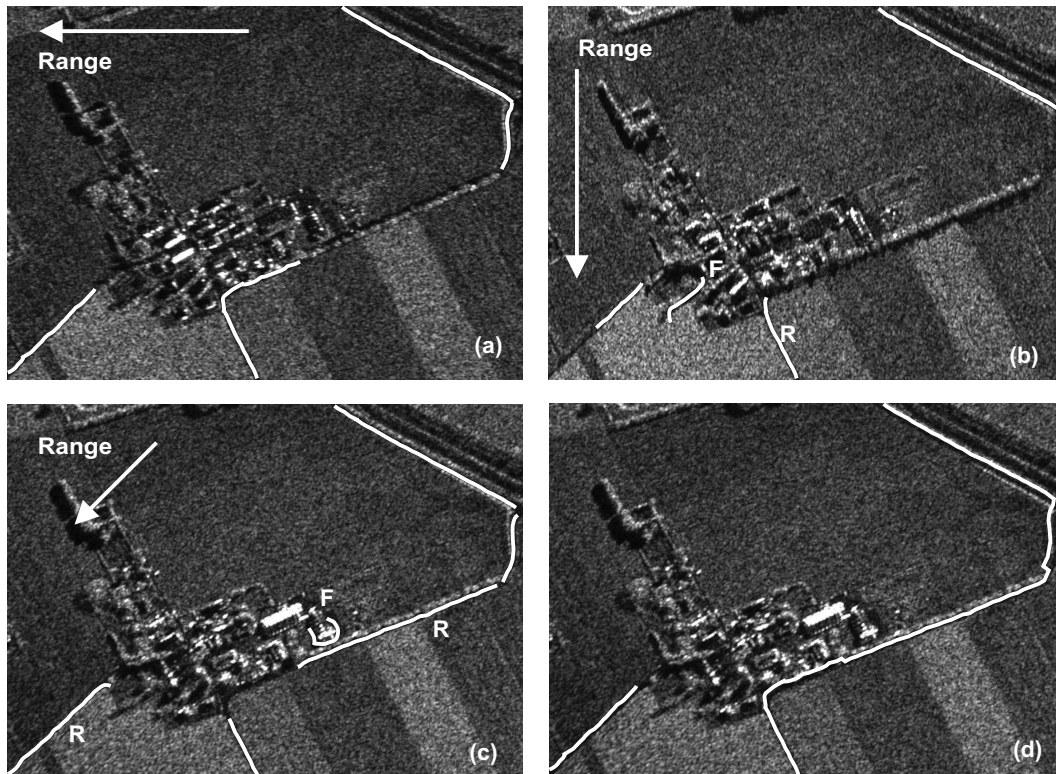


Fig. 4. Road networks extracted with TUM-LOREX were fused based on a fuzzy-fusion strategy (HEDMAN et al., 2005a). TUM-LOREX was first applied to three multi-aspect SAR images (a-c). False alarms are marked by “F” and roads with a favorable direction are marked by “R”. The fused results can be seen in (d).

strategy requires that TUM-LOREX delivers already acceptable results. In addition the fuzzy-functions were set based on an ad-hoc basis.

DELL’ACQUA et al. (2003) used simulated multi-aspect data for testing their approach. Here intermediate results (line segments extracted separately in each image) were fused by a logical OR, followed by a cutting of the overlapping segments. Longer segments are preserved.

So far none of the fusions developed for road extraction from multi-aspect data fully exploit the capabilities of multi-aspect data. Neither the displacement effects nor the SAR specific occlusions are taken into consideration.

Main Conclusions

In account with similar works extracted linear features shall be fused. Furthermore intermediate results shall be fused meaning that the fusion shall be integrated in the road extraction process. Since we have the problem of many gaps and false alarms delivered by the line extraction, the linear features cannot be fused directly. Instead the features shall obtain an uncertainty value before the fusion. Hence a decision-level fusion shall be applied. In previous decision-level fusion approaches both numerical and symbolical methods were utilized.

Fuzzy-theory is already used for one part of TUM-LOREX - the internal evaluation. Fuzzy functions of radiometric and geometric attributes is used for the selection of good road candidates and for sorting out most probable false alarms. However the functions must be defined manually by a user and the parameter setting can be rather time consuming. Including local context and sensor geometry means that the number of fuzzy functions would soon be incalculable. Besides the approach is rather heuristic and not applicable for dealing with the contradicting information extracted from multi-aspect SAR data.

Dempster-Shafer theory is useful when the probabilistic model is incomplete, i.e. when some prior or conditional probabilities are missing. TUPIN et al. (1999) points out that the evidence theory is applicable when the incoming information is imprecise, which is often the case with SAR images. But Bayesian theory can better handle causal probabilities. If most of the probabilities are known, but only some are missing, Bayesian theory allows us to assume reasonable values (PEARL, 1988).

Since TUM-LOREX is based on explicit modeling, the fusion shall also include explicit knowledge. For this Bayesian networks are especially convenient. Bayesian network theory offers us a probabilistic framework based

on the classical Bayesian inference, but allows us a more flexible structure. Contrary to the undirected Markov random fields, Bayesian networks belong to the directed graphs. While Markov graphs are useful for expressing symmetrical spatial relationships, Bayesian networks define causal relationships (PEARL, 2000). Hence we deal with relations rather than with signals or objects. In fact, the structure of a Bayesian network has much in common with human reasoning. The causes (or dependencies) among variables are conveniently described by a network. Directions of the causes are stated which allow top-down or bottom-up combinations of evidence. At the same time independencies among variables can be defined, which allows us to simplify the system if a variable has influence on only a small part of the variables. That reduces computational efforts.

The conclusion drawn from this is that Bayesian network is the most suitable framework for this type of fusion. Hence the aim of this work is to develop a Bayesian network fusion based on a probabilistic model as complete as possible.

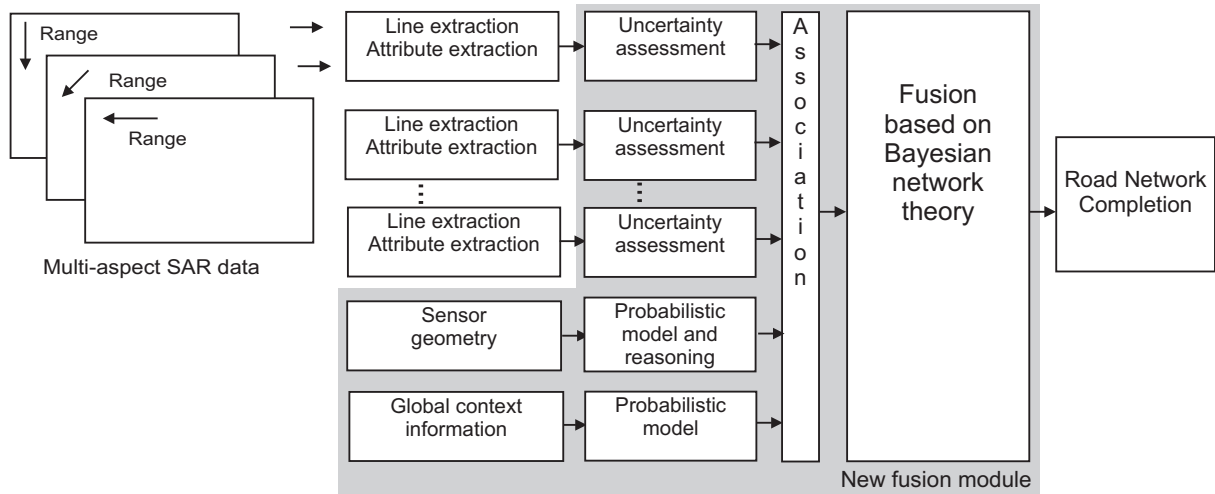


Fig. 5. The fusion and its implementation in TUM-LOREX is illustrated in the figure. The gray area defines those parts that belong to the fusion developed in this work.

The architecture of the fusion and its implementation in TUM-LOREX is illustrated in Fig. 5. Those parts belonging to the new fusion module are placed within the gray region.

In summary, the new fusion module shall accommodate for following aspects:

- ◇ Analysis and probabilistic modeling of the uncertainty of the incoming information (i.e. linear features)
- ◇ Probabilistic modeling of roads and their local and global context depending on sensor geometry
- ◇ Decision-level fusion implemented as a Bayesian network for solving contradicting and supporting hypotheses

3 SAR principles and image characteristics

In this chapter a short summary of the principle and the imaging characteristics of Synthetic Aperture Radar (SAR) will be given. We focus here on the most essential properties, which are relevant for setting up a correct road and context model depending on the viewing and sensor geometry. There are excellent textbooks about SAR, both on the topic of SAR processing (CUMMING and WONG, 2005) and of SAR imaging characteristics (MASSONNET and SOUYRIS, 2008).

3.1 SAR principles

RADAR is an acronym for Radio Detection and Ranging and is essentially a ranging or distance measuring device. Radar is an active system and it operates in the wavelength area between 1 m and 1mm (0.3-300 GHz). The signal characteristics are controlled and allow the utilization of among others interferometry and polarization for a range of applications. An additional advantage of RADAR is its ability to operate during bad weather conditions. Electromagnetic energy with frequencies between 1-15 GHz can practically penetrate through clouds. For shorter frequencies, SAR K-band, there is an atmospheric loss.

The fundamental principle is that the sensor transmits a short, *coherent* signal toward the target and detects the backscattered portion of the signal. By measuring the time delay between the transmission of a pulse and the reception of the backscattered “echo” from different targets, their distance from the radar and thus their location on a reference surface can be determined. As the sensor platform moves forward, recording and processing of the backscattered signals builds up a two-dimensional image of the surface.

In remote sensing there are three kinds of different radar systems; altimeters, scatterometers, and imaging radar systems. In this work we will only consider imaging radar systems. The geometry of an imaging radar system is quite different from an optical imaging system. A side-looking geometry is applied. The platform travels forward in the flight direction and transmits a signal oblique to the flight direction (see Fig. 6). The illuminated area on ground is called *footprint* or *swath*. *Range* refers to the across-track direction perpendicular to the flight direction, while *azimuth* refers to the along-track direction parallel to the flight direction. *Near-range* is the portion of the swath closest to nadir, while *far-range* is the portion of the swath farthest from nadir. In the near-range, the local incidence angle is steep relative to the local incidence angle in far-range.

A radar’s spatial resolution is dependent on the specific properties of the microwave radiation and geometrical effects. Normally we talk about two different resolutions, range and azimuth resolution. Two distinct targets on the surface will be resolved if their distance is larger than half the pulse length. In fact most SAR sensor applies the “chirp” method and makes use of a pulse compression by frequency modulation. The range resolution relates then to the bandwidth of the emitted chirp. The azimuth resolution, however, is limited by the azimuth antenna footprint size. The width of the footprint is proportional to the wavelength and inverse proportional to the antenna length. Better azimuth resolution is normally achieved by either decreasing the wavelength or by obtaining a longer antenna. This technique is utilized by real aperture radar (RAR).

Synthetic aperture radar has the ability to synthesize a longer antenna by exploiting the motion of the platform. The target is then almost continuously illuminated and as a result the target is reconstructed from not one exposure but from several. In principle the azimuth resolution is a function of the synthetic antenna length and the distance to the object is no longer relevant. A shorter real antenna length results in a longer simulated antenna length, which in turn results in a better resolution. An upper band is given, however, by the pulse repetition frequency. In addition, the design of the real antenna length is restricted by the antenna gain. Nonetheless SAR systems, in contrast to RAR systems, are especially suitable as flight- or space-borne sensors.

The generation of SAR images based on the recorded pulse or chirp echoes is a complicated task. Nowadays it is operational implemented involving standardized advanced signal processing.

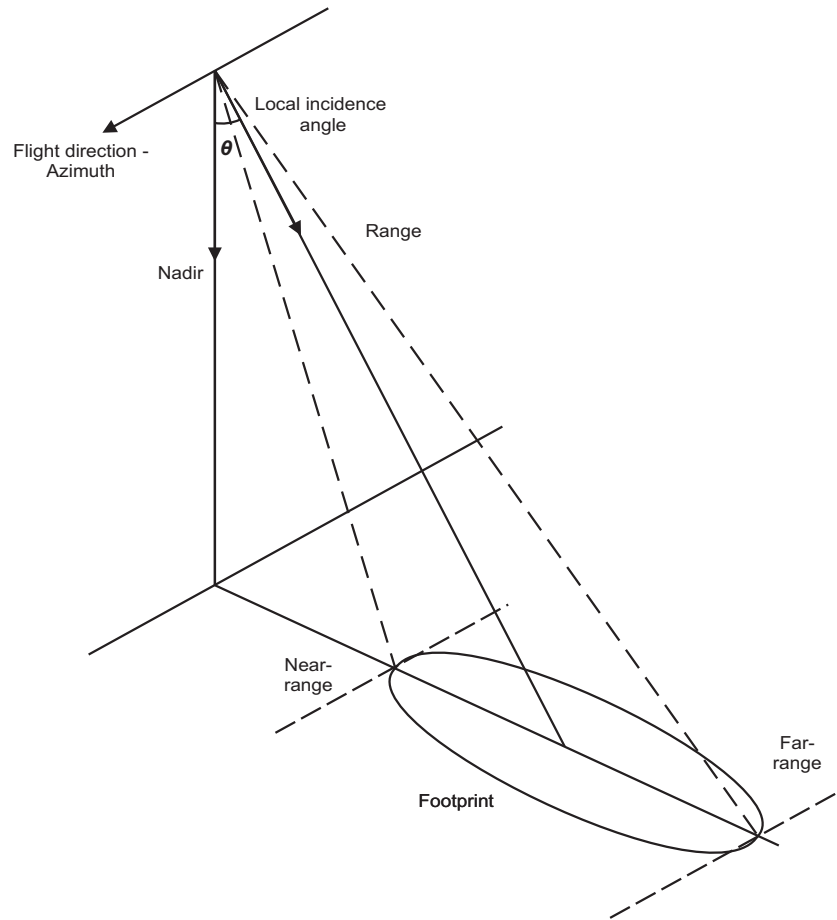


Fig. 6. Side-looking geometry of a SAR-sensor.

3.2 SAR image characteristics

3.2.1 Geometrical effects

The radar measures the distance to features rather in slant range than the true horizontal distance along the ground (ground range). This results in varying image scale moving along the image line from near to far range. Targets in near range tend to appear compressed relative to the far range. This effect is dependent on the flight height and is larger for air-borne systems than for space-borne systems.

An image in slant range can be transformed into ground range format by using trigonometry. Furthermore, the side-looking geometry of the SAR sensor results in certain geometric distortions on the resultant imagery. *Shadow*, *layover* and *foreshortening* are all SAR-specific effects, which occur as soon as high-elevated objects occur on the ground surface (see Fig. 7). These effects cannot be compensated for without additional information but gives clues for the presence of important 3D features.

Foreshortening give rise to a compressed appearance of high objects tilted toward the sensor. The length of the slope will be represented incorrectly and give rise to a bright feature in the resulting image. Foreshortening is dependent on the incidence angle of the sensor and the steepness of the slope. The steeper slope the more significant is the distortion.

Layover occurs by smaller incidence angles (e.g. in near-range), by steep mountains and by building fronts. In this case, the radar beam reaches the top of the target before it reaches the ground. As a result, the signal response from the top is displaced toward the sensor from its true position on the ground and overlaid onto the echoes from the ground.

As soon as layover and foreshortening effects are present, radar shadows are present as well. Shadows occur behind high-elevated objects or steep surfaces, as the radar beam is not able to illuminate the ground surface. In these areas there are no backscattered signal and they appear black in the image. The strong layover and shadow regions of a mountainous region can be seen in Fig. 8.

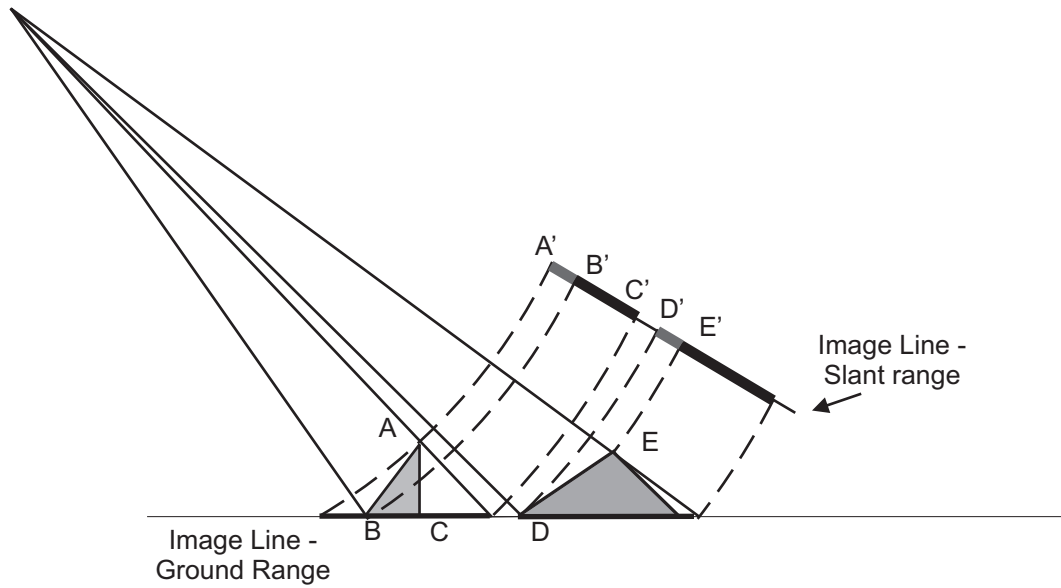


Fig. 7. Image lines in slant- and in ground-range format. Layover effects occurs by steep surfaces. The signal reaches point A before the ground (B). In the image, the signal response from the top is displaced toward the sensor (A'). Radar shadows are present behind steep surfaces or high objects (see C and C'). Tilted surfaces ($D-E$) appear compressed in slant range ($D'-E'$), so called foreshortening.

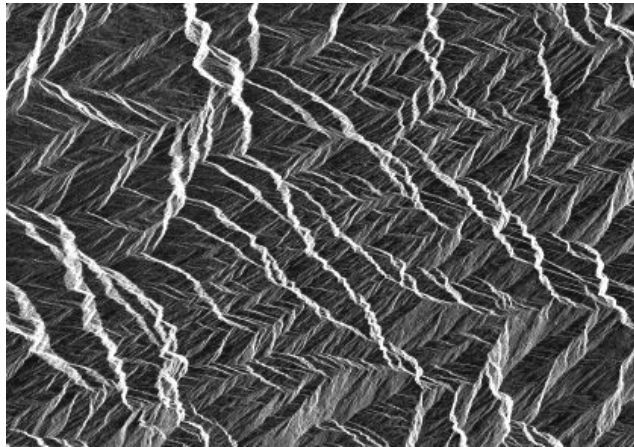


Fig. 8. TerraSAR-X image of a mountainous region, Sichuan province, China.

3.2.2 SAR radiometry

The radiometric properties of a SAR image can be derived from the physical properties of the illuminated object. The radiometry relies therefore on the physical parameters on ground; surface roughness, moisture content, and electrical properties of the object, but also on the sensor and its geometry related to the target; the wavelength of the emitted SAR signal, the local incidence angle and the local ground slope. Surface scattering and volume scattering have different behavior.

Surface scattering occur when electromagnetic waves travel from one homogeneous semi-infinite media to another. These two medias are separated by a surface, which can be described as either rough or smooth. The resulting scattering can be assumed to consist of two components; a reflected, specular component and a scattered, diffuse component. The first component contains coherent reflectance as the second is referred to as the non-coherent scattering (ULABY et al., 1982). A smooth surface causes specular reflection of the incident energy and thus in general only a small amount of the energy (the non-coherent component) is scattered back to the sensor. Hence smooth surfaces appear darker in the resulting SAR image. Rough surfaces cause diffuse reflection, which results in a brighter appearance. In this case the non-coherent component is larger, resulting in power scattered in all directions. Whether a surface appears rough or smooth to the radar is dependent on the wavelength and the incidence angle of the sensor. A surface is considered to be smooth when it fulfills

$$h_{\sigma} \leq \frac{\lambda}{8 \cdot \cos \theta} \quad (4)$$

The variable h_σ represents the surface height variation as defined in (ULABY et al., 1982). Models describing rough scattering normally consider the height variation not only in vertical direction but also in horizontal direction.

A tilted surface toward the sensor appears brighter as a result of a stronger reflected signal. This effect is rather of a specular nature and can be described by a facet model. It is then assumed that the illuminated ground to consist of several flat facets. Each one of these facets has a local ground slope.

Targets, who consist of two or more perpendicular surfaces, give rise to so-called double bounce or trihedral bounce scattering (see Fig. 9). Objects with this property (buildings, walls, etc) are sometimes called corner reflector and are common in urban environments. Metallic objects cause an other kind of strong signal. Due to their high dielectric constant these objects get a re-radiation pattern the same as an antenna causing an resonant effect.

The dielectric constant describes the resistance to the penetration of electromagnetic waves. The moisture content plays here a significant role and contributes more than the texture of the material. The penetration depth is also wave-length dependent. SAR sensors with larger wavelength (such as L-Band) has the ability to penetrate cm/m through snow or soil.

Volume scattering has a different nature than surface scattering (see Fig. 9). Volume scattering is caused when electromagnetic waves propagate through a cloud of scattering elements, each with different dielectric properties, size, and shape. The spatial locations of these elements are random. Hence, in contrary to surface scattering, the media is assumed to inhomogeneous. Volume scattering is often very difficult to predict. Often it is hard to find the boundary when volume scattering and when surface scattering occur. As matter of fact, electromagnetic interaction with materials with a low dielectric constant and hence a large penetration depth may be better described by the volume scattering model. Furthermore, both surface and volume scattering often contributes to the scattering from vegetation.



Fig. 9. Strong scattering caused by metallic objects and by double bounce and trihedral bounce reflections can be seen in the left part of the image. This industrial area contain large buildings. The right part show the irregular volume scattering caused by high vegetation.

Beyond the physical properties of the object, the so-called *speckle* effect has a significant impact on the radiometry of the image. Speckle is caused by random constructive and destructive interference from the multiple scattering returns that will occur within each resolution cell (MASSONNET and SOUYRIS, 2008). If the returning waves within one resolution cell behave constructively, the pixel appears brighter. Destructive interference is the opposite extreme and results in lower pixel intensity. Speckle has the same behavior as multiplicative noise, i.e. its variance increases linearly with the mean intensity. High resolution SAR sensors (about 1 m resolution) show less speckle effect simply since a smaller resolution cell is assumed to have a limited number of scatterers.

Speckle can be reduced by applying speckle filters such as the multiplicative speckle model-based Frost-Filter, Lee-Filter, and Kuan-Filter and product model-based Gamma MAP filter (TOUZI, 2002). An other way of decrease the speckle-effect is to apply multi-look processing. A set of samples illuminating the same area are averaged in power together to produce a smoother image. Each sample is produced by using different parts of the synthetic aperture. The speckle is in the end reduced but at the cost of a worse resolution.

3.2.3 SAR systems and their data

The data used in this work was acquired by an air-borne (E-SAR) and a space-borne (TerraSAR-X) SAR system.

The E-SAR system is a multi-frequency, air-borne SAR system, which was developed by the German Aerospace Center (DLR) in the 90's. The aim of the research project was to get know-how in SAR sensor design and data processing techniques for the support to space missions such as ERS-1 and SIR-C/X-SAR. E-SAR is able to operate in several bands (P-,L-,C- and X Band) (HORN, 1996). A sub-image in X-band can be seen in Fig. 10. The systems has both polarimetric and interferometric modes. A multi-look processor is integrated in the system, enabling multi-look data up to 8 looks. The experience gained from E-SAR was useful for the following space-mission TerraSAR-X.



Fig. 10. Sub-image (X-band) acquired by the E-SAR sensor showing parts of the airport in Oberpfaffenhofen, close to Munich, Germany.



Fig. 11. The football stadium Allianz-Arena can be seen in this TerraSAR-X sub-image. The imaging mode is high-resolution spotlight mode and the data was obtained as radiometrically enhanced data product.

TerraSAR-X is a German space-borne SAR-mission, partly with commercial and partly with scientific interests, developed by the German Ministry of Education and Science (BMBF), DLR and the Astrium GmbH (ROTH et al., 2005). The satellite was launched on 15 June 2007 from the Kazakhstan. The sensor operates in X-band and has a steerable antenna. This enables a range of imaging modes (FRITZ, 2007):

- ◇ *Stripmap mode* - the basic SAR imaging mode with 3.3 m (azimuth resolution)
- ◇ *Spotlight mode* - A phased array beam steering in azimuth direction and thereby increasing the size of the synthetic aperture, resulting in a resolution in azimuth down to 1.7 m. The drawback of this technique is the reduced swathwidth.
- ◇ *High Resolution Spotlight mode* with a higher beam steering velocity than the normal spotlight mode (azimuth resolution down to 1.1 m)

- ◇ *ScanSAR mode* A wider swath is obtained by switching the antenna elevation steering subsequently and scanning several adjacent ground sub-swaths with different incidence angles. In this way the azimuth resolution is reduced to 18.5 m.

All imaging modes have single and dual polarization modes except ScanSAR mode that has single polarization mode. Furthermore spatially and radiometrically enhanced data products are available. Multilook processing and geometric projections such as geocoded ellipsoid correction (assuming one average terrain height) and enhanced ellipsoid correction (using a digital elevation model (DEM)) can be ordered for ground range data. Side-lobe suppression which is especially important in urban areas is applied.

An example of TerraSAR-X data can be seen in Fig. 11.

4 Bayes probability and network theory

This section explains first what plausible reasoning is, second gives an introduction to Bayesian probability theory and third presents Bayesian network theory.

4.1 Plausible reasoning and Bayesian probability theory

Plausible reasoning is very much similar to human's reasoning process of drawing conclusions based on old and new information. In contrast to deductive reasoning, plausible reasoning do not give any *certain* answers but well plausible answers. The introduction of a textbook written by JAYNES (2003) gives a good explanation on the differences between deductive and plausible reasoning:

Deductive reasoning

- ◇ if X is true then Y is true
- ◇ X is true - therefore, Y is true

and its inverse:

- ◇ if X is true then Y is true
- ◇ Y is false - therefore, X is false

This is the kind of reasoning that we would prefer to work with if the world would be perfect. However, the reality looks more like:

Plausible reasoning

- ◇ if X is true, then Y is true
- ◇ Y is true - therefore X becomes more plausible

Y does not prove that X is true, but Y, which is one of the consequences of X, makes us more confident of X. JAYNES (2003) gives an example of this; Assume that X represents the hypothesis that it will rain by 10 AM at the latest and Y that the sky will become cloudy before 10 AM. Observing clouds does not make us certain that it will truly rain, but it will give us a stronger belief in a coming rain. Nevertheless if it would rain, clouds would normally be present. What we deal with in this work is a much weaker reasoning such as:

- ◇ if X is true, then Y becomes more plausible
- ◇ Y is false - therefore X becomes less plausible

The brain has the ability to not only decide whether something is possible or not, but also to evaluate the degree of plausibility. The chances of rain before 10 AM is very much dependent on the type of clouds. The brain make use of experience as well as the present information in making decisions. Thus the brain utilizes *prior and posterior information*. These two categories of information "old" and "present" are also the core of the Bayesian probability theory.

Bayesian probability theory obeys three axioms:

$$\begin{aligned}
 0 &\leq P(X) \leq 1 \\
 P(\text{sure proposition}) &= 1 \\
 P(X \text{ or } Y) &= P(X) + P(Y)
 \end{aligned}
 \tag{5}$$

where the letter P denotes probability, i.e. $P(X)$ stands for the probability that event X is true.

Bayesian probability theory deals with a certain section of probability theory; the conditional probability theory.

- ◇ The conditional probability $P(X|Y)$ expresses the probability that X is true under the assumption that Y is known with absolute certainty
- ◇ which should not be confused with the joint probability: $P(X \text{ and } Y) = P(X, Y) = P(X) \cdot P(Y)$

The inventor of Bayesian theorem, Thomas Bayes (ca. 1702-1761), derived the theorem directly from the *product rule*

$$P(X, Y|I) = P(X|Y, I) \cdot P(Y|I) \tag{6}$$

The Bayes' theorem:

$$P(Y|X, I) = \frac{P(X|Y, I) \cdot P(Y|I)}{P(X|I)} \quad (7)$$

where $P(X|Y, I)$ is called the *conditional* probability or *likelihood function*, which specifies the belief in X under the assumption that Y is true. $P(Y|I)$ is called the *prior* probability of Y that was known before the evidence X became available. $P(Y|X, I)$ is often referred to as the *posterior* probability. The denominator $P(X|I)$ is called the *marginal* probability, i.e. the belief in the evidence X . The marginal probability expresses the probability that X is true irrespective of Y :

$$P(X|I) = \int_{-\infty}^{+\infty} P(X, Y|I) dY. \quad (8)$$

This is merely a normalization constant, which nevertheless is important in Bayesian network theory. All probabilities are conditional on I , which is made to denote the relevant background information at hand. In this work we leave I out and write $P(X)$ instead of $P(X|I)$.

The strength of Bayes' theorem is that it relates the probability that the hypothesis Y is true given the data X to the likelihood probability that we have observed the measured data X if the hypothesis Y is true. The latter term is in most applications much easier to estimate. For example, estimating the probability that a patient with a certain disease will develop a certain symptom X is manageable as soon as it is established that a group of patients suffer from a given disease (PEARL, 1988).

4.2 Bayesian networks

Bayesian networks expound Bayes' theorem into a directed acyclic graph (DAG) (JENSEN, 1996) (PEARL, 1988). The *nodes* in a Bayesian network represent the variables, such as temperature of a device, gender of a patient or feature of an object. Variables may have discrete states or continuous states. A variable is in exactly one of its states, but most of the time these states are unknown to us. The *links*, or in other words the *arrows*, represents the informational or causal dependencies between the nodes. If there is an arrow from node Y to node X ; this means that Y has an influence on X . Y is called the parental node and X is called the child node. X is assumed to have n states x_1, \dots, x_n and $P(X = x_i)$ is the probability of each certain state x_i .

Bayesian networks are examples of causal networks. Important are not only the dependencies but as well the independences between the set of variables. This is controlled by the connection between the variables and the current information about the variables. If the state of one variable is already known, we call this *hard evidence* or we say that the variable (or node) is instantiated. If not, the evidence is called *soft*. Below we will give a couple of examples of networks when variables can be considered dependent or not given hard or soft evidence (JENSEN, 1996). These three examples are illustrated in Fig. 12.

Serial connection: Assume that X has influence on Y which in turn has influence on Z (see Fig. 12(a)). Knowledge about X will have an impact on belief in Z through Y . Also knowledge about Z will influence the belief in Y and then also X . If the state of Y is given (i.e. hard evidence), information is blocked and the two variables X and Z become independent. X and Z are *d-separated* given Y :

$$P(Z|Y, X) = P(Z|Y) \quad (9)$$

Diverging connection: In this diverging connection, variable X is the parental node of the two child nodes Y and Z (see Fig. 12(b)). If X is given, the two child nodes are independent. Otherwise information can flow between the nodes (see Fig. 12(b)). Y and Z are *d-separated* given X :

$$P(Z, Y|X) = P(Z|X) \cdot P(Y|X) \quad (10)$$

Converging connection: Now assume that variable X is the child node of the parental nodes Y and Z . If no knowledge about X is known, the parental nodes are all independent of each other. But as soon as evidence about X or about any of child nodes of X is known, then there exist a dependency between Y and Z (see Fig. 12(c)). Y and Z are *d-separated* given that neither X nor any child nodes of X have received evidence:

$$P(X|Y, Z) = P(X|Y) \cdot P(X|Z) \quad (11)$$

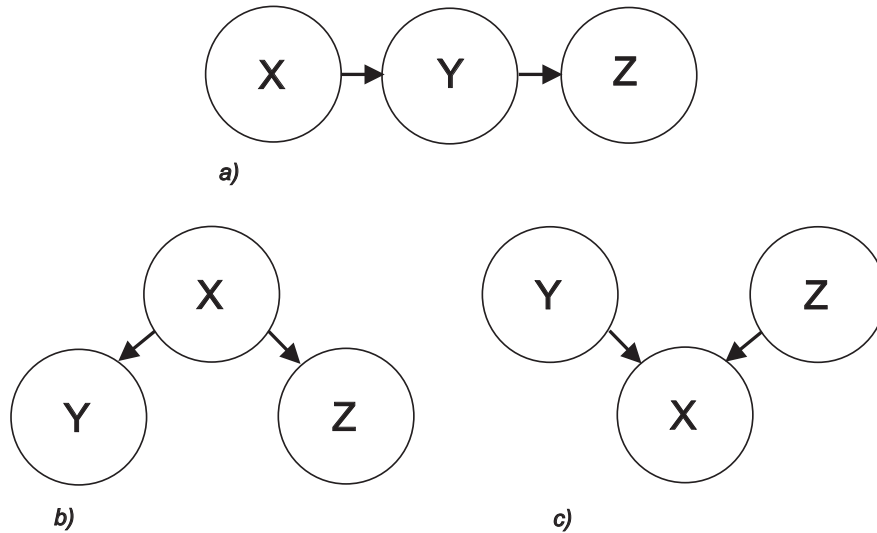


Fig. 12. Bayesian networks with: (a) serial connection, (b) diverging connection, (c) converging connection.

If two nodes are not d-separated, they are called *d-connected*.

The mathematical definition of Bayesian networks is as follows (JENSEN, 1996)(PEARL, 1988)

The Bayesian network U is a set of nodes $U = \{X_1, \dots, X_n\}$, which are connected by a set of arrows $\mathbf{A} = \{(X_i, X_j) | X_i, X_j \in \mathbf{U}, i \neq j\}$. Let $P(u) = P(x_1, \dots, x_n)$ be the joint probability distribution of the state values \mathbf{x} . Lowercase letters stand for particular values (e.g. TRUE or FALSE). For being a Bayesian network, U has to satisfy the Markov condition, which means that a variable must be conditionally independent of its nondescendants given its parents. $P(x_1, x_2, \dots, x_n)$ can therefore be defined as

$$P(x_1, x_2, \dots, x_n) = \prod_{i=1}^n P(x_i | \text{pa}(X_i)) \quad (12)$$

where $\text{pa}(X_i)$ represent the parents states of node X_i . If this node has no parents, the prior probability $P(X_i = x_i)$ must be specified.

Assume a Bayesian network composed by two child nodes, X and Z , and one parental node, Y (see Fig. 13). Since X and Z are considered to be independent given the variable Y , the joint probability distribution $P(y, x, z)$ can be expressed as

$$P(y, x, z) = P(y)P(x|y)P(z|y) \quad (13)$$

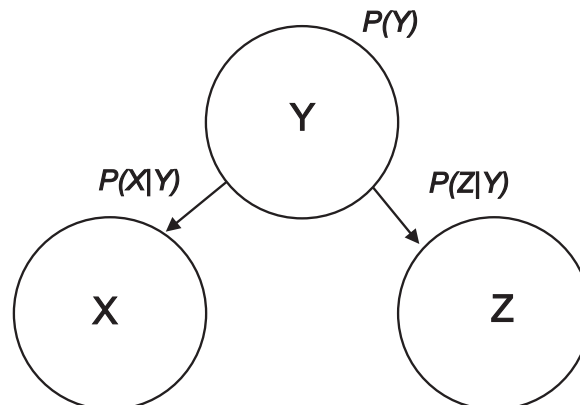


Fig. 13. A Bayesian network with one parental node (Y) and its two child nodes (X and Z) and their corresponding conditional probabilities.

4.2.1 Belief propagation in Bayesian networks

Until now the Bayesian network has been described as the joint probability of all variables contained in the network (see Eq. 13). However in many applications one is interested in the probability related to one variable, the *hypothesis variable*. Hypothesis variables are normally impossible to observe, but are the variables with the states we would like to estimate. The estimation is done by means of known or partly known states of observable variables, the *information variables*. PEARL (1988) describes a belief updating system which will be applied in this work. In this system each variable will obtain a processor, which controls the information running from one variable to its neighboring variables. Information run only via the links and these links are supposed to be always open.

The evidence arriving to an information node in such a system may be sent from both neighboring parental and child nodes at the same time. Information coming from a parent, e^+ is named *causal* or *predictive* evidence. Predictive information propagates in a top-down direction. Information from child nodes, e^- , flow in the opposite direction and is called *diagnostic* evidence. Information coming from the top (the parents) and from the bottom (the children) are differentiated and therefore expressed by different Greek letters (see Fig. 14):

$$\pi(x) = P(x | e^+) \quad (14)$$

and

$$\lambda(x) = P(e^- | x) \quad (15)$$

The total belief in node X is obtained by fusing evidence coming from the top and from the bottom:

$$BEL(x) = \alpha \lambda(x) \pi(x) \quad (16)$$

where α is a normalizing constant assuring that $\sum_{i=1}^N BEL(x_i) = 1$ for all n states x of X .

Each arrow between two nodes ($X \rightarrow Y$) is quantified by conditional probability functions. Probability functions in a Bayesian network can have a countable (discrete) or a continuous set of states. Conditional probabilities for discrete states are usually realized by conditional probability tables. Conditional probabilities for continuous states can be estimated by probability density functions.

By such tables' definition, the nodes in a Bayesian network are variables with a finite number of mutually exclusive states. If the variable X has states $x_1 \dots x_n$ and the variable Y has states $y_1 \dots y_m$ then $M_{Y|X}$ is an $m \times n$ table containing numbers $P(y_i | x_j)$ such as

$$M_{Y|X} = p(Y = y | X = x) = \begin{bmatrix} p(y_1 | x_1) & p(y_1 | x_2) & \dots & p(y_1 | x_n) \\ p(y_2 | x_1) & p(y_2 | x_2) & & p(y_2 | x_n) \\ \vdots & \vdots & & \vdots \\ p(y_m | x_1) & p(y_m | x_2) & \dots & p(y_m | x_n) \end{bmatrix} \quad (17)$$

The sum of the columns should preferably be one.

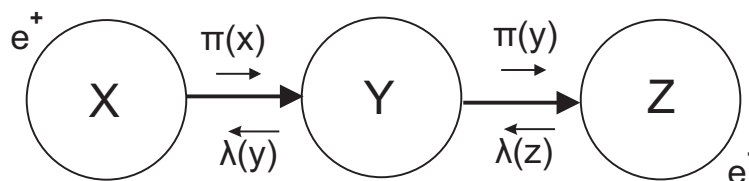


Fig. 14. The belief update is illustrated for a serial connection.

Assume a Bayesian network consisting of one parental node X and two child nodes Y and Z (see Fig. 14). Assume that evidence arrive at node X , some prior information expressed by the vector $\pi(x)$. Node Y is not observed directly but is supported by node Z , which state is observed, $e^{-} \{Z = z_{observed}\}$. This information propagates to node Y and then later to node X . Based on this information $\lambda(y)$ can be estimated. The states in node Y is not known for sure, but the vector $\lambda(y)$ contains for each state of Y an uncertainty value entirely based on Z . The belief in node X can the be expressed as:

$$BEL(x) = \alpha \lambda(x) \pi(x) = \alpha M_{Y|X} \lambda(y) \pi(x) \quad (18)$$

where

$$\lambda(x) = M_{Y|X} \lambda(y) \quad (19)$$

is a matrix product.

More detailed information on Bayesian network theory can be found in JENSEN (1996) and in PEARL (1988).

5 A Bayesian fusion approach for road extraction from SAR

As already stated in Sect. 2.2.2 Bayesian networks express causal relationships and enable us to model data fusion similar to a human's reasoning process. Hereby we need to define all the information variables and find dependencies/independencies among them. Important here is to realize the causal relationships among the variables. In addition Bayesian networks requires us to give all its entities a probabilistic definition. Hence an underlying probabilistic model as complete as possible must be found. That means that all incoming information must be analyzed before the network is structured. As soon as the correct structure of the network is found, the network shall be learned. That means that the conditional probabilities among the nodes shall be estimated.

Doing this in practice for road extraction from multi-aspect SAR data involves following five steps:

- (1) Definition of a road model and its local context in multi-aspect SAR data (Sect. 5.1)
- (2) Analysis of the feature extraction, i.e. the dark and bright linear extractor and the classification of global areas (Sect. 5.2)
- (3) Building a Bayesian network model, which means defining the nodes and their states (Sect. 5.3). This part also comprises finding dependencies and independencies and modeling of the flow of information (i.e. belief updating) between the nodes.
- (4) Learning, which means a quantification of the arrows between the nodes by conditional probabilities. The estimation of conditional probability functions (Sect. 5.4) and of conditional probability tables (Sect. 5.5) requires training data. The prior term shall also be approximated for which global context information plays an important role (see Sect. 5.6).
- (5) Associate the observations (i.e. the linear features), which means that it is decided which features are the observations of the same object(Sect. 5.7).

5.1 Modeling of roads and their context for SAR data

Extraction of man-made objects such as buildings or houses relies in general on any kind of modeling. An *object model* describes properties of an object in the real world, while an *image model* explains the characteristics of the appearance of the object in the image. Based on these models, rules and/or a priori knowledge can be defined. These later underlie the coming fusion module and the road extraction system.

In this section we will present the object- and image models, which are the basis for not only TUM-LOREX, but also for the fusion approach presented in this work.

5.1.1 Modeling of roads

Object Model: In the real world, roads may look very different depending on the road type (e.g. motorway, highway, side roads). Furthermore the characteristics of these road types might differ within one category depending on the country, terrain, etc. A road can be described by its geometrical, radiometrical, topological and contextual properties (see Tab. 1). All roads have a certain geometry and appear usually as a long linear shape, are normally straight or lightly curved, but with a constant width. Roads have specific radiometric properties which are dependent on the material (e.g. asphalt, concrete, etc.). Some roads have many lanes such as a motorway. Common for all roads is that they are somehow connected to each other in a road network. Cities are normally connected by roads. The underlying object model for TUM-LOREX take principally geometrical (1, 2, 4, 5), radiometrical (7) and topological (10) properties into consideration (WIEDEMANN, 2002). WESSEL (2006) also considered the properties 6, 12, 13, and 14 in her work. The fusion presented in this work concentrates on some geometrical properties (1,4), radiometrical (7,8) and contextual properties (13, 14). Topological properties are included in the network generation but this is a separate step and is carried out after the fusion.

Image Model: The image model presented in this work shall describe objects appearing in high resolution SAR ground range data. The appearance of roads in SAR data can be explained by their physical properties and the SAR sensor properties (see Sect. 3.2.2). Normally, roads appear as long dark linear structures in SAR data. Roads show a low radiometry in SAR imagery, no matter whether the imagery is of X-band or C-band data. Due to the side-looking geometry of the SAR sensor, the appearance of roads in SAR data is highly affected by nearby objects. It is therefore more important to consider contextual relationships when working with SAR data than other image data such as optical data. As in all image data, the resolution of the SAR data affect the

Geometrical Properties:
<ol style="list-style-type: none"> 1. Roads have a long, linear shape 2. In general roads have a constant width 3. Roads have parallel edges 4. In general, roads feature a low curvature 5. Roads show a typical width (dependent on the road type) 6. Roads are normally flat with low or no inclination
Radiometrical Properties:
<ol style="list-style-type: none"> 7. Roads consist of homogeneous materials such as asphalt, concrete or gravel 8. The surface of roads can be considered to be smooth 9. Roads are stationary objects
Topological Properties:
<ol style="list-style-type: none"> 10. Roads are usually connected in a network 11. Roads end with a connection or as a dead end
Contextual Properties:
<ol style="list-style-type: none"> 12. Roads connect cities 13. Roads feature a relation to nearby objects (local context) 14. In different surroundings (global context), the appearance of roads differs

Tab. 1. Characteristics of the object model for roads - adapted from (WESSEL, 2006).

appearance of roads as well. In low resolution SAR data, roads tend to look like long lines, as in high resolution SAR data, separate lanes, crash barriers and traffic lights may be discerned. Due to the strong impact caused by nearby objects, the road appearance differ due to the surrounding area (e.g. global context).

5.1.2 Modeling of context

Local context represents all objects that have direct influence on the geometrical and radiometrical properties. Examples of local context are buildings, high vegetation such as trees, big traffic signs and traffic lights, and moving vehicles. Buildings and high vegetation cause typically shadow and layover effects. Traffic signs, traffic lights, buildings and all sorts of metallic objects causes strong reflections. These effects may occlude the road and hinder important road information. The extent of the occlusion depends on the position of the road in relation to the SAR sensor as well as the type of the local context object on the surface.

In this work we are on one hand interested in the influence of local context on the appearance of road in the image but on the other hand also in the identification of different local objects. Identification of local context alone is a good evidence in case of conflicting hypotheses. Therefore the first part is about the relation between local context objects and the road (i.e. in the image model) and the second part is about how different local context objects look like in the SAR image.

Including Shadow and and Layover in the Road Image Model

Shadow and layover effects are present as soon as high objects are present. The extent of the effect in ground range data depends on the local incidence angle θ , the height of the target (H) and the slope of the target surface. In Fig. 15, the length of a shadow S and a layover L of a tree is depicted. Assuming a horizontal reference surface and an image in ground range the length of the shadow, S :

$$S = H \cdot \tan \theta \quad (20)$$

and the length of the layover, L :

$$L = H \cdot \cot \theta. \quad (21)$$

The shadow and layover effects raised by an object vary with the location of the object in relation to the position of the SAR sensor. Roads are preferably located in range direction to get the best possible visibility. The shadow lengths projected to the normal of the road S_n can be expressed as

$$S_n = H \cdot \tan \theta \cdot \sin \beta \quad (22)$$

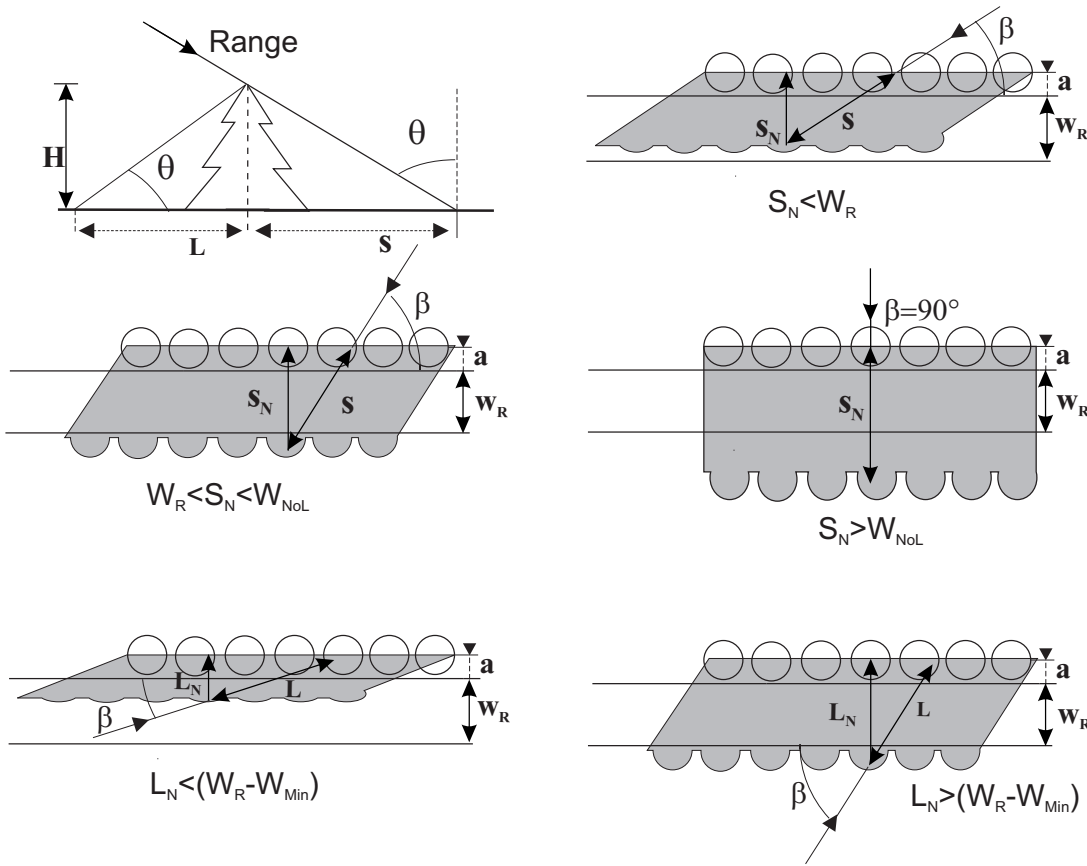


Fig. 15. The shadow and layover effects caused by a row of trees is depicted first as a side view. The shadow regions are illustrated three times and the layover two times as top view for different β angles. The length of the occlusions, S and L , stays the same, but the occlusions projected as normal to the road, S_n and L_n , increases as soon as the β angle increase. W_R is the assumed width of the road and W_{NoL} is the maximum width for the line extraction, which is a parameter that has to be set during the line extraction.

and the layover:

$$L_n = H \cdot \cot \theta \cdot \sin \beta \quad (23)$$

where β is the angle between the range direction and the direction of the road. In this work, β is called the *road visibility angle* (HEDMAN et al., 2005b). The larger β is, the higher is the probability that the road is occluded by a shadow or a layover.

Objects Located at One Side When trees or houses are located at just one side of the road, either layover or shadow might occlude parts of the road. Depending on β , the height of the object, H , and the width of the road W_R , the road can either be partly or completely covered. If the shadow cover only a little part of the road, the linear shape is kept and the road show about the same characteristics as a road without any high objects nearby in the SAR image (see Fig. 16). Hence, in favorable cases the road has kept its linear shape and is likely to be detected by a line extraction. If β increases further the road can be completely covered. If the linear shape is kept, it still might be detected but shows then the characteristics of a shadow, meaning that the backscattered intensity is almost zero. If β approaches 90° the width of the shadow region is likely to exceed the width parameter set by the line extraction and is hence not detected by the line extraction.

If a road of width 10 m is bordered by 15 m high trees on one side and is viewed by a SAR sensor with a local incidence angle of 45° , then the road is totally covered by the shadow for road visibility angles larger than 42° (see Tab. 2). For less β angles the shadow occludes only a part of the road and can be viewed for the extraction as a part of the road itself. The maximum road visibility angle for which the road is still detectable is called β_{max} .

The main problem by layover effects is the decrease of the road width. Even though parts of the road are visible, the width of the remaining road pixels is below the width limitations for road extraction (W_R). Hence, roads

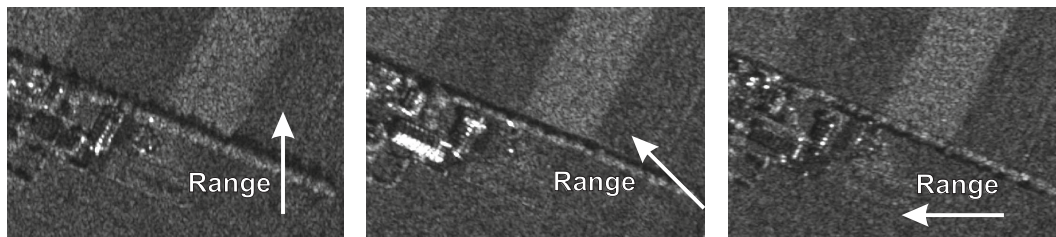


Fig. 16. Multi-aspect SAR images of a road with trees on the lower side. The effect of the shadow depends on the range direction and the incidence angle of the SAR sensor.

HIGH OBJECTS ON ONE SIDE OF THE ROAD			
<i>Shadow effects</i>	β_{Max}	<i>Layover effects</i>	β_{Max}
$W_R > S_N$	$< 42^\circ$	$(W_R - W_{Min}) > L_N$	$< 32^\circ$
HIGH OBJECTS ON BOTH SIDES OF THE ROAD			
$(W_R - W_{Min}) > (S_N + L_N)$	$< 15^\circ$		

Tab. 2. Different road visibility angles β_{Max} when high objects are present ($H = 15\text{m}$, $W_R = 10\text{m}$, $\theta = 45^\circ$, $W_{Min} = 2.7\text{m}$).

affected by forest layover are restricted to a smaller limited number of road visibility angles (see Tab. 2). Dark shadow pixels however can be “included” into the road width and the extraction is possible, even in cases of large road visibility angles.

Objects located at both sides When a road is surrounded by high objects at both sides, the situation is more difficult. Both shadow and layover regions cover the road. The road direction should not differ too much from the range direction otherwise the road is covered by layover and shadow regions (see Tab. 2). Fortunately the shadow regions caused by vegetation on both sides are often detected by the line extraction even for large β angles. However the displacement can be pretty large.

High Objects One problem with road extraction from SAR images is that long-linear shadow regions caused by a row of trees or a row of houses show the same characteristics as a road with high objects nearby. Except for $\beta < \beta_{Max}$ it is impossible to say whether a road is present or not. Fig. 17 shows a shadow caused by a row of trees illuminated with different β angles. The height of the trees (about 16 m) could be estimated by looking at the length of the shadow. Here one can see that if the object is pretty high, a line extraction is possible rather for small β angles than larger ones.

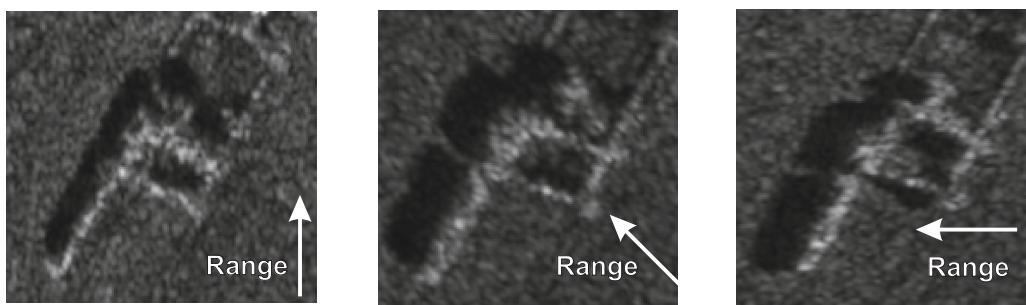


Fig. 17. Multi-aspect SAR images showing a row of trees. The width of the shadow and layover region depends on the range direction and the incidence angle of the SAR sensor.

Image Model of Local Context

Highways are often surrounded by crash barriers. These barriers are usually long, made out of metal and less than one meter high. The parallel lanes of the highway can also be separated by low vegetation such as small bushes or grass areas. Common for both crash barriers and the low vegetation is that both appear much brighter than the lanes of the highway. In the image the highway appear as dark parallel lines separated by brighter lines in the middle and/or on the outer side (see Fig. 18(a)). Crash barriers are easy to identify since they appear very bright in the image. The brightness is caused by a strong direct reflection due to the metal and by a crash barrier-lane double-bounce reflection. The reflected back-scattering is especially intensive as the sensor looks in a perpendicular direction toward the crash-barriers.

Buildings are even harder to categorize than roads. Industrial, residential and administration buildings differ greatly in terms of size, material and shape. Common for all buildings is that they give rise to shadow- and

layover regions as well as strong double-bounce reflections. The main contributors to the total backscattering in the image are: 1) direct backscattering from the roof, 2) direct backscattering from the wall, 3) direct backscattering from the ground, 4) wall-ground double-bounce scattering (STILLA and SOERGEL, 2006) (see Fig. 18(b)). The signal response from the roof can be both weak and strong depending on the roof structure. A gabled roof oriented perpendicular to range leads to a strong direct reflection which position in the image is affected by layover. A smooth and flat roof causes a specular reflection away from the sensor. The double-bounce reflections between the ground and the wall leads to a strong signal response, which occur at the position of the wall. As soon as buildings stand closer to each other the complexity arises due to mixed backscattered signals from several buildings. If the heights of the buildings vary, high buildings may totally occlude small buildings. Differentiation between layover and shadow regions becomes more and more complicated.

As the resolution of the SAR sensor improves, the amount of strong backscatterers increases and become more and more dominant in the image. These are a result of the direct specular reflection due to metallic objects as window details, balconies, roof details, etc. A detailed description of complicated building shapes in SAR images is a hard task and include both geometrical (even fine details) and electromagnetic properties of the building (GUIDA et al., 2008).

Higher *vegetation* (i.e. trees) is characterized by an overall medium backscattering intensity. The total backscattering for a radar resolution cell is a result of several backscattering components. According to the forest model described in the work of SUN and RANSON (1995), which is also presented in WESSEL (2006), there are five main components: 1) direct crown backscatter (i.e. volume scattering), 2) direct backscattering from ground, 3) direct backscattering from trunk, 4) crown-ground double-bounce scattering, and 5) trunk-ground multiple scattering (see Fig. 18(c)). The direct volume scattering from the crown and the specular reflection from the trunk are affected by layover. The double-bounce scattering range delay represent the position of the tree on ground. X-band SAR cannot penetrate the vegetation (dependent on the extent of the biomass), which give rise to clear shadow regions behind the trees. Trees are easily identified in high resolution SAR images. Sometimes even the structure of the trunk and the tree crown can be identified.

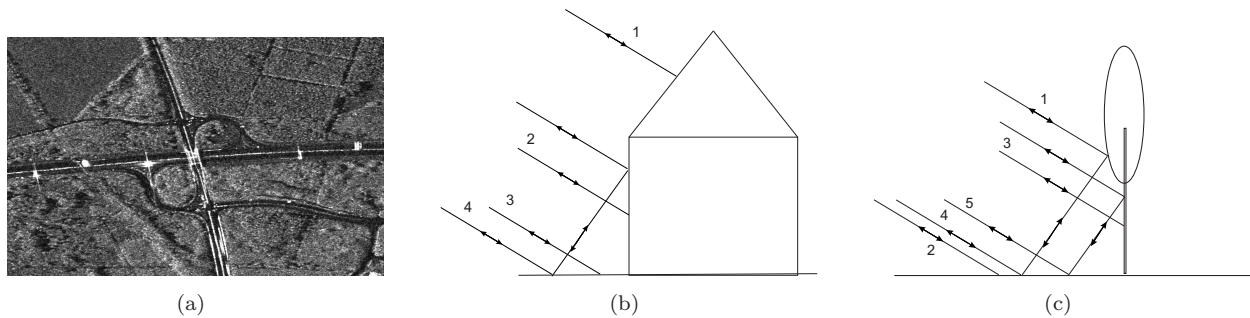


Fig. 18. (a) Highways surrounded by crash barriers. (b) Main contributors of the total backscattering from buildings. (c) Main components of the total backscattering from trees - adapted from SUN and RANSON (1995) and WESSEL (2006).

Global Context

Global context relies to larger image regions where roads show certain typical characteristics. In this work we differentiate between urban (built-up areas), forest and rural (fields) areas.

In *rural areas*, long lines, constant width and low curvatures signify the appearance of roads (see Fig. 19(a)). Some parts of the roads might be occluded by adjacent objects, like high trees. But in general, roads are always connected to each other in a network. The frequency of roads is rather low.

An *urban* scene with built-up areas is much more complex than rural scenes, which makes road extraction in cities much harder (see Fig. 19(b)). The road frequency is high, but the roads are often occluded. In cities, building structures, traffic signs and metallic objects give rise to dominant scattering. The most prominent scatters are double-bounce scattering due to reflections between the front of a house and the ground and triple-bounce scattering at trihedral corner structures at buildings. Also side-lobes, due to specular reflections from house roofs or metallic structures, appear frequently in urban scenes and might thus hinder road information. Among the mentioned high scattering phenomena “normal” shadow- and layover effects might occlude a road totally. A road network in built-up areas is characterized by shorter streets with many intersections. Modern North American cities often has a regular network with parallel streets and perpendicular intersections as in Europe where old cities generally contain a much more complex network, often with a curved and irregular network.

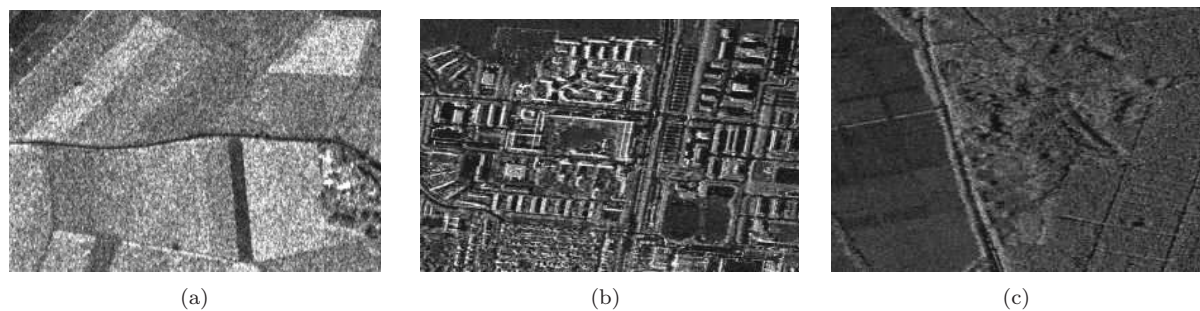


Fig. 19. (a) Roads in rural areas are often undisturbed from nearby object. (b) Roads in urban areas are usually shorter. The frequency of roads in these areas is in general high. (c) Roads in forest areas are usually occluded by shadow from the high trees.

Roads in *forestry areas* are often occluded by shadow regions of the nearby trees (see Fig. 19(c)). The shadow regions are characterized by an irregular shape. In general it is very hard to distinguish if a road is truly present or if the shadow is caused by a clear cut area. The frequency of roads per unit area is very low.

5.2 Feature extraction

The aim of this section is to present and analyze the feature extraction. The main feature involved in the road extraction process are the extracted line primitives. Hence it is important to fully understand and to analyze the behavior of the extraction in order to design the fusion correctly.

5.2.1 Extraction and analysis of dark and bright linear features

Our approach is based on Steger's differential geometry approach (STEGER, 1998a), which belongs to the more sophisticated ones. Contrary to the line detectors mentioned in Sect. 2.1.1 it was originally developed for optical images. The applicability for extracting roads from SAR data was shown in previous research (WESSEL, 2006).

Steger's line detector is able to extract both dark and bright linear features. A bar-shaped profile of roads is assumed, which is allowed to be asymmetrical (e.g. different contrasts on each side of the line). The extraction is done by using a partial derivatives of a Gaussian smoothing kern. First, the user defines some parameters such as: 1) a preferred width of the lines, which determines the Gaussian smoothening, 2) two threshold values, one *higher* and one *lower*, which is related to the minimum absolute response of the second derivative. These parameters control the process of linking individual line pixels into pixel chains. Pixels with a second derivative larger than *the higher threshold* are immediately accepted while pixels with a second derivative smaller than the *lower threshold* are rejected. All other line points are accepted if they connect together to one path. In addition the bias of the line position induced by asymmetrical contrast on both sides is corrected. As output local line attributes like width, direction, and contrast are obtained. The result of the line extraction is a set of pixel chains with subpixel precision (e.g. linear primitives).

In general open roads are well detectable since they appear as clear lines with a good contrast to the surroundings (see Fig. 20). Roads with buildings or high trees nearby are not as easy to detect as open roads, but the probability of detecting the road at its correct position improves as the direction of the road approaches the SAR range direction (as discussed thoroughly in Sect. 5.1). The line extractor is also able to extract the lanes of the highway (see Fig. 21).

Unfortunately there are many gaps in the line extraction. Usually the gaps occur where the road is not visible due to any of the local context objects listed in Sect. 5.1.2. A big problem is of course the layover and shadow effects caused by trees or nearby building. But the line extractor might fail even though the road is visible in the SAR image. Depending on the parameter settings very wide or very narrow roads are sometimes not extracted (see Fig. 22). A solution in that case would be to combine two or more line extractions with different parameter settings. A second problem is low contrast between the road and the surrounding area. If the surrounding has similar surface scattering properties as a road, the contrast might be too low for the line extractor to work. As soon as there are unconventional crossings such as highway crossings or crossings including bridges the line extractor has problem to detect all lanes (see Fig. 22).

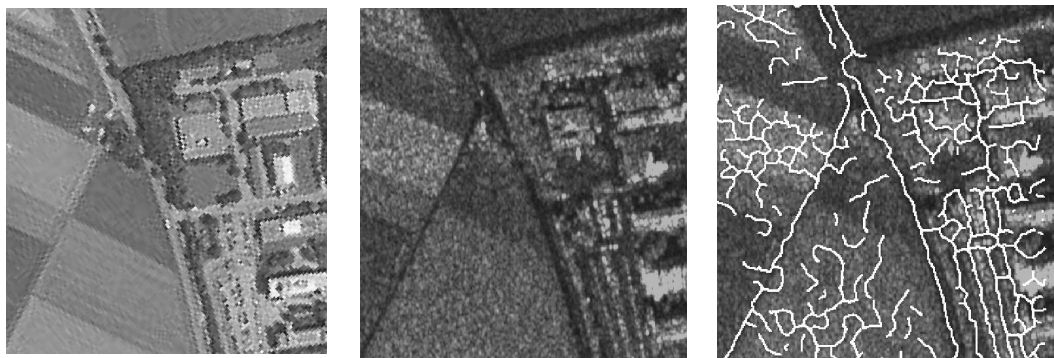


Fig. 20. Dark line extraction from a SAR image. The line extractor successfully extracted the diagonal open road to the left. Also the vertical road is nicely detected since the road is situated in range direction (Optical data - copyright: Stadtplandienst).

Over-segmentation occurs especially frequently in forestry (see Fig. 21) and in urban areas. The line extraction detects not only roads, but also linear shadow regions (shadows) and relatively bright line extractions mainly occurring in forest areas (false alarms), caused by volume scattering. Also in fields these false alarms due to structure are sometimes extracted. Paved areas such as parking places or very small roads which are not included in the reference are also often detected by the line extraction.

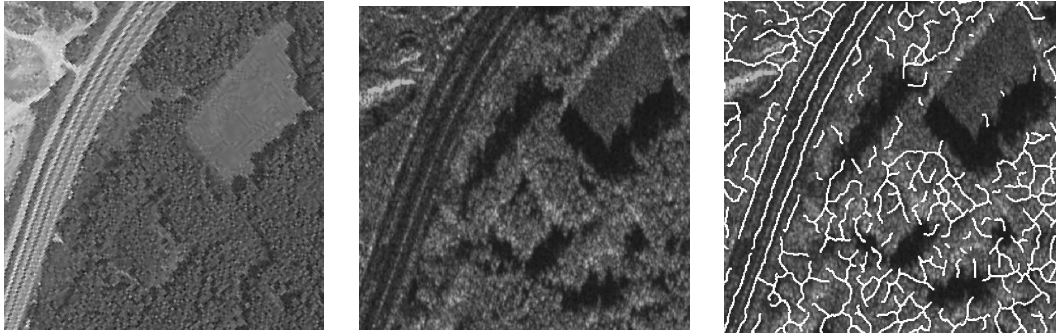


Fig. 21. The line extraction manages well to detect the lanes of the highway. There is a clear over-segmentation in forestry areas (Optical data - copyright: Stadtplandienst).

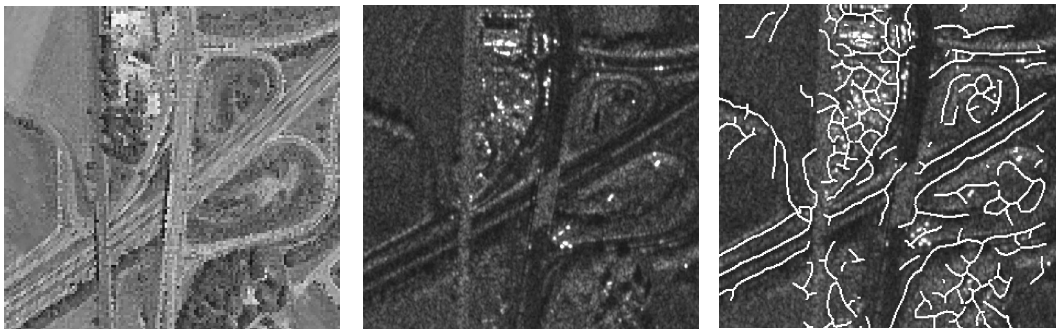


Fig. 22. The line extractor has problem with complicated crossings such as this highway crossing. Also the wide road was not extracted (Optical data - copyright: Stadtplandienst).

Since shadows are included as one class in the Bayesian fusion we need to analyze when the line extractor manages to detect shadow regions and when not. In general the line extractor is very successful as soon as the linear shadow region is not too irregular or when the width is not too wide (Fig. 24).

The bright line extraction succeeds to detect rows of trees and most highway borders (see Fig. 23). Interesting is that the bright scattering which is present on the side of the vegetation which faces the sensor (partly caused by layover) is always detected (see Fig. 24). Here the detection is not dependent on the width as in the case of the shadows. Please note that the line extractor detects either this bright scattering facing to the sensor or row of trees, but not vegetation itself. As soon as no layover effect is present edges of forestry regions are not extracted. Due to the structure of forestry regions over-segmentation appear frequently. The extraction of buildings is far more complicated. Instead of detecting layover regions, dominant scattering is usually detected. The dominant scattering has seldom a linear shape. The shape is rather irregular and sometimes the appearance looks more like dots. The line extractor is therefore not the optimum for detecting buildings. Still small scattering is detected and this is a good indicator of that any kind of man-made objects are present. These man-made objects can be big traffic signs, vehicles, and metallic objects. Also balconies or roof structures give rise to dominant scattering. The sensor geometry plays often here an important role, which is unfortunately very hard to model. The problem with gaps and over-segmentation is also present but is not as widespread as for the dark feature extraction.

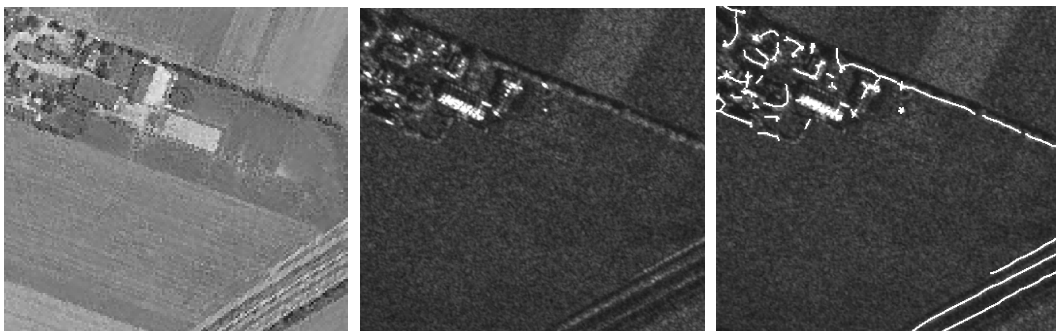


Fig. 23. The bright line extractor is able to detect row of trees and the grass between the highway lanes very well. Buildings are more complicated to detect but also here the line extractor detects at least some scattering of each building. One can also see that the frequency of false alarms is less than for dark features (Optical data - copyright: Stadtplandienst).

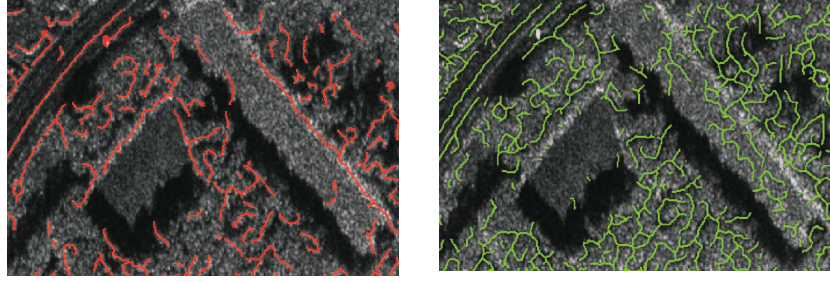


Fig. 24. Bright line extraction in red and dark line extraction in green from a small subimage of Fig. 25. The small cut shows that the detection of shadow regions are highly dependent on the width of the shadow region. However the detection of the bright reflection of the vegetation toward the sensor works still very good.

The performance of the line extractor for different classes was tested on a small subimage (see Fig. 25). The results of a line extraction were compared to reference data. The quality measure *completeness* were applied (see Eq. 1). The completeness tells us how much of the reference data was detected by the line extractor. It is defined as the percentage of the reference data which lies within a buffer around the extracted line primitives.

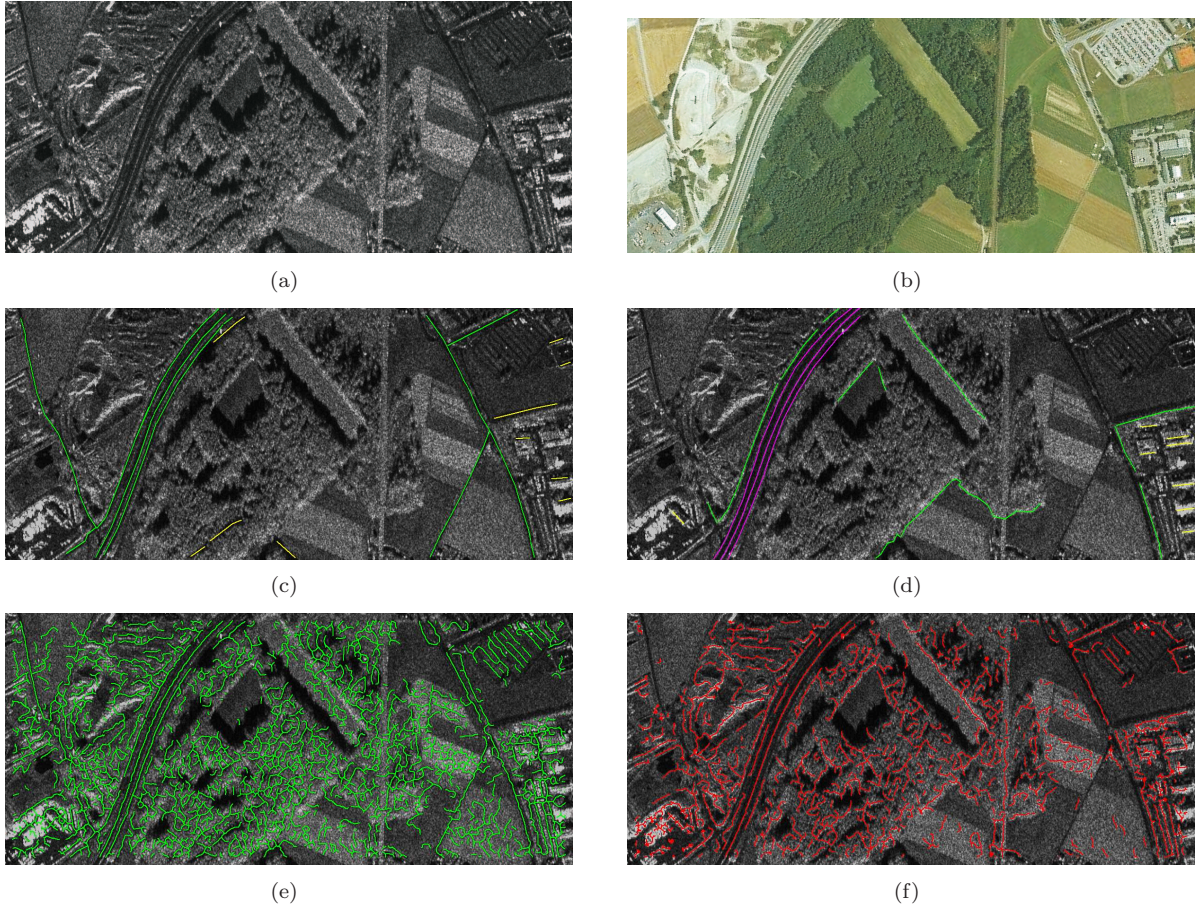


Fig. 25. (a) E-SAR data. (b) Optical image (copyright: Stadtplandienst). (c) Reference for dark line extraction (Green=roads, Yellow=shadows). (d) Reference for bright line extraction (magenta=highway (crash barriers or lower vegetation), yellow=buildings, green=vegetation). (e) Dark linear primitive extraction. (f) Bright linear primitive extraction.

Other quality measures such as *correctness* and geometric accuracy (*RMS*) are not applied at this stage.

The conclusion that can be made from Tab. 3 is that the line extractor works very well.

Dark features	Completeness	Bright features	Completeness
ROAD	87 %	HIGHWAYS	80%
SHADOW	73 %	MAN-MADE OBJECTS	92 %
		VEGETATION	94 %

Tab. 3. Completeness of the line extractor for detecting different classes.

5.2.2 Classification of global areas

Global context regions can be derived from maps or GIS before road extraction, or can be segmented automatically by a texture analysis. Previous work of TUM-LOREX contained a segmentation of dark areas for reducing the search area. Then dark regions were obtained by a threshold of dark pixels followed by a morphological dilation (WESSEL, 2006). This step shall be replaced by a global classification step. Several texture-based approaches for automatic extraction of land cover classes from SAR data have been proposed:

DEKKER (2003) presented a study on texture analysis and classification of ERS SAR Images for map updating. He investigated not only different texture measures, such as various histogram measures (mean, standard deviation, variance, skew, kurtosis, entropy, and energy), but also wavelet energy measures, fractal-based dimensions, lacunarity and semivariograms, for five classes (urban, industry/greenhouses, forest, water, and other). In order to find the best characteristic measures, the nonparametric distance was used. The conclusions made from this work was that the best texture measures were mean intensity, variance, weighted-rank fill ratio (mainly high average separability for water-bodies) and semivariograms.

TISON et al. (2004) proposed a classification method for urban areas based on Markovian classification with good results for urban areas. It was proved that the underlying statistical model can be assumed to follow a Fisher distribution. One of the advantages of the Fisher distribution is that different kind of tails are allowed. Six classes are differentiated; ground, dark vegetation, bright vegetation, dark roof, mean roof and bright roof.

Our aim is not to achieve such detailed classification results as the ones presented in (DEKKER, 2003) and (TISON et al., 2004). Instead regions should be extracted on a large-scale. We use a similar approach as the one presented by (DELL'ACQUA et al., 2009). The group in Pavia has developed an approach for discrimination between urban, vegetated areas and water bodies by applying texture analysis followed by morphology. The textural measures used are histogram measures and linear features (frequency and direction). Our approach originates from a classification applied to optical data (HINZ, 2004). Global context regions are segmented automatically by a texture analysis followed by a morphological filter. The textural measures used are histogram measures and linear features (frequency and direction). Also in this work we concentrate on three regions; *built-up areas*, *field* and *forest*. The following measures are applied:

Statistical measures The mean μ , standard deviation σ , and data range were investigated. Data range is defined as the range of data (i.e. difference between the maximum and the minimum intensity) within one small window around a pixel (DELL'ACQUA et al., 2009). In order to obtain a large-scale classification, the image is strongly resampled to a lower resolution. In this work the resolution was reduced to almost 10%. After estimating the standard deviation and the data range were estimated a median filter was applied in order to smooth the result further.

Linear features An extraction of dark and bright curvilinear structures was done by a HALCON operator *lines facet*. The extraction applies a facet model (i.e. a least squares fit) (BUSCH, 1994). Parameter can be adjusted for the degree of smoothing of the image, as well as higher and lower thresholds for the second directional derivative perpendicular to the line direction. Only lines with a higher second derivative as these two thresholds are accepted. An advantage of this line extractor is that for each line point two attributes, the *direction* and the *magnitude of the second derivative* are estimated. Based on these two attributes the *local line frequency* and the *homogeneity of local line orientation* were estimated.

After the classification a morphological filter is applied for eliminating noise and smoothing the contours of the regions. For this aim a filter consisting of an opening followed by a closing is suitable (GONZALEZ and WOODS, 2001).

The textural measures of each training area were plotted in scatterplots in order to make sure that the correlation and overlap is not too large (see Fig. 26). Based on these scatterplots and the results presented in Fig. 27 one can draw the following conclusions about the different global context areas:

- ◊ *Built-up areas* are characterized by its bright scattering and shadow regions, hence showing both high mean intensity and large data range. Also there is a high line frequency. Unlike the case with optical data (HINZ and BAUMGARTNER, 2003) the local line direction is very irregular.
- ◊ *Fields* are easy to identify due to their homogeneity. Both data range, standard deviation and the number of lines are relatively low.
- ◊ *Forest areas* show an irregularity similar to built-up areas but has a lower data range and standard deviation. The frequency of extracted linear features as well as their directions are very irregular.

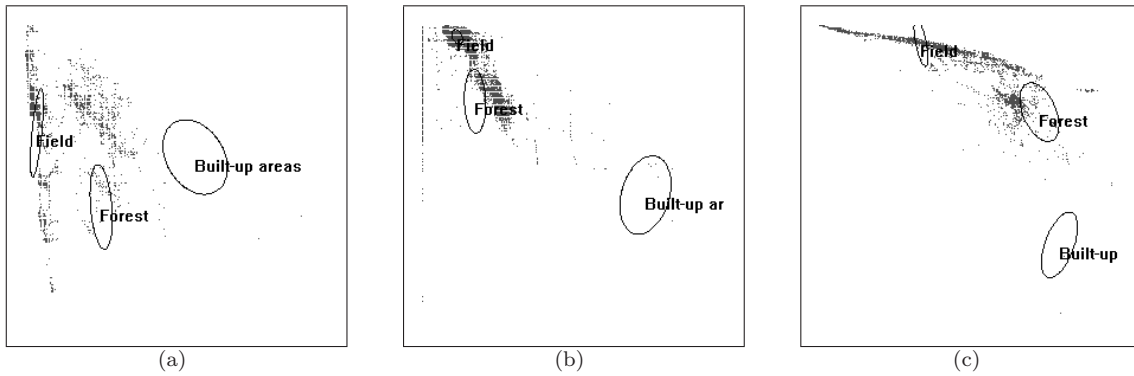


Fig. 26. Scatterplots showing the correlation between the different statistical and textural measures: (a) Mean and standard deviation, (b) Standard deviation and data range, (c) Line frequency and line direction.

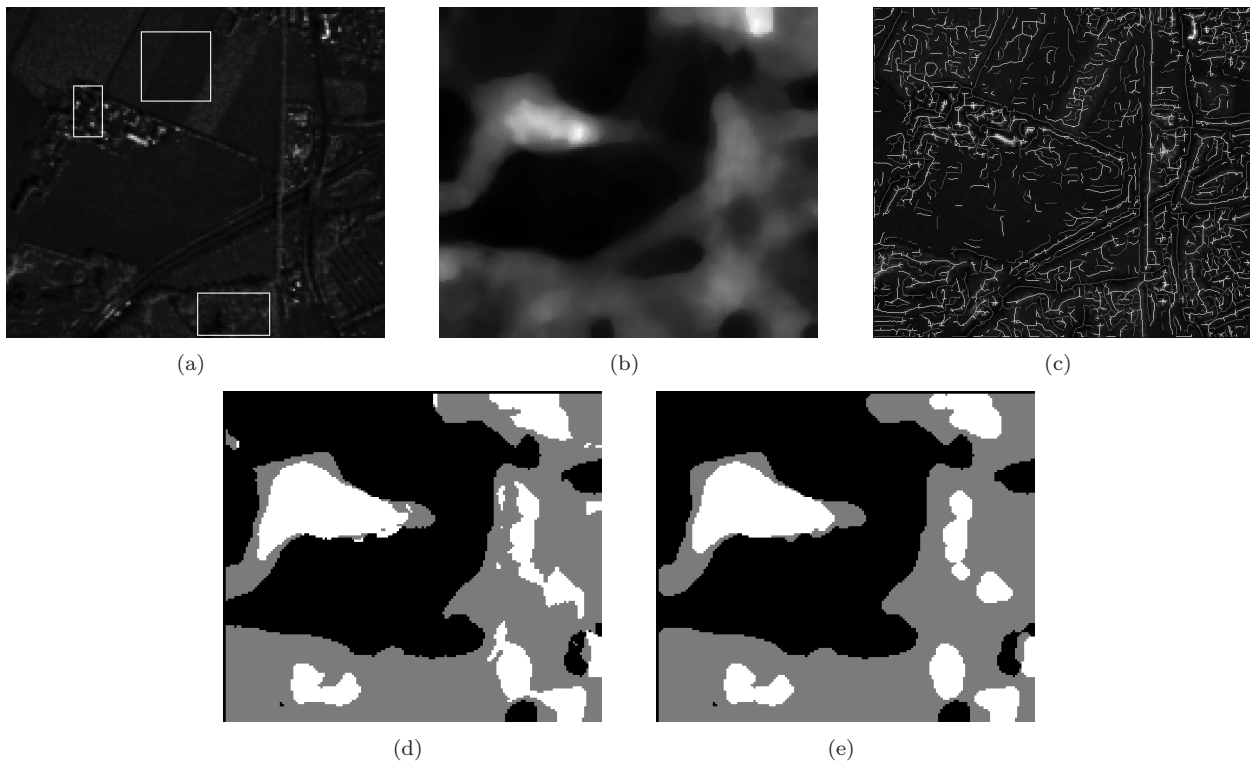


Fig. 27. The classification tested on a small SAR scene. (a) Training regions are defined in the resampled image. (b) Standard deviation σ is calculated followed by a median filter. (c) Extraction of bright and dark linear feature for estimating the line frequency and the homogeneity of line direction. (d) Results after classification (white=built-up areas, black=fields, gray=forest). (e) The classification results are smoothed by a morphology filter.

The accurate delineation of texture boundaries is in general a hard problem since the texture boundaries are typically calculated and estimated within a local neighborhood (i.e. sliding window). Thus whenever two or more textures fall within the window to be analyzed, the same problem as for classifying “mixed pixels” occur. That together with the hard smoothing should be one of the reasons why urban regions are often surrounded with some pixels assigned to forest. But one should also keep in mind that there are often trees in the outer regions of built-up areas. Even though there is a clear over-classification of forest areas, the classification manages to correctly classify most regions.

5.3 Setting up a Bayesian network for fusion of multi-aspect SAR data for automatic road extraction

Finding the optimal structure of the Bayesian network is the crucial and most important step in the process of designing a Bayesian network fusion. A correct structure makes the estimation of the conditional probabilities more straightforward. However finding the needed variables and the causal relationship among them can be rather difficult depending on the complexity of the task. In general one would have to start with a simple structure and gradually increase the complexity, which is also expressed in this quotation:

... we start with the simplest possible structure (i.e. the one with the minimum number of links) and try to find parameters that fit the data; if this attempt fails, we try more complex structures, and so on...

(PEARL, 1988)

In the following section we define different Bayesian networks, starting with the most simplest one and ending with a rather complex structure. We will also define the joint probabilities and will discuss how the information will flow between the nodes.

The main feature involved in the road extraction process is the line primitive. The dark line extraction detects not only roads, but also linear shadow regions and false alarms. Bright features extracts highway crash barriers, bright scattering from man-made objects and rows of vegetation. In this section we will present different Bayesian networks for combining the extracted features from multi-aspect data. For the sake of simplicity we will start with a Bayesian network for dark features only (also presented in STILLA and HEDMAN (2010)).

A ROAD, a SHADOW and a FALSE ALARM may be differentiated by means of their characteristic attributes (intensity, length, etc.). For this task two nodes are defined; L , which is our extracted line primitive and X , the attributes of the line primitives. L has an influence on X . The variable L is assumed to have the following states:

- ◇ $l_1 = \text{an extracted line primitive belongs to a ROAD}$
- ◇ $l_2 = \text{an extracted line primitive belongs to a FALSE ALARM}$
- ◇ $l_3 = \text{an extracted line primitive belong to a SHADOW}$

Depending on which state L has, the line primitive has certain attribute values (X). Therefore L is the parental node, while X is the child node in this at the beginning simple Bayesian network (see Fig. 28a). The joint probability can be expressed as:

$$P(L, X) = P(X|L)P(L) \quad (24)$$

If relevant, the hypotheses above can be extended with more states l_4, \dots, l_n (e.g. river, etc.). The flow of evidence may come from the top (state of L is known) or from the bottom (state of X is known). On one hand, if a shadow is present, one expects that the linear primitive has low intensity. On the other hand, if a linear primitive has got the same low intensity, one can assume that a shadow region has been extracted.

Exploiting sensor geometry information relates to the observation that road primitives in range direction are less affected by shadows or layover of neighboring elevated objects. A road beside a row of trees, for instance, can be extracted at its true position when oriented in range direction. However, when oriented in azimuth direction, usually only the parallel layover and shadow areas of the trees are imaged but not the road itself. As described in Sect. 5.1.2 the angle between the direction of the road and the aspect angle of the sensor, β has a high impact on the characteristics of the extracted line primitive. Hence a third variable may be incorporated into the Bayesian network, the sensor geometry, G , which considers the look and incidence angle of the sensor in relation to the direction of the detected linear feature. Since an extracted linear shadow can be an indication of that a road exist or not depending on the different sensor geometries it is no longer enough with what was detected in the image (node L). We must also consider what kind of object exists in the real world. Hence a fourth variable Y with the following four states is included:

- ◇ $y_1 = \text{A road exists in the scene}$
- ◇ $y_2 = \text{A road with high objects, such as houses, trees or crash barriers, nearby}$
- ◇ $y_3 = \text{High objects, such as houses, trees or crash barriers}$
- ◇ $y_4 = \text{Clutter}$

If relevant, the variable Y can easily be extended with further states y_5, \dots, y_n , which makes it possible to describe road with buildings and road with trees as separate states. Y and G cause both together L , which in

turn influence X . Our Bayesian network is now extended with two further variables (see Fig. 28b). Eq. 24 can now be expressed as:

$$P(Y, G, L, X) = P(X|L) P(L|G, Y) P(Y) P(G) \quad (25)$$

Finding independencies and dependencies is a crucial point for belief updating in a Bayesian network. This network comprises a converging connection (see Sect. 4.2) with two parental nodes, Y and G , and a child node L . As the sensor geometry is known and as soon as the attributes of the line primitive are extracted, evidence will enter via G and X . X is a child node of Y . By the incoming evidence e^- the communication link between Y and G is opened. Y and G are d-connected, meaning that evidence e^+ has now an impact on the $BEL(Y)$.

This work deals with fusion of several SAR images. That means that we shall combine line primitives extracted from two or more images. In that case one has to deal with the case that a road might be detected in one scene, but maybe not in the second scene. Hence, we need to add a fourth state to our variable L ;

- ◇ $l_4 =$ a line primitive has **not** been extracted in that scene

By introducing this state, we also consider the case that the road might not be detected by the line extraction in all processed SAR scenes. In fact, the sensor geometry G has a high impact on the chance of the road at being detected at all (see Fig. 15). For each SAR scene a sensor geometry node, a line extraction node and attribute node need to be defined. The nodes belonging to different SAR scenes are separated by superscript indices (i.e. G^1, G^2, \dots). A Bayesian network for two SAR scenes becomes a *polytree* structure with the joint probability:

$$P(Y, G^1, G^2, L^1, L^2, X^1, X^2) = P(X^2|L^2) P(X^1|L^1) P(L^2|G^2, Y) P(L^1|G^1, Y) P(Y) \quad (26)$$

Please note that the two prior probabilities for $P(G^1)$ and $P(G^2)$ are not included in Eq. 26. The reason for this is that the information contained in these nodes is of course well known with a better accuracy far beyond the one required in this work. Both local incidence and aspect angles of the SAR sensor are delivered as metadata together with the SAR image data. Hence these two nodes are considered as "hard" evidence.

Next Bayesian network contains local context information in terms of bright linear primitives. Parallel dark and bright linear primitives are fused. The Bayesian network is now extended with two new nodes; B_{left} and B_{right} represent now the fact that not only the single dark linear primitive is extracted but also parallel bright features. Here we distinguish between bright features found on the left or on the right side. Therefore the variable L changes now name to D .

The variable representing the dark linear feature, D , has the same states as before:

- ◇ $d_1 =$ an extracted line primitive belongs to a ROAD.
- ◇ $d_2 =$ an extracted line primitive belongs to a FALSE ALARM.
- ◇ $d_3 =$ an extracted line primitive belongs to a SHADOW.
- ◇ $d_4 =$ missing dark line extraction.

The variable representing the bright linear feature, B_{left} and B_{right} becomes the following four states:

- ◇ $b_1 =$ an extracted bright line primitive belongs to bright scattering from HIGHWAYS.
- ◇ $b_2 =$ an extracted line primitive belongs to bright scattering from high VEGETATION.
- ◇ $b_3 =$ an extracted line primitive belongs to bright scattering from BUILDINGS.
- ◇ $d_4 =$ missing bright line extraction.

The bright linear primitives as an additional input to the Bayesian network bring new information and allow us to define new states of the variable Y . We are now able to get layover information. Hence we are able to define on what side of the road the high local context object is situated. Further the extracted bright scattering can inform us about what kind of local context is available. The variable Y is therefore extended with some additional states:

- ◇ $y_1 =$ An open road exist in the scene.
- ◇ $y_2 =$ A highway with parallel lanes separated by crash barriers or low vegetation exist in the scene.
- ◇ $y_3 =$ A road and higher vegetation exist in the scene. The higher vegetation is on the left side of the road.
- ◇ $y_4 =$ A road and higher vegetation exist in the scene. The higher vegetation is on the right side of the road.
- ◇ $y_5 =$ A road with higher vegetation on both sides of the road exist in the scene.
- ◇ $y_6 =$ Higher vegetation only - the vegetation is on the left side of a detected dark feature.
- ◇ $y_7 =$ Higher vegetation only - the vegetation is on the right side of a detected dark feature.
- ◇ $y_8 =$ A building exist in the scene. The building is on the left side of a detected dark feature.

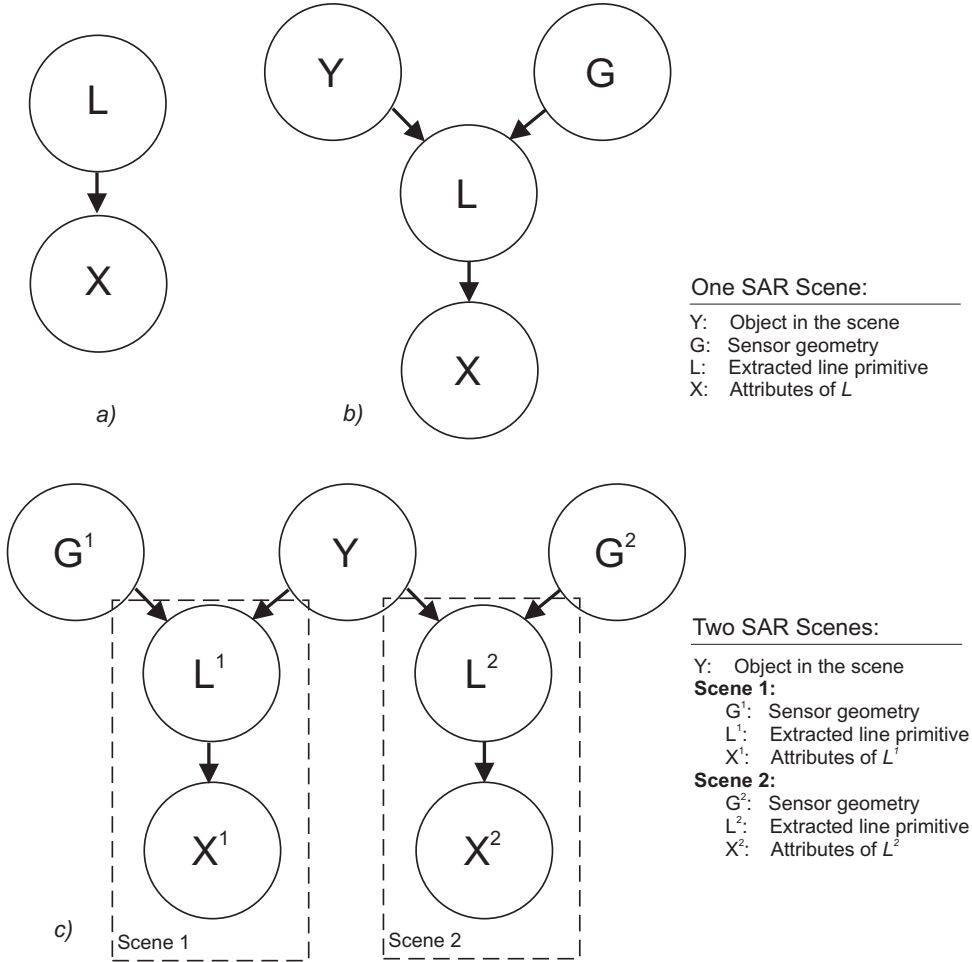


Fig. 28. Three different Bayesian networks: (a) Bayesian network including two nodes, the line primitive L and its attributes X , (b) Bayesian network including also sensor geometry (G) and the true object Y , (c) Bayesian network for a line extraction from two different scenes with different sensor geometries (G^1 and G^2).

- ◇ y_9 = A building exist in the scene. The building is on the dark side of a detected dark feature.
- ◇ y_{10} = Clutter.

The resulting Bayesian networks for one image (BN_4) and for two images variables (BN_5) can be seen in Fig. 29. All the three variables, D , B_{left} and B_{right} , are independent of each other, but are both dependent on their two parents, Y and G .

The joint probability for BN_4 :

$$P(Y, G, D, B_{left}, B_{right}, X_D, X_{Bl}, X_{Br}) = P(\bullet|Y) \cdot P(Y)$$

$$\text{where } P(\bullet|Y) = P(X_D|Y, G, D) \cdot P(X_{Bl}|Y, G, B_{left}) \cdot P(X_{Br}|Y, G, B_{right}) \cdot$$

$$\cdot P(D|Y, G) \cdot P(B_{left}|Y, G) \cdot P(B_{right}|Y, G)$$
(27)

The joint probability for BN_5 is the product of the contribution from image 1 and image 2:

$$P(Y, G^1, G^2, D^1, D^2, B_{left}^1, B_{left}^2, B_{right}^1, B_{right}^2, X_D^1, X_D^2, X_{Bl}^1, X_{Bl}^2, X_{Br}^1, X_{Br}^2) = P^1(\bullet|Y) \cdot P^2(\bullet|Y)$$
(28)

with $P^1(\bullet|Y)$ and $P^2(\bullet|Y)$ being expounded as in Eq. 27.

Belief Update

The next step is to describe how information can flow upwards and downwards in these systems. Let us start with the Bayesian networks which includes only the dark features (see Fig. 28 and Eq. 25). Evidence shall propagate from nodes which have observable states to nodes with unknown states. Observable nodes are the attributes of the line primitive (X), the sensor geometry (G) and to some extent L (i.e. when no line primitive is detected). Hard evidence will enter by X , G and L (only by missing line detection). Since child nodes of Y and G obtain evidence, the two nodes are dependent and can be regarded as d -connected (see Sect. 4 for

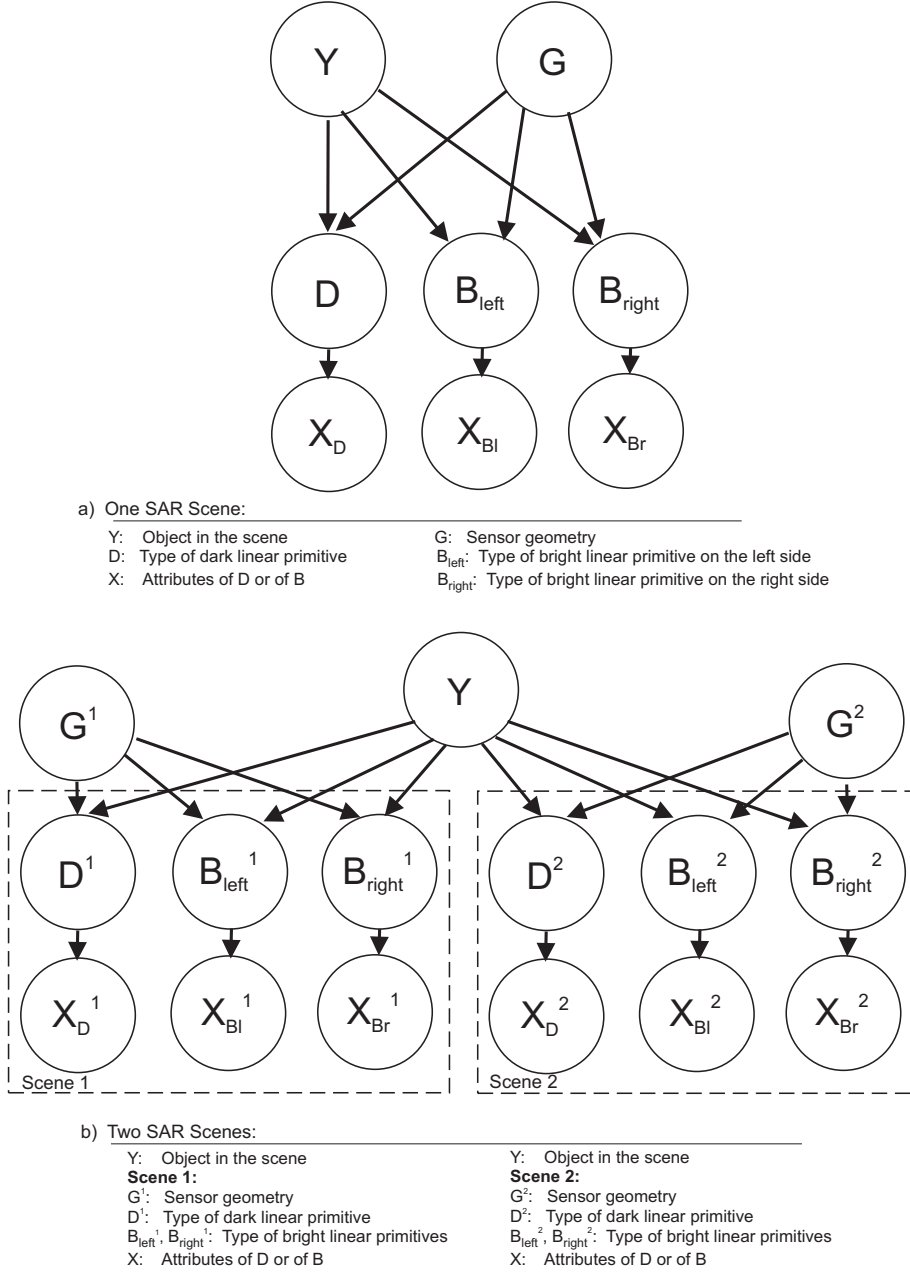


Fig. 29. Two different Bayesian networks: (a) Bayesian network including both dark and bright line extraction as well as the sensor geometry, (b) Bayesian network for a line extraction from two different scenes with different sensor geometries (G^1 and G^2).

a definition). Both predictive and diagnostic information flow in the system. The node Y is the hypothesis variable of interest. Hence the state of Y shall be the outcome of the fusion module.

Based on Eq. 16 the belief in node Y can be expressed as

$$BEL(y) = \alpha \lambda(y) \pi(y) \quad (29)$$

where

$$\lambda(y) = \pi(g) M_{L|G,Y} \lambda(l) \quad (30)$$

The node L has got two parents. The sensor geometry has no influence on what kind of object that exist in the scene, but the combination of the sensor geometry and what kind of object truly exists in the scene has a high impact on what can be seen in the SAR image. Hence these two parental nodes have a strong common impact on L . Therefore $M_{L|G,Y}$ must be defined for all combination of states of G and Y .

Luckily we can treat the information coming from two images as independent. The propagation of belief based on two images is illustrated in Fig. 30. If a second image is available the belief in node Y is simply the product

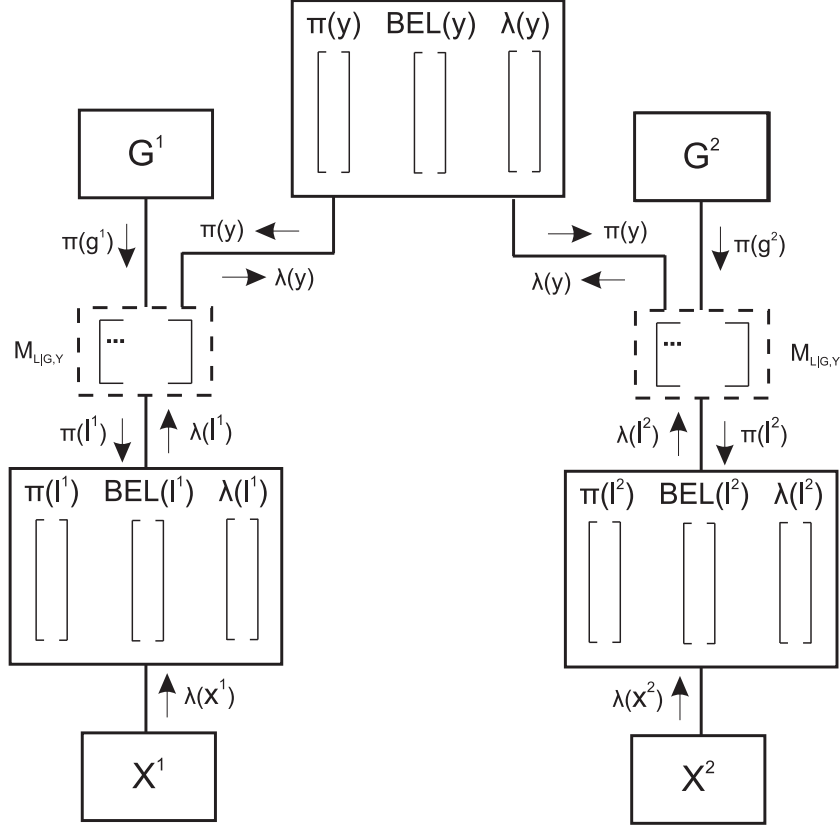


Fig. 30. Belief update for the Bayesian network in Fig. 28. Evidence enters by the nodes G^1 , L^1 , X^1 , G^2 , L^2 , and X^2 .

of the evidence coming from the two images:

$$BEL(y) = \alpha \pi(g^1) M_{L|G,Y} \lambda(l^1) \pi(g^2) M_{L|G,Y} \lambda(l^2) \pi(y) \quad (31)$$

If we incorporate also the bright features the belief update gets more complicated (see Fig. 31). The three nodes D , B_{left} and B_{right} are treated as independent of each other, since the line extractions are independent on each other. Again the two parental nodes have a strong common causation on the three child nodes. The resulting belief in Y can be written as

$$BEL(y) = \alpha (\pi(g) M_{D|G,Y} \lambda(d)) (\pi(g) M_{B_{left}|G,Y} \lambda(b_{left})) (\pi(g) M_{B_{right}|G,Y} \lambda(b_{right})) \pi(y) \quad (32)$$

and for two images the belief in Y is:

$$BEL(Y) = \alpha (\pi(g^1) M_{D|G,Y} \lambda(d^1)) (\pi(g^1) M_{B_{left}|G,Y} \lambda(b_{left}^1)) (\pi(g^1) M_{B_{right}|G,Y} \lambda(b_{right}^1)) \cdot (\pi(g^2) M_{D|G,Y} \lambda(d^2)) (\pi(g^2) M_{B_{left}|G,Y} \lambda(b_{left}^2)) (\pi(g^2) M_{B_{right}|G,Y} \lambda(b_{right}^2)) \cdot \pi(y) \quad (33)$$

We have the problem that the three nodes D , B_{left} and B_{right} have two parents. These two parental nodes have a strong common impact on the three child nodes, meaning that the definition of the conditional probability tables, $M_{D|G,Y}$, $M_{B_{left}|G,Y}$ and $M_{B_{right}|G,Y}$ becomes rather complicated. This is solved by introducing hidden nodes. Since the main purpose of the hidden nodes is to simplify the definition of the conditional probability tables the procedure is explained in Sect. 5.5.2. In reality the structure of the Bayesian network is not influenced.

Now we have designed the structures of the networks and have estimated how information propagates in these networks. What is left is to do the learning and to estimate the conditional probabilities between the nodes. That we will do in the following sections, namely:

- ◇ Estimation of $\lambda(l)$ ($\lambda(l) = \lambda(d)$), $\lambda(b)$ ($\lambda(b_{left}) = \lambda(b_{right})$) which quantifies the link between the detected line primitive (l, D, B_{left} , and B_{right}) and their attributes, X (see Sect. 5.4).
- ◇ The definition of the conditional probability tables $M_{L|G,Y}$, $M_{D|G,Y}$, $M_{B_{left}|G,Y}$ and $M_{B_{right}|G,Y}$ (see Sect. 5.5).
- ◇ Approximation of the prior term $\pi(y)$ where global context information plays an important role (see Sect. 5.6).

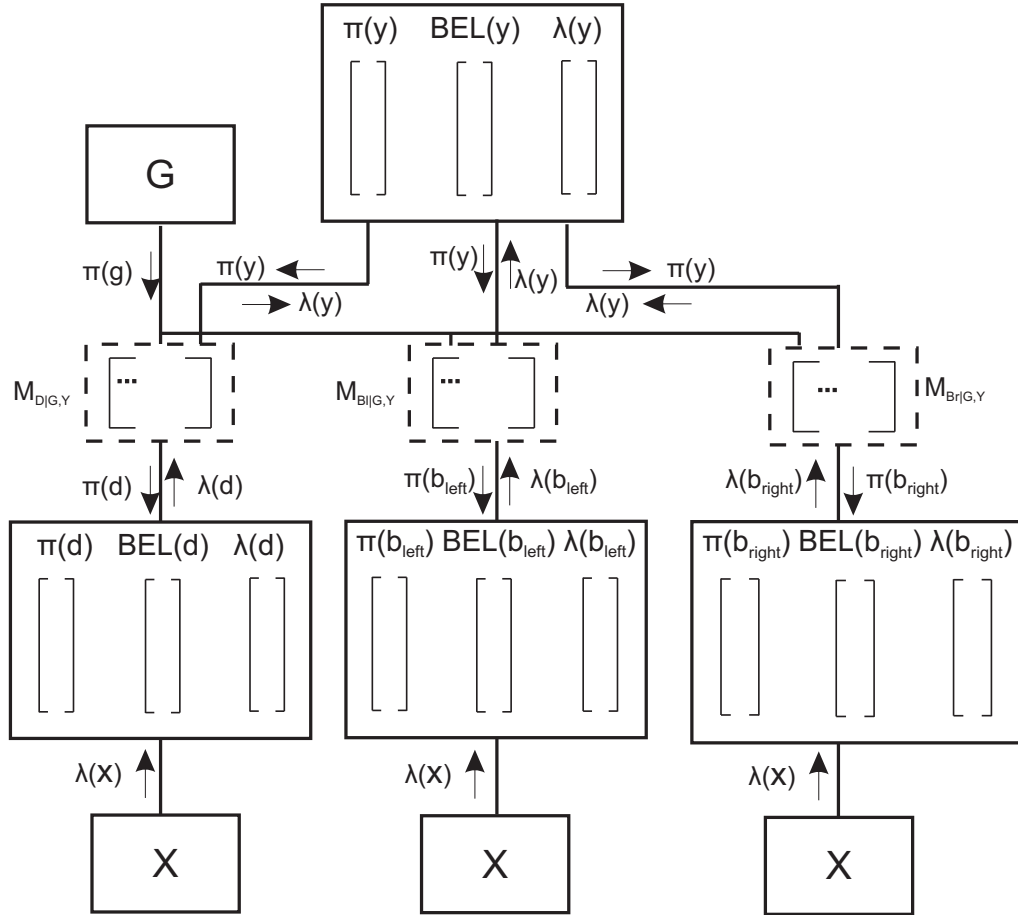


Fig. 31. Belief update for the Bayesian network in Fig. 29. Evidence enters by the nodes G , D , B_{left} , B_{right} and all the X .

5.4 Estimating continuous conditional probability density functions

The selection of attributes of the dark line primitives is based on the knowledge about roads. Radiometric attributes such as contrast, mean and constant intensity as well as geometrical attributes like length and straightness are all good examples (see Sect. 5.1). It should be pointed out that more attributes does not necessarily yield better results, instead rather the opposite occurs. In that case more uncertainty is introduced through new attributes. In addition the risk of correlation among the attributes increases. A selection including a few, but significant attributes is recommended. Several attributes such as length, intensity, width, contrast, constant intensity and constant width, etc. were tested. In this work, we have decided to concentrate on three attributes, *length* of the line primitive, *straightness* and *intensity*. Based on the analysis of the training data these three attributes turned out to be neither correlated nor had little overlap compared to other attributes. The others were excluded due to either their high overlap or due to a high correlation with the selected ones. In order to be consistent the selected three attributes were later on examined also for the bright linear primitives. The linear primitives consist each of a pixelchain (coordinate) with subpixel accuracy. For each coordinate, the direction, the width, and the intensity are estimated already during the line extraction process. The length is defined as the length of the complete pixelchain corrected with the pixel resolution. The straightness is estimated as the standard deviation of the direction calculated for all coordinates. The intensity is the median of the intensity for all coordinates.

Learning from training data means that the extracted line segments are sorted manually into three groups; roads, shadows, and false alarms. Optical data and maps were used as reference. Attributes of the line primitives are dependent not only on a range of factors such as characteristics of the SAR scene (rural, urban, etc.), but also on the parameter settings by the line extraction. The aim is to achieve probability density functions which represent a degree of belief of a human interpreter rather than a frequency of the behavior of the training data. For this reason, different training data sets have been used and for each set the line primitives have been selected carefully.

5.4.1 Independency criteria

Information reaches node L from node X via $\lambda(l)$. Since L in this work has 4 states $\lambda(l)$ is a vector with the length 4, where each element is estimated by means of predefined conditional probability functions. These functions quantify the link between L and X and represent the probability that the variable L belongs to the state l_i under the condition that its attributes \mathbf{x} (an attribute vector) are known. For instance, $\lambda(l)$ is estimated for each extracted dark line primitive by

$$\lambda(l) = [P(l_1|x), P(l_2|x), P(l_3|x), P(l_4|x)] \quad (34)$$

where each separate posterior probability $P(l_i|\mathbf{x})$ is equal to

$$P(l_i|\mathbf{x}) = \frac{P(\mathbf{x}|l_i) P(l_i)}{P(\mathbf{x})} \quad (35)$$

If there is no correlation between the attributes, the likelihood $P(\mathbf{x}|l_i)$ can be assumed equal to the product of the separate likelihoods for each attribute

$$P(\mathbf{x}|l_i) = P(x_1, x_2, \dots, x_n | l_i) = P(x_1 | l_i) P(x_2 | l_i) \dots P(x_n | l_i) \quad (36)$$

Hence assuming n attributes, $\lambda(l)$ can be expressed by

$$\lambda(l) = \begin{pmatrix} P(l_1|\mathbf{x}) \\ P(l_2|\mathbf{x}) \\ P(l_3|\mathbf{x}) \\ P(l_4|\mathbf{x}) \end{pmatrix} = \begin{pmatrix} \alpha^{-1} \prod_{i=1}^N p(x_i|l_1) \\ \alpha^{-1} \prod_{i=1}^N p(x_i|l_2) \\ \alpha^{-1} \prod_{i=1}^N p(x_i|l_3) \\ 0 \end{pmatrix} \quad \text{where } \alpha = \sum_{j=1}^4 \left(\prod_{i=1}^N p(x_i|l_j) \right) \quad (37)$$

α represents here the marginal probability. $p(l_4|\mathbf{x}) = 0$, since a line primitive was extracted for sure.

The independence condition has been empirically proved by a correlation test using the training data. The correlation coefficient ρ_{ij} for each attribute is calculated:

$$\rho_{ij} = \frac{\sigma_{ij}^2}{\sigma_{ii}\sigma_{jj}} \quad (38)$$

where σ_{ii} is the variance of the attribute x_i ,

$$\sigma_{ii}^2 = \frac{1}{N} \sum_{t=1}^N (x_{i,t} - \mu_i)^2 \quad \text{where } \mu_i = \frac{1}{N} \sum_{t=1}^N x_{i,t} \quad (39)$$

and σ_{ij} is the covariance of the attributes x_i and x_j ,

$$\sigma_{ij}^2 = \frac{1}{N} \sum_{t=1}^N (x_{i,t} - \mu_i)(x_{j,t} - \mu_j) \quad (40)$$

ρ_{ij} indicates the strength of a linear relationship between two attributes, x_i and x_j . The value ranges from 1 to -1, where

- ◇ $\rho_{ij} \rightarrow 1$ means that there is a positive linear relationship between the two attributes
- ◇ $\rho_{ij} \rightarrow -1$ means that there is a negative linear relationship between the two attributes
- ◇ $\rho_{ij} \rightarrow 0$ shows that there is no linear relationship and the two attributes can be treated as independent.

Attributes of dark linear features	Correlation coefficient ρ	Attributes of dark linear features	Correlation coefficient ρ
Length - Straightness	0.0061	Straightness - Constant intensity	-0.054
Length - Intensity	-0.28	Straightness - Contrast	-0.23
Length - Constant intensity	-0.27	Intensity - Constant intensity	0.77
Length - Contrast	-0.34	Intensity - Contrast	0.88
Straightness - Intensity	-0.024	Constant intensity - Contrast	0.72

Tab. 4. Correlation coefficient for different attributes of dark linear features (results for the training data of roads). Strong correlation values are in bold.

From Tab. 4 we can draw the conclusion that only the attributes *mean intensity*, *constant intensity* and *contrast* show a high correlation. This can in fact be expected due to the speckle characteristics of SAR data. As a conclusion, the factorized likelihoods can not be applied for these two attributes. The rest of the attributes did not indicate any dependence. Fig. 32(a) exemplifies this for the two attributes length and intensity.

5.4.2 Histogram fitting

Each separate likelihood $P(x_i|l_j)$ can be approximated by a probability density function learned from training data (HEDMAN et al., 2006b)(HEDMAN et al., 2006a).

Histograms are one of the most common tools for visualizing and estimating the frequency distribution of a data set. The Gaussian distribution

$$p(x|l_i) = \frac{1}{\sigma\sqrt{2\pi}} e^{-\frac{(x-\mu)^2}{2\sigma^2}} \quad (41)$$

is most often assumed to describe random variation that occurs in data used in most scientific disciplines. However, if the data as in this case, shows a more skewed distribution, has a low mean value, large variance and values cannot be negative, the distribution fits better to a log-normal distribution (LIMPERT et al., 2001). Skewness of a distribution is measured by estimating the coefficient of skewness, which includes the second and the third central moments, μ_2 and μ_3 :

$$\gamma_1 = \frac{\mu_3}{\frac{\mu_2}{3/2}}, \quad \text{where } \mu_n = \frac{1}{N} \sum_{t=1}^N (x_t - \bar{x})^n \quad (42)$$

A random variable X is said to be log-normally distributed if $\log(X)$ is normally distributed. The rather high skewness and remarkable high variance of the data indicated that the histograms might follow a log-normal distribution, i.e.

$$p(x|l_i) = \frac{1}{S\sqrt{2\pi}x} e^{-\frac{(\ln x - M)^2}{2S^2}} \quad (43)$$

where M and S are the mean and standard variation of the variable's natural logarithm. The shape of a histogram is highly dependent on the choice of the bin size. Larger bin width normally yields histograms with a lower resolution and as a result the shape of the underlying distribution cannot be represented correctly. Smaller bin widths produce on the other hand irregular histograms with bin heights having great statistical fluctuations. Several formulas for finding the optimum bin width are well-known, such as Sturges' rule or the Scott's rule. However most of them are based on the assumption that the data is normally distributed. Since the histograms show a large skewness, a method, which estimates the optimal bin size out of the data directly (SHIMAZAKI and SHINOMOTO, 2007), is used instead. Here the optimal bin width is chosen by minimizing a certain cost function, which is estimated based on the assumption that the data in each bin obeys a Poisson distribution. The optimal bin width is found by varying the cost function for varying bin widths (see Fig. 32(b)).

The probability density functions have been fitted to the histograms by a least square adjustment of S and M since it allows for introducing a-priori variances (GARCIA, 2000). Figs. 33, 34 and 35 show the histogram of all attributes and their fitted log-normal distributed curve. A fitting carried out in a histogram with one

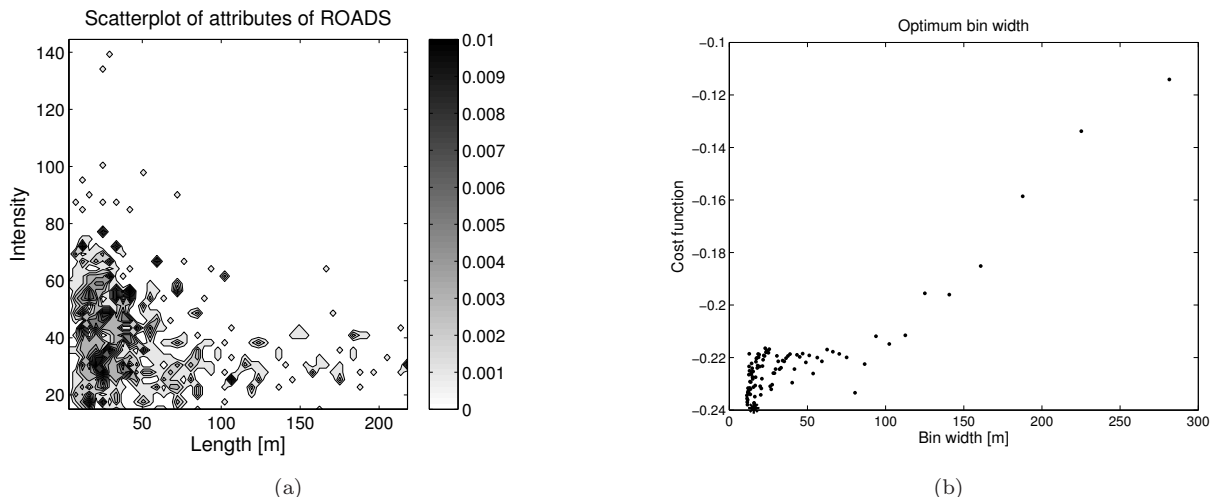


Fig. 32. (a) Scatter plot of the attributes length and intensity. (b) Cost function as a function of bin width for histogram below: ROADS - Length. The optimum bin width is marked as a dark star.

dimension is relatively uncomplicated, but as soon as the dimensions increase, the task of fitting becomes more complicated. As soon as attributes tend to be correlated, they cannot be treated as independent. A fitting of a multivariate log-normal distribution shall then be carried out. We avoid this by only selecting attributes with little or no correlation.

The obtained probability assessment shall correspond to our knowledge about roads. At a first glance, the histograms in Figs. 33(a) and 33(b) seem to overlap, but one should also consider the different scales of the figures. Fig. 33(d) exemplifies for the attribute length that the discriminant function

$$g(x) = \ln(p(x|l_1)) - \ln(p(x|l_2)) \quad (44)$$

increases as the length of the line segment increases. When $g(x)$ is positive, the probability density function for l_1 is larger than l_2 . With other words, all linear segments with a length larger than x_0 given that $g(x_0) = 0$ are classified into ROADS, under the condition that only the attribute length is considered. The behavior of the discriminant function corresponds to the belief of a human interpreter. By means of the discriminant function we can also estimate the range when we can assume that the density functions are valid. The tails of probability density functions are hard to estimate accurately because of lack of training data. The further from the peak the less measurements exist in the training set. Sometimes the estimated functions show a particular strange behavior for either very small or large values. Either a strange peak or valley close to the tails can then be observed (see for instance the discriminant function for the attribute intensity in Fig. 34(d)). By estimating the position of the peaks and valleys the validity range of the approximated functions can be defined. Outside of this range, fixed numerical values are assumed. The behavior of the discriminant function was tested for all attributes.

5.4.3 Results: probability density functions

In this section the fitted probability density functions are presented and analyzed for each attribute. The section is divided into two parts, one for the dark linear features and one for the bright linear features.

Dark linear features

The aim of the analysis of the probability density functions is to make sure that the probability functions correspond to the belief of a human interpreter. Hence it should be assured that long, dark, and straight linear features shall get a high certainty of being ROADS. Very dark, irregular and short linear features shall be likely to be SHADOWS, as well as brighter, irregular and short linear features shall be assigned to the class FALSE ALARMS.

Length and Straightness: The training data set used for the attributes length and straightness is a comprehensive data set consisting of more than 1400 line primitives. In this training data set, false alarms and shadows were categorized into the same group: FALSE ALARMS AND SHADOWS. Not until later, the idea about discriminating also shadows from the rest of the false alarms came up. These two attributes can stay in the same group

since both of them are assumed to be irregular and short. Even though a slight majority of false alarms are represented in the group, the part belonging to shadows should be big enough for being statistically represented. FALSE ALARMS AND SHADOWS are in majority and represent about 4/3 (75 %) of the line primitives. The line primitives come from different global context regions; one small part comes from forest areas (6 %), some from built-up areas (37 %) and almost the half from fields (49 %). The rest were assigned to an undefined global context - OTHER (7 %).

The length of the line primitive is scaled by means of the pixel resolution. Straightness is defined as the standard deviation of the orientation. Steger's line extractor is able to define the coordinates (i.e. the points) of the extracted line primitives with sub-pixel precision. Furthermore, for each point the width and the orientation is returned. After smoothening and re-sampling the standard deviation of the orientation for each point is calculated.

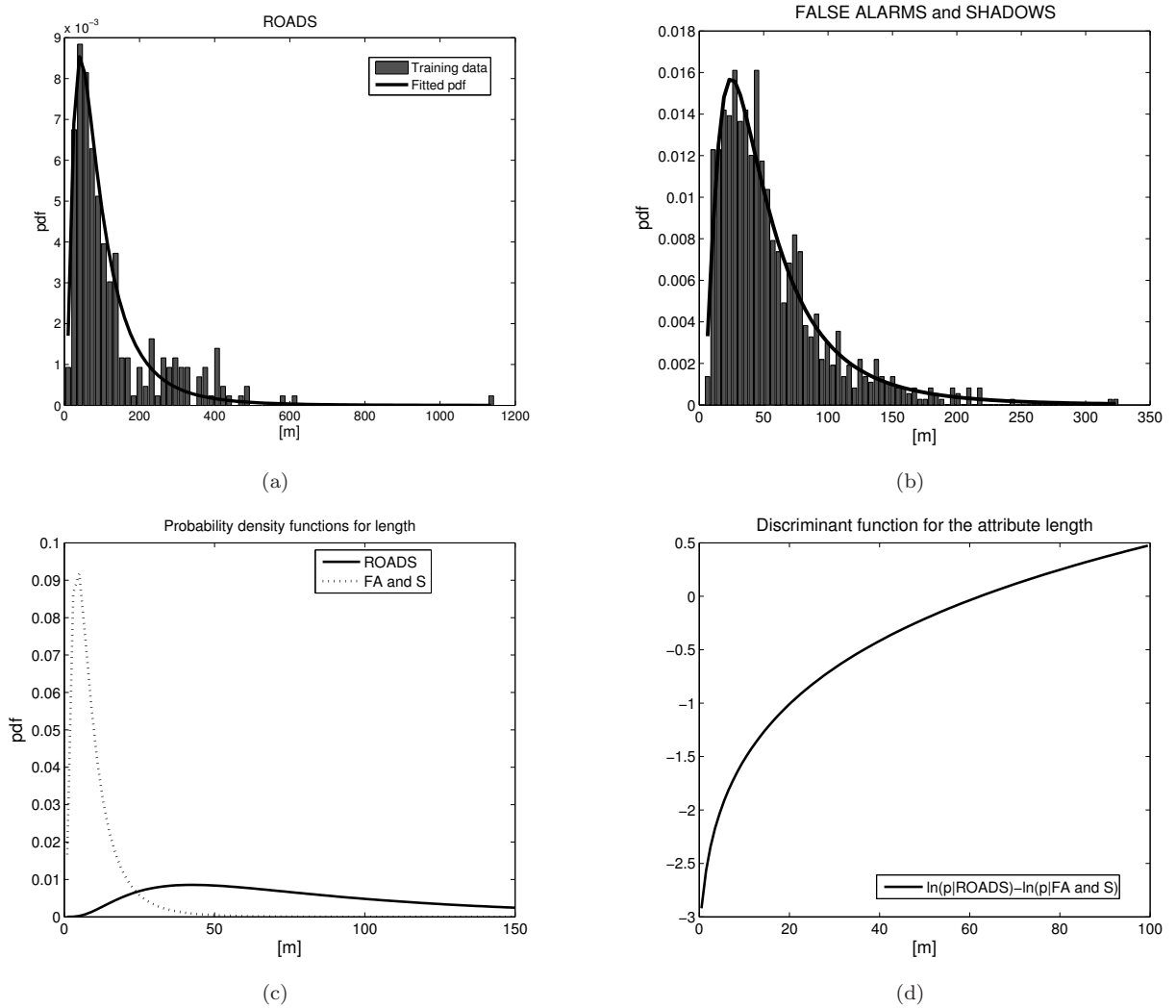


Fig. 33. **Length:** Log-normal distributions are fitted to histograms of ROADS (a) and FALSE ALARMS AND SHADOWS (b). The approximated distributions for the two classes are plotted together (c). (d) The discriminant functions based on these two distributions.

Fitted probability density functions to histograms for the attributes as well as the discriminant functions for both length and straightness can be seen in Figs 33 and 34. The estimated values for mean, variance and skewness are listed in Tab. 5.

The plotted discriminant function for straightness shows a strange decrease close to 0 (see Fig. 34(d)). Most probably this is due to very short line primitives with only a few pixels length. In the training data these short line primitives are normally assigned to the class FALSE ALARMS AND SHADOWS. Statistical attributes addressing deviation and mean measures are unreliable for line primitives of only a few pixels length. Later during the fusion procedure, very short line segments are simply sorted out. Despite of this we can make the conclusion that line primitives belonging to a ROAD are believed to be straighter than FALSE ALARMS AND SHADOWS.

For this reason a threshold is defined:

$$\begin{aligned} p(x|ROAD) &= \frac{1}{S\sqrt{2\pi}x_L} e^{-\frac{(\ln x_L - M)^2}{2S^2}} & \text{for } x < x_L \\ p(x|ROAD) &= \frac{1}{S\sqrt{2\pi}x} e^{-\frac{(\ln x - M)^2}{2S^2}} & \text{for } x_L < x < 2\pi \end{aligned} \quad (45)$$

and

$$\begin{aligned} p(x|FA_S) &= \frac{1}{S\sqrt{2\pi}x_L} e^{-\frac{(\ln x_L - M)^2}{2S^2}} & \text{for } x < x_L \\ p(x|FA_S) &= \frac{1}{S\sqrt{2\pi}x} e^{-\frac{(\ln x - M)^2}{2S^2}} & \text{for } x_L < x < 2\pi \end{aligned} \quad (46)$$

where $x_L = 0.06$, a local maximum obtained from the discriminant function (see Fig. 34(d)).

	ROADS			FALSE ALARMS and SHADOWS		
	Mean	Variance	Skewness	Mean	Variance	Skewness
Length	67.8	4690	-1.88	29.4	510	-2.00
Straightness	0.257	0.0318	-3.41	0.477	0.197	-2.95

Tab. 5. Mean, variance and skewness estimated for two attributes, straightness and length.

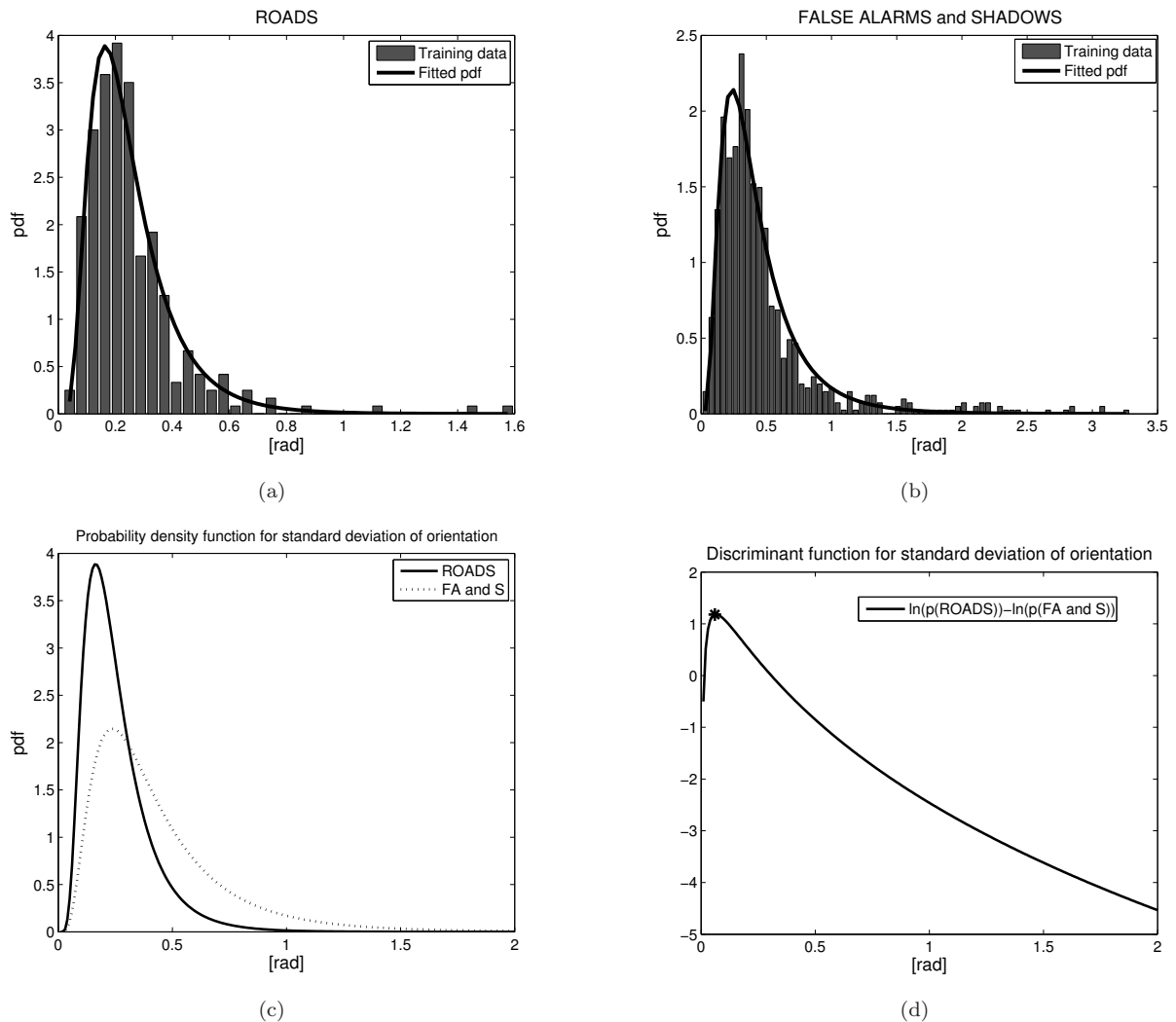


Fig. 34. **Straightness:** Log-normal distributions are fitted to histograms of ROADS (a) and FALSE ALARMS AND SHADOWS (b). The approximated distributions for the two classes are plotted together (c). (d) The discriminant functions based on these two distributions. The star indicates the local maximum, defined as x_L .

Intensity: Including intensity as an attribute was introduced for the differentiation between FALSE ALARMS and SHADOWS. ROADS and SHADOWS show both very low intensities and finding separable peaks is only possible by exploiting the full 16-bit data range of the SAR data.

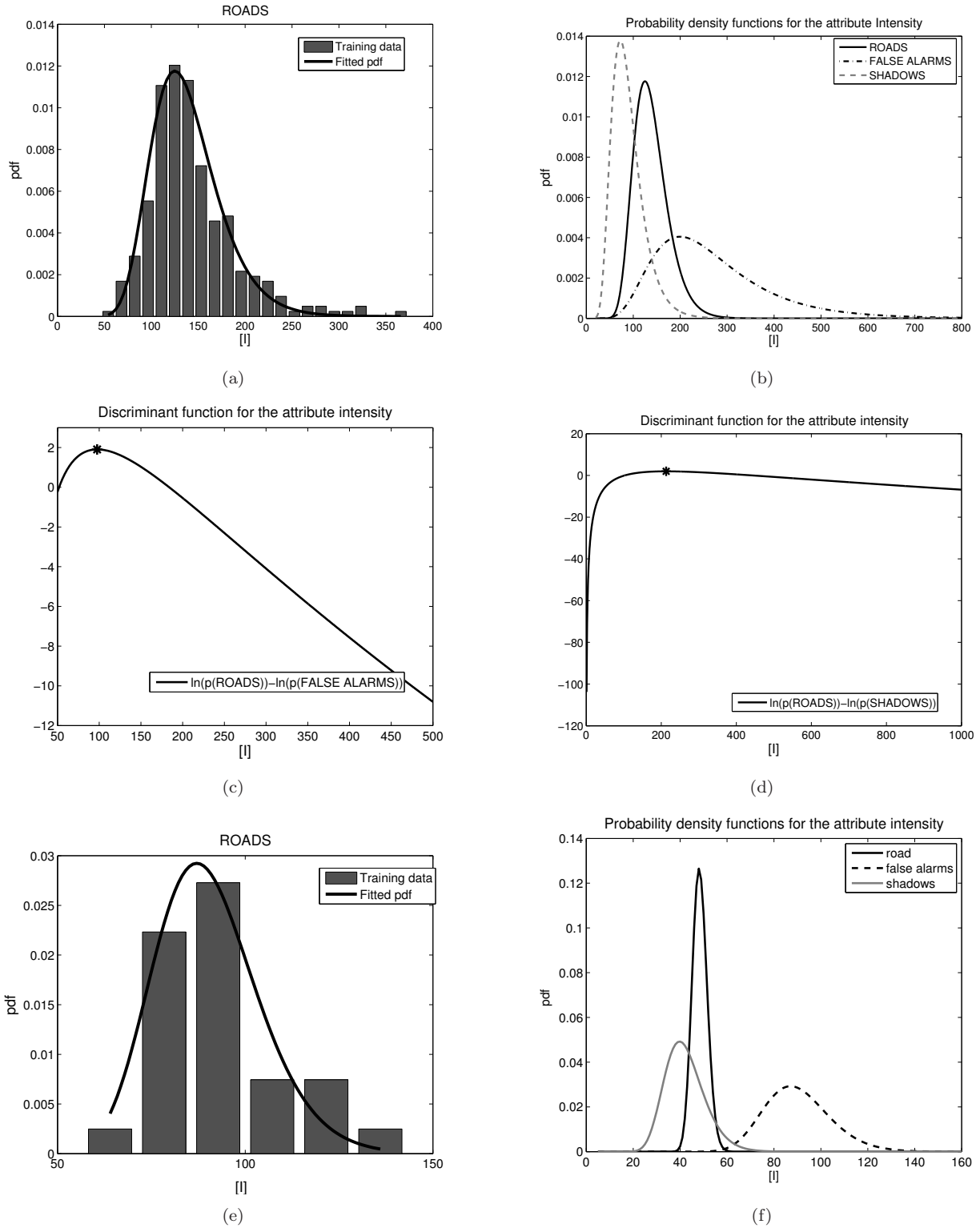


Fig. 35. **Intensity - E-SAR data:** (a) Log-normal distribution is fitted to histograms of ROADS. (b) The approximated distributions for three classes are plotted together. (c) The discriminant functions based on the fitted distributions for ROADS and FALSE ALARMS. The star indicates the local minimum, defined as x_L . (d) The discriminant function for ROADS and SHADOWS. The star is in this case the local maximum x_H . **Intensity - TerraSAR-X data:** (e) Log-normal distribution is fitted to histograms of ROADS. (f) The approximated distributions for three classes are plotted together.

The discriminant functions seen in Figs. 35(c) and 35(d) show both strange behavior in the lower intensity regions. Irrespective of the data we can make the following conclusions:

- (1) Line primitives belonging to shadows have most likely a low intensity compared to false alarms and roads.
- (2) From the definition of FALSE ALARMS (see Sec. 5.3) we can make the conclusion that its line primitives have a rather bright intensity.

Hence thresholds are defined also for the attribute intensity:

$$\begin{aligned} p(x|FALSE_ALARM) &= 0 && \text{for } x < x_L \\ p(x|FALSE_ALARM) &= \frac{1}{S\sqrt{2\pi}} e^{-\frac{(\ln x - M)^2}{2S^2}} && \text{for } x > x_L \end{aligned} \quad (47)$$

and

$$\begin{aligned} p(x|SHADOW) &= \frac{1}{S\sqrt{2\pi}} e^{-\frac{(\ln x - M)^2}{2S^2}} && \text{for } x < x_H \\ p(x|SHADOW) &= 0 && \text{for } x > x_H \end{aligned} \quad (48)$$

where $x_L=97.5$ and $x_H=213$ are local maximum and minimum points also obtained from the discriminant function (see Figs. 35(c) and 35(d)). Please, note the difference between the thresholds defined here and the thresholds defined for the attribute straightness. As $p(x < x_L|FALSE_ALARMS)$ is equal to 0, no line primitives with intensities below x_L can be assigned to the class FALSE ALARMS. At the same time, all line primitives with an intensity higher than x_H are excluded to be SHADOWS. Whereas for straightness the probability density functions are assumed to be only valid for the regions $x_L < x < 2\pi$. For $x < x_L$ the likelihood probability is assumed to be $P(x|l) = P(x_L|l)$. Otherwise very straight line primitives would be assigned to roads regardless of its length and intensity.

Transferring the estimated probability density functions to other SAR scenes would save the user work but would be especially difficult for the attribute intensity when different SAR sensors are used. Hence, the probability density functions for intensity should preferably be adjusted as soon as new data sets are included. Also a training data set from TerraSAR-X data was collected for testing the intensity range of the data. The training data set was not as large as for the E-SAR data but large enough for the estimation of the probability density functions (see Fig. 35(e)). While comparing the estimated functions for E-SAR data (see Fig. 35(b)) and for TerraSAR-X data (see Fig. 35(f)) one can clearly differentiate the different intensity ranges. When the estimated probability density functions are applied on true data, adequate thresholds must be defined as in the case with E-SAR data.

Bright linear features

An E-SAR training data set showed that bright features extracted from BUILDINGS (i.e. strong scattering) are characterized by a very strong intensity and are in general short compared to the other classes. The bright features closed to HIGHWAYS are usually very long, sometimes even extremely long. The intensity is low compared to the others. At the beginning a group of false alarms (e.g. undefined bright features extracted in fields and forest) were examined. The first idea was to differentiate between straight rows of trees and other vegetation. However these two groups showed very similar characteristics. The two classes cannot be separated based solely on their length and intensity and it was decided to merge them into one class - VEGETATION. The characteristics of VEGETATION turned out to be in between highways and man-made objects in terms of both intensity and length. The attribute straightness was excluded since the overlap was too large for all classes. There was no strong correlation between the attributes intensity and length (see Tab. 6), except for buildings, where there seem to be some correlation between the two attributes. This is probably due to very small but strong scatterers from metallic objects. The magnitude of the correlation is still less than 0.5 and the two attributes are therefore handled as independent in this work.

Correlation between attributes: <i>Length - Intensity</i>	HIGHWAY	BUILDINGS	VEGETATION
Correlation coefficient ρ	-0.14	-0.43	0.07

Tab. 6. Correlation coefficient estimated for the bright linear feature training set for the attribute length and intensity.

The training data set was rather small compared to the training data set of dark features and contains only 115 linear features. Compared to dark linear features it was simply harder to find adequate linear primitives. Especially the number of linear primitives belonging to the class HIGHWAY was low (see Fig. 36(b)). Due to the lack of training data the tails are especially hard to define. Therefore thresholds need to be defined for each attribute. Within the data range defined by these thresholds, the probability density functions can be considered reliable.

Not all functions were as skewed as those estimated for the dark features. In particular the two attributes of HIGHWAY showed a skewed distribution, which could not be described by a normal distribution. Since a log-normal distribution is able to approach a normal distribution, log-normal distribution was assumed for all classes.

Length:

The following assumptions were made:

- (1) Bright features belonging to crash barriers of highways are usually very long, sometimes even extremely long and are extracted with hardly any gaps.
- (2) Bright features of buildings are often short. A maximum length for buildings is introduced here. However this threshold can be adjusted according to the scene. Industrial large buildings or blocks of houses might also cause very long bright features. Then it is more likely though that gaps occur.
- (3) Extracted bright vegetation features are in general not as long as highways, but longer than buildings.

The following thresholds were defined:

$$\begin{aligned}
 p(x|HIGHWAYS) &= \frac{1}{S\sqrt{2\pi}x} e^{-\frac{(\ln x - M)^2}{2S^2}} \quad \text{for } 0.1 < x < x_H \\
 p(x|HIGHWAYS) &= \frac{1}{S\sqrt{2\pi}x_H} e^{-\frac{(\ln x_H - M)^2}{2S^2}} \quad \text{for } x > x_H
 \end{aligned} \tag{49}$$

$$\begin{aligned}
 p(x|VEGETATION) &= \frac{1}{S\sqrt{2\pi}x} e^{-\frac{(\ln x - M)^2}{2S^2}} \quad \text{for } 0.1 < x < x_H \\
 p(x|VEGETATION) &= \frac{1}{S\sqrt{2\pi}x_H} e^{-\frac{(\ln x_H - M)^2}{2S^2}} \quad \text{for } x > x_H
 \end{aligned} \tag{50}$$

where $x_H = 87m$ were estimated as a local maximum in the discriminant function.

$$\begin{aligned}
 p(x|BUILDINGS) &= \frac{1}{S\sqrt{2\pi}x} e^{-\frac{(\ln x - M)^2}{2S^2}} \quad \text{for } x < x_H \\
 p(x|BUILDINGS) &= 0 \quad \text{for } x > x_H
 \end{aligned} \tag{51}$$

The threshold value of x_H for BUILDINGS can be adjusted for each scene. It should be less than the threshold x_H for vegetation and highways. In this work we set x_H equal to 50 m.

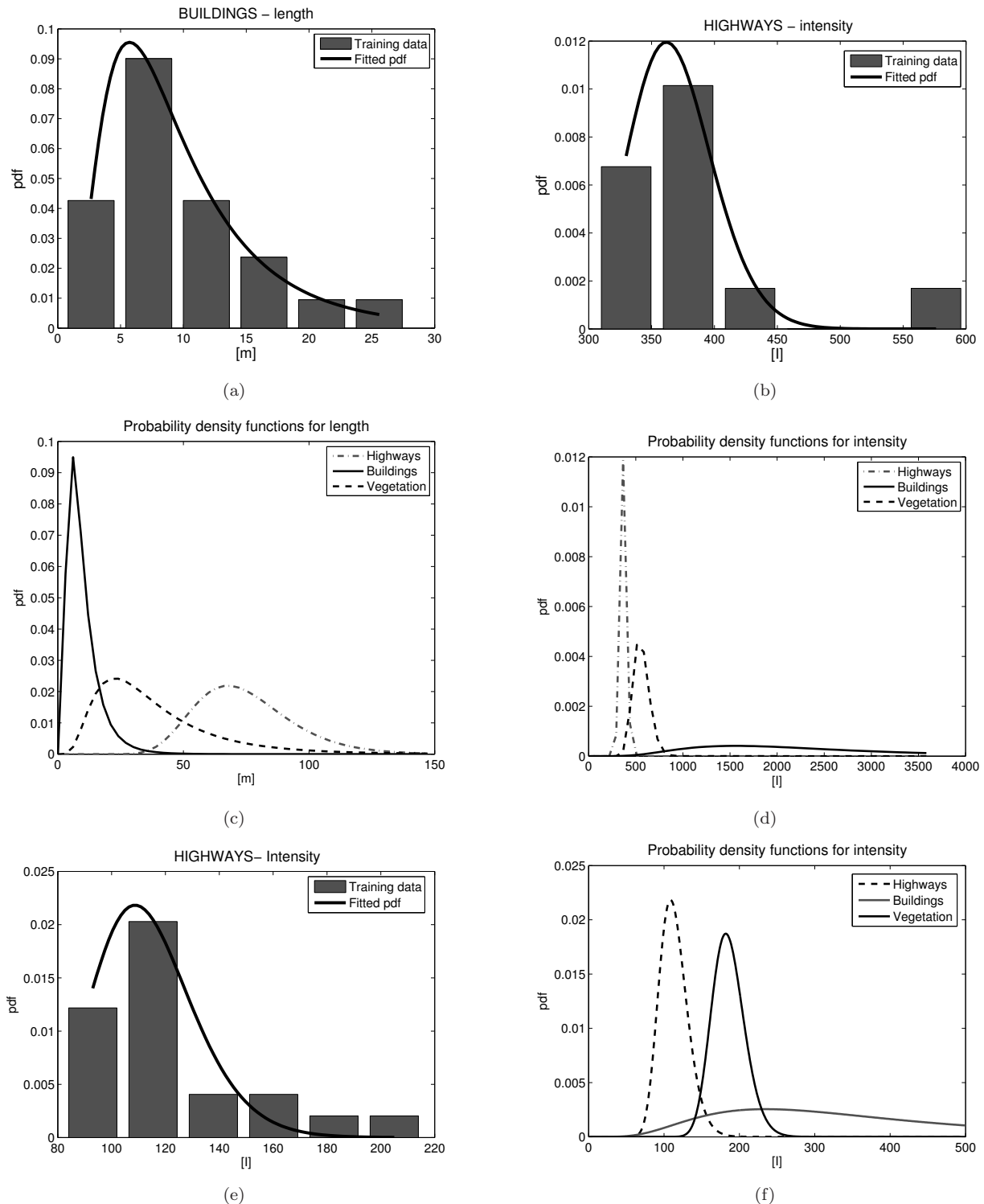


Fig. 36. Log-normal distributions are fitted to histograms of E-SAR training data (a) Buildings - length and (b) Highways - intensity. The resulting fitted distributions for bright linear features for three classes are plotted together; (c) length and (d) intensity. Distributions were also fitted to a small TerraSAR-X training data set. Here an example for highways is shown (e). The estimated functions for TerraSAR-X data are plotted together (f).

Intensity:

The probability density functions for intensity showed a good behavior for large intensities. Even going to maximum intensities, BUILDINGS became a high assessment. Therefore we concentrated on the definition of thresholds for the lower intensity area.

$$\begin{aligned}
 p(x|BUILDINGS) &= 0 && \text{for } x < x_L \\
 p(x|BUILDINGS) &= \frac{1}{S\sqrt{2\pi}x} e^{-\frac{(\ln x - M)^2}{2S^2}} && \text{for } x_L < x < x_H \\
 p(x|BUILDINGS) &= \frac{1}{S\sqrt{2\pi}x_H} e^{-\frac{(\ln x_H - M)^2}{2S^2}} && \text{for } x > x_H
 \end{aligned} \tag{52}$$

where $x_L = 493$. x_H has got the same numerical value for all classes ($x_H = 1585$).

$$\begin{aligned}
 p(x|VEGETATION) &= \frac{1}{S\sqrt{2\pi}x_L} e^{-\frac{(\ln x_L - M)^2}{2S^2}} && \text{for } x < x_L \\
 p(x|VEGETATION) &= \frac{1}{S\sqrt{2\pi}x} e^{-\frac{(\ln x - M)^2}{2S^2}} && \text{for } x_L < x < x_H \\
 p(x|VEGETATION) &= \frac{1}{S\sqrt{2\pi}x_H} e^{-\frac{(\ln x_H - M)^2}{2S^2}} && \text{for } x > x_H
 \end{aligned} \tag{53}$$

where $x_L = 288$ was estimated as a local minimum based on the discriminant function.

$$\begin{aligned}
 p(x|HIGHWAY) &= \frac{1}{S\sqrt{2\pi}x_L} e^{-\frac{(\ln x_L - M)^2}{2S^2}} && \text{for } x < x_L \\
 p(x|HIGHWAY) &= \frac{1}{S\sqrt{2\pi}x} e^{-\frac{(\ln x - M)^2}{2S^2}} && \text{for } x_L < x < x_H \\
 p(x|HIGHWAY) &= \frac{1}{S\sqrt{2\pi}x_H} e^{-\frac{(\ln x_H - M)^2}{2S^2}} && \text{for } x > x_H
 \end{aligned} \tag{54}$$

where the same value ($x_L = 288$) as for VEGETATION was used.

As in the case with the dark linear features the intensity probability density functions should be adjusted if they are applied to data acquired from other SAR sensors. A training data set of bright features collected from TerraSAR-X data showed indeed that the intensities differ compared to the E-SAR data (see Figs 36(e) and 36(f)). Hence the probability density functions should be adjusted as soon as the sensor characteristics are too different.

5.4.4 Evaluating and testing the classification

As soon as the training data contains a large data sample, we can use some samples for evaluating the classification. In this work the data is randomly separated into one training set (80 % of the data) and one testing set (20 % of the data). The first set is used for the histogram fitting (i.e. building the classifier) and the second set is used for evaluating the performance of a classifier. This classifier is nothing else than our estimated probability density functions. The result of the evaluation is presented in a so called classification error matrix, which is presented for each attribute. Error matrices are useful for showing the relationship between known reference data and the corresponding results of the classification (LILLESAND et al., 2008). The matrices are square matrices with rows corresponding to the known reference and with columns with the number of the classified line primitives. Those line primitives correctly classified can be found along the diagonal.

Producer's accuracies are estimated from the number of correctly classified line primitives within one class divided by the total number of line primitives of this class (the reference). It gives us an idea about how well the testing set of one specific class is correctly classified. *User's accuracies* on the other hand shows us how reliable our classification result is. This one is calculated by dividing the number of correctly classified line primitives within each class by the total number of line primitives that were classified in that class. *Overall accuracy* is calculated by dividing the number of correctly classified line primitives with the total number of line primitives.

The error matrices give information about how well the classification works for each attribute and for each class. This information is of particular importance for the design of the conditional probability table (see Sect. 5.5). The overall accuracies for the dark linear features range from 63 % to 69 % with a better performance for the combination of length and straightness (81 %) (see Tab. 7). The producer's accuracies (57-83 %) and the user's

accuracies (37-99 %) vary both highly between the attributes and the classes. Here there are also slightly better results for the combination of length and straightness (57-96 %). Normally these values give us an idea about how well separable and homogeneous the classes are. In this case the number of FALSE ALARMS dominates the testing set that much (76 % of the first set and 72 % of the second set) that it is hard to evaluate the performance of the two other classes.

The error matrix for the linear bright features (see Tab. 8) shows that the different bright features can be much better differentiated than the dark ones. The attribute intensity alone shows an overall accuracy of 87 %. The bright backscattering covers a large intensity range and due to the different backscattering characteristics of the different classes, the classes can be very well distinguished. The two classes ROAD and SHADOWS are both very close in intensity range. Applying both attributes to the bright features resulted in a very good accuracy - 96 %! However one shall keep in mind that the training data set is very small, especially the reference class HIGHWAY. Therefore the results from the error matrix shall be handled carefully. One shall also keep in mind that the training data was picked selective with the purpose to get homogeneous and separable classes.

One should also remember that the error matrices only give an evaluation of the classifier and not of the uncertainty assessment. The actual input to the fusion is a percentage and not an assignment to a specific class. The uncertainty assessment is also a result of the product of all probabilities (Eq. 36).

Error Matrix: Dark Features							
Length							
	R	FA and S	Total	User's Accuracy	Producer's Accuracy	Overall Accuracy	
r	47	70	117	0.40	0.66		
fa and s	24	145	169	0.86	0.67		
Total	71	215	286			0.67	
Straightness							
	R	FA and S	Total	User's Accuracy	Producer's Accuracy	Overall Accuracy	
r	59	93	152	0.39	0.83		
fa and s	12	122	134	0.91	0.57		
Total	71	215	286			0.63	
Intensity - E-SAR data							
	R	FA	S	Total	User's Accuracy	Producer's Accuracy	Overall Accuracy
r	41	59	11	111	0.37	0.71	
fa	1	156	0	157	0.99	0.69	
s	16	11	17	44	0.39	0.61	
Total	58	226	28	312			0.69
Length, Straightness, Intensity							
	R	FA	S	Total	User's Accuracy	Producer's Accuracy	Overall Accuracy
r	39	24	9	72	0.54	0.67	
fa	9	187	2	198	0.94	0.83	
s	10	15	17	42	0.40	0.61	
Total	58	226	28	312			0.78

Tab. 7. Error matrix for the attributes; length, straightness and intensity. Capital letters indicate the reference and the classification results are referred to as the lowercase letters (such as R=reference for ROADS, r=classified line primitives into the class ROAD).

In order to get an idea of how the classifier works it was also tested on a line extraction from real data. The line extraction is carried out with a different parameter setting compared to the training data. The small sub-images come from the same scene as the training data, but the training data was collected from different parts. A visual inspection of the results implies that the classification delivers overall good results. Especially open roads (see Fig. 37) and highways (see Fig. 38) are in most cases correctly classified. Here the line extraction is successful. The extracted line primitives are usually long and straight. The classification also works well for most of the false alarms extracted in fields (see Fig. 37) and forest areas, as well as for very dark irregular shadow regions (see Fig. 38).

There are certain problematic areas where it is hard to achieve a reliable classification. Built-up areas is in

Error Matrix: Bright Features							
Length							
	H	B	V	Total	User's Accuracy	Producer's Accuracy	Overall Accuracy
h	2	1	2	5	0.40	0.67	
b	0	10	1	11	0.91	0.83	
v	1	1	5	7	0.71	0.63	
Total	3	12	8	23			0.67

Intensity							
	H	B	V	Total	User's Accuracy	Producer's Accuracy	Overall Accuracy
h	2	0	0	2	1.00	0.67	
b	0	11	1	12	0.92	0.92	
v	1	1	7	9	0.78	0.88	
Total	3	12	8	23			0.87

Length and Intensity							
	H	B	V	Total	User's Accuracy	Producer's Accuracy	Overall Accuracy
h	3	0	0	3	1.00	1.00	
b	0	11	0	11	1.00	0.92	
v	0	1	8	9	0.89	1.00	
Total	3	12	8	23			0.96

Tab. 8. Error matrix for the attributes; length and intensity for the bright features belonging to the classes HIGHWAY, BUILDING, and VEGETATION. Capital letters indicate the reference and the classification results are referred to as the lowercase letters (such as H=reference for HIGHWAYS, h=classified line primitives into the class highways).

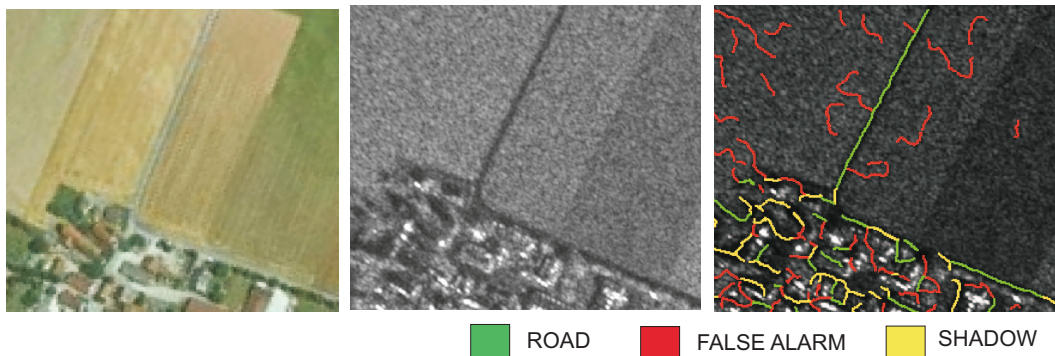


Fig. 37. Classification of dark linear primitives extracted from a SAR image (E-SAR data). The open road is extracted and correctly classified as road. The classification also manages to correctly assign the extracted features from the field to false alarms. Unfortunately in built-up areas many false alarms and shadows are falsely classified as roads.

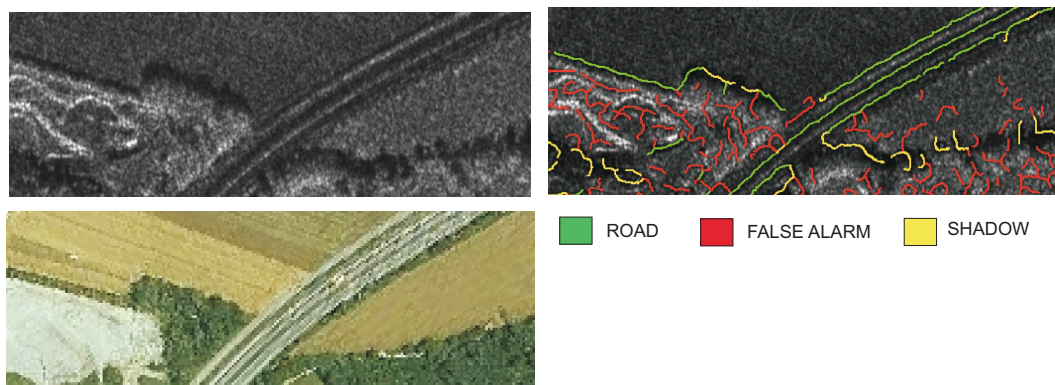


Fig. 38. Classification of dark linear primitives extracted from a SAR image (E-SAR data). The highway lanes are extracted and correctly classified as roads. Most of the shadow regions are correctly classified. However the long shadow region in the left part was wrongly assigned to the class road because of its long straight shape.

general very difficult (see Fig. 37). But these areas are also difficult to interpret even for an experienced user and it is almost impossible to know whether the extracted line primitives belong to shadows, roads or false alarms. Further there is a difficulty to differ between shadow regions and roads when the shadows appear very straight and regular. Unfortunately the intensity values of the two classes are close to each other, resulting that geometrical attributes (e.g. length and straightness) matter for a good discrimination.

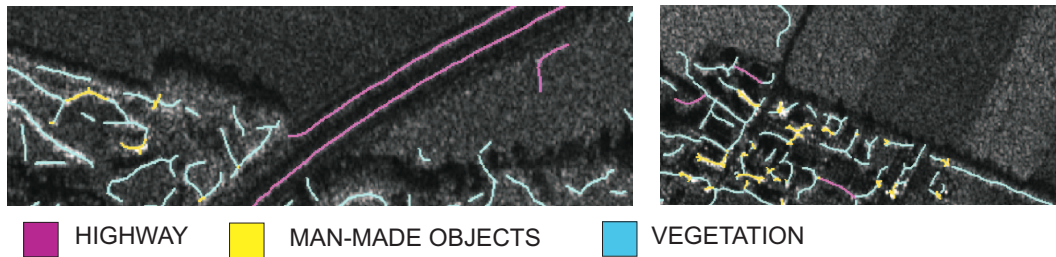


Fig. 39. Classification of bright linear primitives extracted from a SAR image (E-SAR data). (a) The backscattering surrounding the highway is correctly classified as highway (see optical image in Fig. 38). (b) Built-up areas is a problematic area for the classification (see optical image in Fig. 37). Some linear features are also wrongly classified as highways.

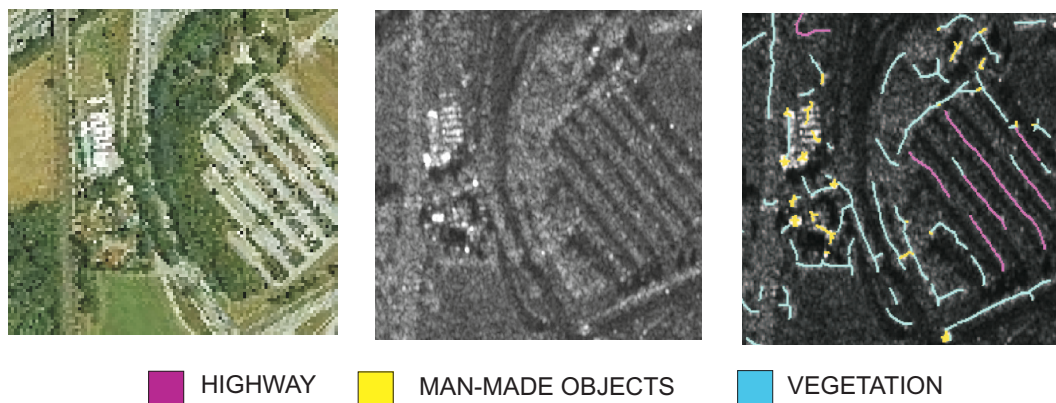


Fig. 40. Classification of bright linear primitives extracted from a SAR image (E-SAR data) showing a parking area

As expected the classification of the bright features works very well and even better than the classification of the dark features. All the three classes, highways, man-made objects and vegetation are in most cases correctly classified (see Fig. 39). The few errors originates from very long features extracted from lower vegetation which are classified into highways. Another problematic area is a parking area (see Fig. 40), but this area is of course exceptional. Built-up areas is a problem also for bright features. Here we have got the same problem as with the dark features. There is a lot of vegetation between the houses, which makes it hard to say whether the classification is correct or not. Mixed backscattering from built-up areas is a problem, since the backscattering from houses are sometimes assigned to the class vegetation.

The conclusion drawn from the test on true data is that the "classification" seems robust enough to be applied to the fusion. However we should keep in mind that it is not a true classification. Instead of giving the line primitives a label, each element of the vector $\lambda(l)$ becomes a value ranging from 0 to 1 (see Eq. 37). Hereby we keep the information if the "classification" is a certain "classification" or not. The advantage of keeping the uncertainty assessment was demonstrated in STILLA and HEDMAN (2010) by investigating some simple examples. Some line features were selected and looked at in detail during the fusion. By using either the uncertainty assessment or the classification labels as input to the fusion, the different results were plotted and further investigated. These plots showed that keeping the uncertainty assessment was of advantage for the final results.

In the following section the link between node Y , G , and L will be quantified. Instead of using continuous conditional probability functions, discrete probability tables will be defined.

5.5 Conditional probability tables

While the conditional probability functions defined in the previous section (see Sect. 5.4) quantify the link between the detected line primitive L and their attributes X , the conditional probability table defined in this section shall express the relation between the existing object, Y , and the extracted line primitives, L . Since we move in the same direction as the arrow (i.e. from causes to effects) the conditional probability table should quantify the probability that a certain object in the scene should give rise to detected line features. During the process of defining the conditional probability table three points must be taken into consideration;

- (1) the road model considering different sensor geometries (Sect. 5.1.1),
- (2) the performance of the line extractor (Sect. 5.2.1)
- (3) the performance of the probability density functions - our "classifier" (Sect. 5.4)

5.5.1 Definition of conditional probability table - without local context

The capacity of estimating conditional probability density functions is dependent on the availability of training data. If one has no access to sufficient training data, one is forced to express the belief by tables consisting of discrete probabilities. At best, probabilities can be numerically estimated directly from training data. In the worst case they have to be estimated based on subjective belief. In this work most numerical values representing the conditional probabilities originates from the previous analysis of training data and the model of road and its local context. But due to lack of training data some conditional probabilities needed to be estimated based on a subjective belief.

We will start with the Bayesian network (s. Eq. 26) which do not include the bright features. The conditional probability table, $M_{L|Y,G}$ should quantify the arrows $Y \rightarrow L$ and $G \rightarrow L$. If the two parental nodes were assumed to have independent causation on L the arrows could be treated individually. However the two parental nodes have a strong correlated influence on L meaning that the conditional probability table ($P(l|y, g)$) needs to be defined for both variables. This means that every combination of conditions that might cause L must be stored. As stated in Sect. 5.3, Y and G are d-connected as soon as evidence will enter variable L .

Each column of $M_{L|Y_i}$ shall comprise the following two questions:

- ◇ "What is the probability that a possible object Y_i illuminated with a certain sensor geometry will be detected by the line extractor?"
- ◇ "... and if detected, what is the probability that the line primitive is assigned to the state l_i ?"

Hence the node L also comprises the information if a line extraction succeeded or not. We assume that e_1 represent that a line feature was extracted and e_2 that nothing was detected. The probability that the line extraction will be successful can be as in earlier work be estimated based on subjective belief (HEDMAN et al., 2007)(HEDMAN et al., 2008), but estimating numerical values based on training data is a better option. In this work the probability of detecting a line primitive with the characteristics of being a road $P(e_1|y_1) = 0.87$ if the road is visible is given by the completeness values of the line extractor (see Tab. 3). Next we should find $P(l_1, e_1|y_1, g_k)$ which is the answer to the second question above. The product rule allows the following expression:

$$p(l_i, e_1|y_j, g_k) = p(l_i|e_1, y_j, g_k) p(e_1|y_j, g_k) \quad (55)$$

where $p(l_i|e_1, y_j, g_k)$ can be estimated based on the error matrix (see Tab. 7) assuming that all objects y_i were visible during the SAR acquisition. The error matrix gives us information about the performance of the classifier. Producer's accuracies tell us the probability that a line feature is correctly assigned to a class. Indeed some line primitives of the reference class ROAD are falsely classified. Furthermore the error matrix gives us the useful information that a ROAD is more likely to be falsely classified as a SHADOW as a FALSE ALARM.

Since e_2 is equal to the state $L = l_4$ we can simply write $P(l_4, e_2|y_j, g_k)$ as $P(l_4|y_j, g_k)$. The notation $p(l_i|y_j, g_k)$ is used for simplicity in the following text but is in reality equal to $p(l_i, e|y_j, g_k)$.

Assessing the numerical values for $p(l_i|y_j, g_k)$ for each state y_j is more complicated for those objects Y which are influenced by the sensor geometry. We need to answer on the question when we can expect to see our road in the SAR image. And if the road cannot be seen, what do we expect then? Fig. 41 shows how the object Y and the sensor geometry G are likely to cause different states of L . Here one can see that the node G is quantified through the width of an assumed shadow S_N . Certainly G can enter all kind of states g_k but

there is not a chance that we can collect training data enough for covering the range of S_N . Most difficult is the estimation of $p(e_1|y_j, g_k)$ for some states of Y . For instance no reference data could be defined for clutter, meaning that $p(e_1|clutter)$ had to be defined by the user. In this work we call these manually defined assumptions *subjective probabilities*. In addition the line extractor is restricted by the width, meaning that $p(e_1|y_j, g_k)$ can vary dependent on the object Y . This would be straight forward to estimate numerically if the height of the object was either known before or estimated during the fusion. Since the height of high objects is set by the user the definition of $p(e_1|y_j, g_k)$ should not be too severe since a false estimation of the height must be included as well.

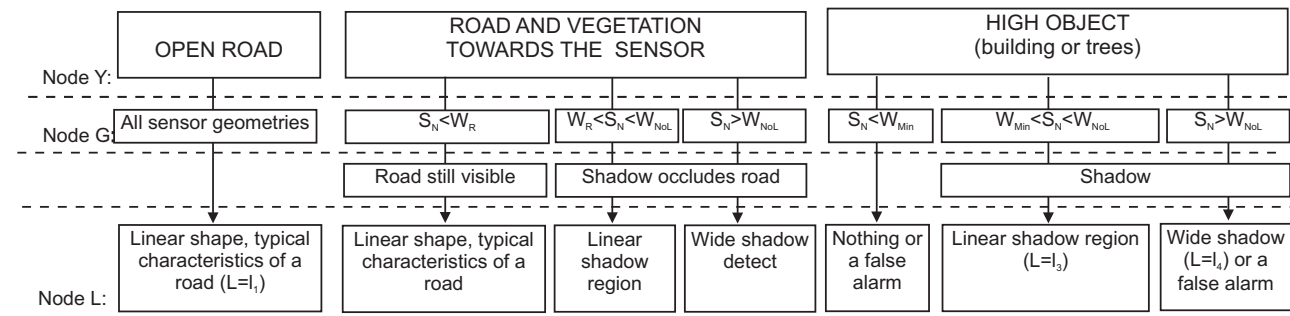


Fig. 41. The relation between roads, local context, sensor geometries and the appearance in the SAR image, which is the underlying model behind the Bayesian network.

Open roads (y_1): The sensor geometry has no influence on the appearance of the road. There are no local context that might influence the appearance of the road in the SAR image. The road shall show the same characteristics, no matter from what direction the SAR image is acquired.

Roads with high objects nearby (y_2): As discussed in Sect. 5.1.2, the road with trees or houses nearby show different characteristics in the SAR scene depending on the β angle. Based on Fig. 15 following assumptions can be made:

- (1) $S_n < W_R$: The shadow occludes only a part of the road and the typical road characteristics are supposed to be kept.
- (2) $W_R < S_n < W_{NoL}$: The shadow occludes the whole road. A line extraction is still possible and an extracted line primitive will have the same characteristics as an extracted shadow region.
- (3) $S_n > W_{NoL}$: Range is almost perpendicular to the direction of the road. The width of the shadow is assumed to be too large for the line extraction.

The conclusion drawn from these statements is that depending on the sensor geometry different states of L are expected. For each state g_k not only each $p(l_i|y_2, g_k)$ is different, but also $p(e_1|y_2, g_k)$ must vary. When the road is assumed to be visible ($S_n < W_R$) the same chances of a line extraction and characteristics as an open road is assumed. Hence the column $p(l|y_1)$ is equal to $p(l|y_2)$. As we continue to the next domain, $W_R < S_n < W_{NoL}$, a shadow is expected. The column should therefore express the performance of the line extractor for detecting shadow regions as well as the performance of the classifier. For the domain $S_n > W_{NoL}$ the numerical estimates are much harder. The following subjective probabilities are assumed:

- ◇ There is a 50% chance that the line extractor will work anyway.
- ◇ Among these detected 50%, 25% of these will have the same characteristics as FALSE ALARMS

High Objects

- (1) $S_n < W_{MinL}$: Either no shadow is present or the linear shadow region is supposed to be too thin for the line extractor. If something is extracted it is assumed to be only clutter.
- (2) $W_{MinL} < S_n < W_{NoL}$: A line extraction is possible and the extracted line primitive will have the typical characteristics of an extracted shadow region.
- (3) $S_n > W_{NoL}$: Range is almost perpendicular to the high object. The width of the shadow is assumed to be too large for the line extraction.

For the domain $S_n < W_{MinL}$ nothing or a false alarm is expected. It is assumed that a width larger than W_{MinL} is needed for a line extraction to succeed. The reasoning behind the definition of $p(l|y_4)$ can be found under "Clutter". The definition of $p(l|y_3)$ for the domain $W_{MinL} < S_n < W_{NoL}$ is based on the same calculations as for roads with objects nearby ($W_R < S_n < W_{NoL}$) resulting in $p(l|y_3) = p(l|y_2)$. That is also valid for

$S_n > W_{NoL}$. The conclusion is that the differentiation between ROADS WITH AN OBJECT NEARBY and HIGH OBJECTS can only be made if $S_n < W_R$!

Clutter Clutter is assumed to look the same no matter where the SAR sensor is. In most cases clutter does not belong to any special object. They appear often in forest regions. It is extremely hard to estimate the performance of the line extractor for clutter since clutter is not really defined. Clutter is not expected to cause any line structure in the SAR data and therefore represents all pixels in the image except those pixels that belongs to roads and high objects. Based on that definition the chance of detecting clutter must be low. Since all probabilities are related to each other each factor defined in the conditional probability table needs to be defined with care. We will discuss later why.

Here we assume the following:

- ◇ There is a 50% chance that clutter will detected.

In the end four different states for G are defined;

- ◇ $g_1 =$ Line primitives with a direction very close to range - $S_N < W_{Min}$
- ◇ $g_2 =$ A possible shadow would still not occlude the road $W_{Min} < S_N < W_R$
- ◇ $g_3 =$ Shadows are assumed to occlude the road $W_R < S_N < W_{NoL}$
- ◇ $g_4 =$ A possible shadow is too large for the line extraction $W_R < S_N < W_{NoL}$

The value of S_N is estimated by Eq. 22. The height H of the assumed object can either be estimated iteratively based on the width of an extracted shadow or can be assumed to be a fixed value for one scene. As written before W_{Min} is supposed to be 3 pixels wide. W_R could also be estimated out of the data but is in this work assumed to be about 8 m. W_{NoL} was empirically estimated as the highest maximum width of all extracted line features.

In the end four tables have to be defined. There should be one for each defined state g_k :

Conditional probability tables, $p(l_i y_j, g_k)$									
$G = g_1 : S_n < W_{Min}$					$G = g_2 : W_{Min} < S_n < W_R$				
$p(l_i y_j)$	$Y = y_1$	$Y = y_2$	$Y = y_3$	$Y = y_4$	$p(l_i y_j)$	$Y = y_1$	$Y = y_2$	$Y = y_3$	$Y = y_4$
$L = l_1$	0.59	0.59	0.05	0.05	$L = l_1$	0.59	0.59	0.26	0.05
$L = l_2$	0.14	0.14	0.41	0.41	$L = l_2$	0.14	0.14	0.06	0.41
$L = l_3$	0.15	0.15	0.03	0.03	$L = l_3$	0.15	0.15	0.50	0.03
$L = l_4$	0.13	0.13	0.50*	0.50*	$L = l_4$	0.13	0.13	0.18	0.50*
$G = g_3 : W_R < S_n < W_{NoL}$					$G = g_4 : S_n > W_{NoL}$				
$p(l_i y_j)$	$Y = y_1$	$Y = y_2$	$Y = y_3$	$Y = y_4$	$p(l_i y_j)$	$Y = y_1$	$Y = y_2$	$Y = y_3$	$Y = y_4$
$L = l_1$	0.59	0.26	0.26	0.05	$L = l_1$	0.59	0.11	0.11	0.05
$L = l_2$	0.14	0.06	0.06	0.41	$L = l_2$	0.14	0.23	0.23	0.41
$L = l_3$	0.15	0.50	0.50	0.03	$L = l_3$	0.15	0.17	0.17	0.03
$L = l_4$	0.130	0.18	0.18	0.50*	$L = l_4$	0.13	0.50*	0.50*	0.50*

Tab. 9. Numerical values for the conditional probabilities $p(l_i|y_j, g_k)$ expressed in the conditional probability table $M_{L|Y,G}$. The subjective probabilities are marked with a "*".

One can see in the first conditional probability table that ($G = g_1$, Tab. 9) some states will obtain the same probability even though G has entered two different states. For instance the two states ROAD WITH OBJECT NEARBY and HIGH OBJECTS will obtain the same probability for the two states g_3 and g_4 . Having only these SAR images at disposal one could not say whether the detected line primitive belongs to y_2 or y_3 . Preferably at least one of the images shall be acquired from an aspect angle close to the roads direction. This does not automatically mean that the images shall be perpendicular to each other. Instead it is important to try to get the range of at least one image to approach the direction of the main road axes of the scene.

5.5.2 Definition of conditional probability table - including local context

A conditional probability table for a fusion that includes the bright feature extraction must also take the performance of the bright line extractor, the performance of “the bright classifier” and the relation between the object, the sensor geometry and the extracted dark and bright features in consideration.

The conditional tables that needs to be defined are far more complex than the previous one. Since there are three nodes, D , B_{left} and B_{right} , three tables are constructed. In addition the node G is no longer quantified by only S_n , but also the length of layover, L_N . In addition the bright features are on the side which faces or is opposite to the sensor plays a certain role. Hence the number of states of G is further increased. If we would design the conditional probability table in the same way as in the previous section (Sect. 5.5.2) we would end up with an endless number of states and several conditional probability tables.

The difficulty lies in the modeling. It is hard to find a model which on one side is detailed enough for including the characteristics for each object. On the other side the model should not be too detailed in order to avoid over-fitting.

The three classes open road, highway and clutter have all in common that these are independent on the sensor geometry. No matter the sensor geometry, the performance of the line extractor and the classifier stay the same. Next to open roads we do not expect to find any local context. If a bright feature is extracted then it can be assumed to be only bright clutter. Next to highways we can expect to find bright extracted feature classified as HIGHWAYS. These are assumed to be well detectable no matter the sensor geometry. Also these are expected to be extracted on both sides of the road. Clutter is assumed to consist of dark and bright false alarms only.

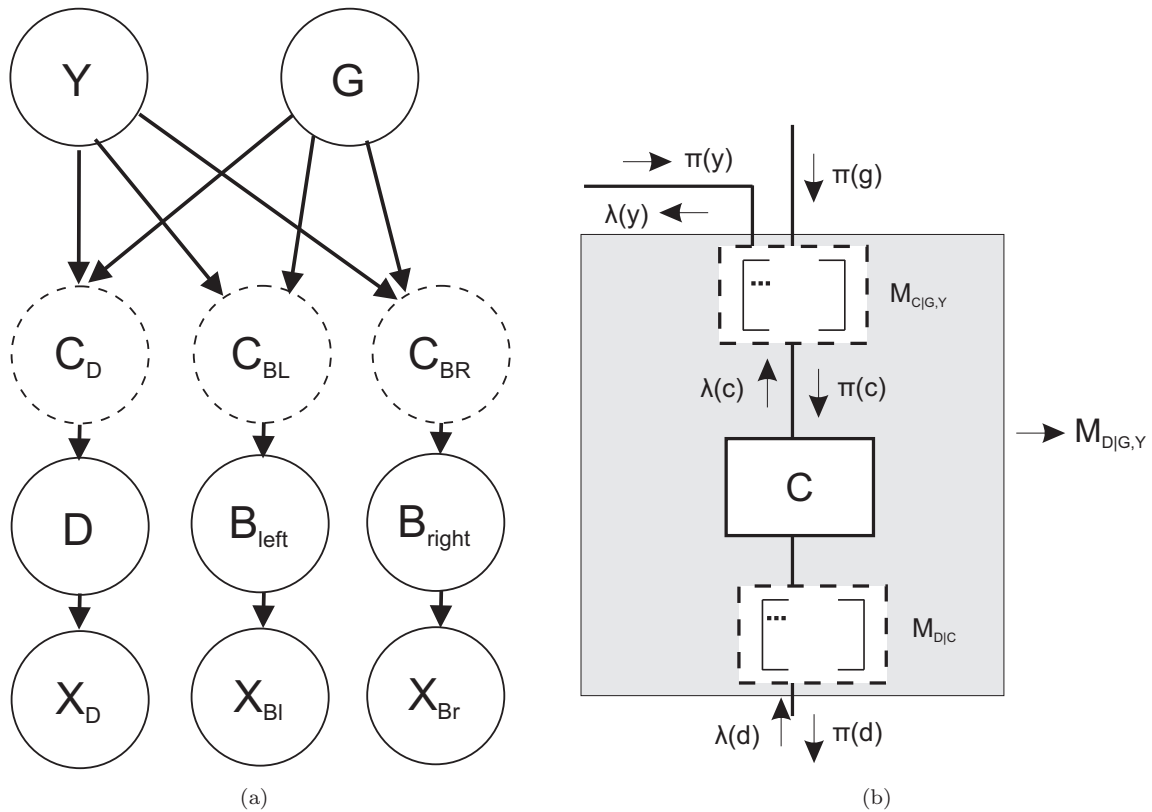


Fig. 42. (a) The hidden nodes C_D , C_{BL} , and C_{BR} are inserted in the Bayesian network BN_4 . (b) The belief update including the hidden node C is illustrated. $M_{C|G,Y}$ and $M_{D|C}$ create together $M_{D|G,Y}$.

As soon as local context represents high objects such as high trees or high buildings, the sensor geometry has a strong impact on what the local context and the road (if existing) look like in the SAR image. For instance if a row of trees exists next to the road, the sensor geometry is the critical factor for the possibility to extract a linear dark feature and if this extracted linear feature belongs to a road or a shadow. Furthermore the sensor geometry influences the possibility that the bright line extractor detects the row of trees. Common for the classes $y_3 - y_9$ (see definition in Sect 5.3) is that all classes comprise high objects meaning that the sensor geometry needs to be incorporated in the definition of the conditional probability tables. In previous section we could not differentiate whether the local context was on the left or on the right side of the road. The assumed shadow was

calculated based on the road visibility angle, β , only. Luckily here we can differentiate whether the local context is on the left or on the right side. Also the fact that the left or the right side faces the sensor or not matters, since this informs us where to expect the shadow and layover regions. Hence a large number of different states of the sensor geometry needs to be defined.

In order to make the design of the conditional probability tables and the implementation of the fusion easier we define some hidden nodes C . Hidden nodes represent unobservable variables and were introduced by PEARL (1988). The aim was to verify causal directionality (i.e. ensure that causes flow only in one direction between the nodes). But hidden nodes can also be used for obtaining a more compact structure or to handle joint distribution among observable nodes (BINDER et al., 1997) (KIM and NEVATIA, 2003). Three hidden nodes are inserted between Y and each one of the child nodes; D , B_{left} , and B_{right} (see Fig. 42(a)). For the node C between Y and D the conditional probabilities $p(d_i|c_n)$ (quantified by $M_{D|C}$) and $p(c_n|y_j, g_k)$ (quantified by $M_{C|Y,G}$) are linked. While $M_{C|Y,G}$ is binary (consists of 1 and 0 only), the numerical definition of $M_{D|C}$ is similar to $M_{L|Y,G}$. $M_{C|Y,G}$ and $M_{D|C}$ creates together $M_{D|Y,G}$ (Fig. 42(b)). Hence $M_{D|Y,G}$ becomes a dynamic conditional probability table which is created for each line primitive as soon as the sensor geometry is known.

The matrix $M_{C|Y,G}$ expresses the relation between Y , G , C_D , C_{Bl} , and C_{Br} . These are quantified by rules, which defines what states c are expected if object y_i is illuminated by a sensor with the certain sensor geometry g_k . Examples of how these rules are defined can be seen in Figs. 43 and 44. Here one can see that for those objects that are dependent on the sensor geometry, the modeling is rather complex. This modeling is simplified by the new hidden nodes.

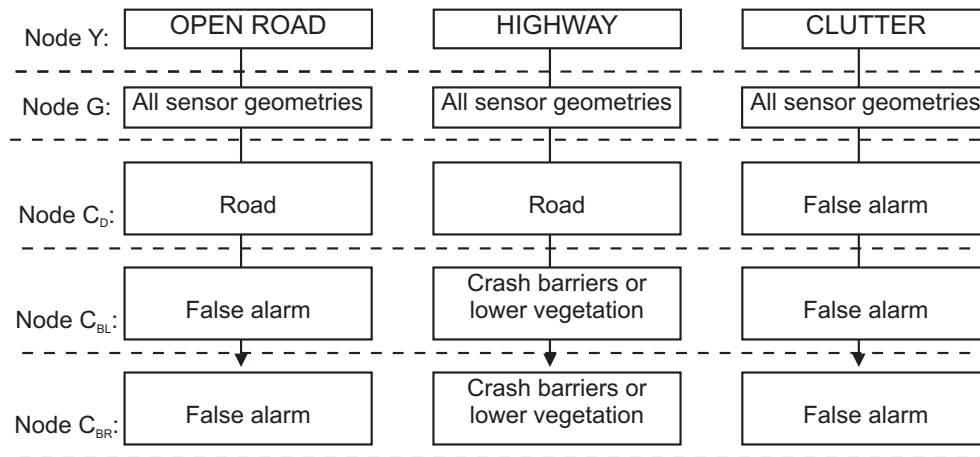


Fig. 43. The relations between some objects, their local context, and the appearance in the SAR images by different sensor geometries are illustrated in the figure. For each node a certain state is expected. Based on these relations, the conditional probability table $M_{C|Y,G}$ is defined.

The states of C_D are the following;

- ◇ $c_{d1} = \text{road}$ (a road can be seen)
- ◇ $c_{d2} = \text{false alarm}$ (actually nothing is expected)
- ◇ $c_{d3} = \text{shadow 1}$ (a linear shadow region, $S_N < W_{NoL}$)
- ◇ $c_{d4} = \text{shadow 2}$ (a wide shadow region, $S_N > W_{NoL}$)

The numerical estimation of the conditional probability table $M_{D|C_D}$ follows the same procedure as for $M_{L|Y,G}$. The reason behind the definition of two states for linear shadow regions, c_{d3} and c_{d4} , is that the probability that the line extractor detects the shadow decreases when the width of the shadow increases. The subjective probabilities are assumed:

- ◇ There is a 50% chance that clutter will be detected as dark false alarms.
- ◇ The probability that the line detector extracts a wide shadow region is 50%.

The numerical values for $M_{D|C_D}$ can be seen in Tab. 10.

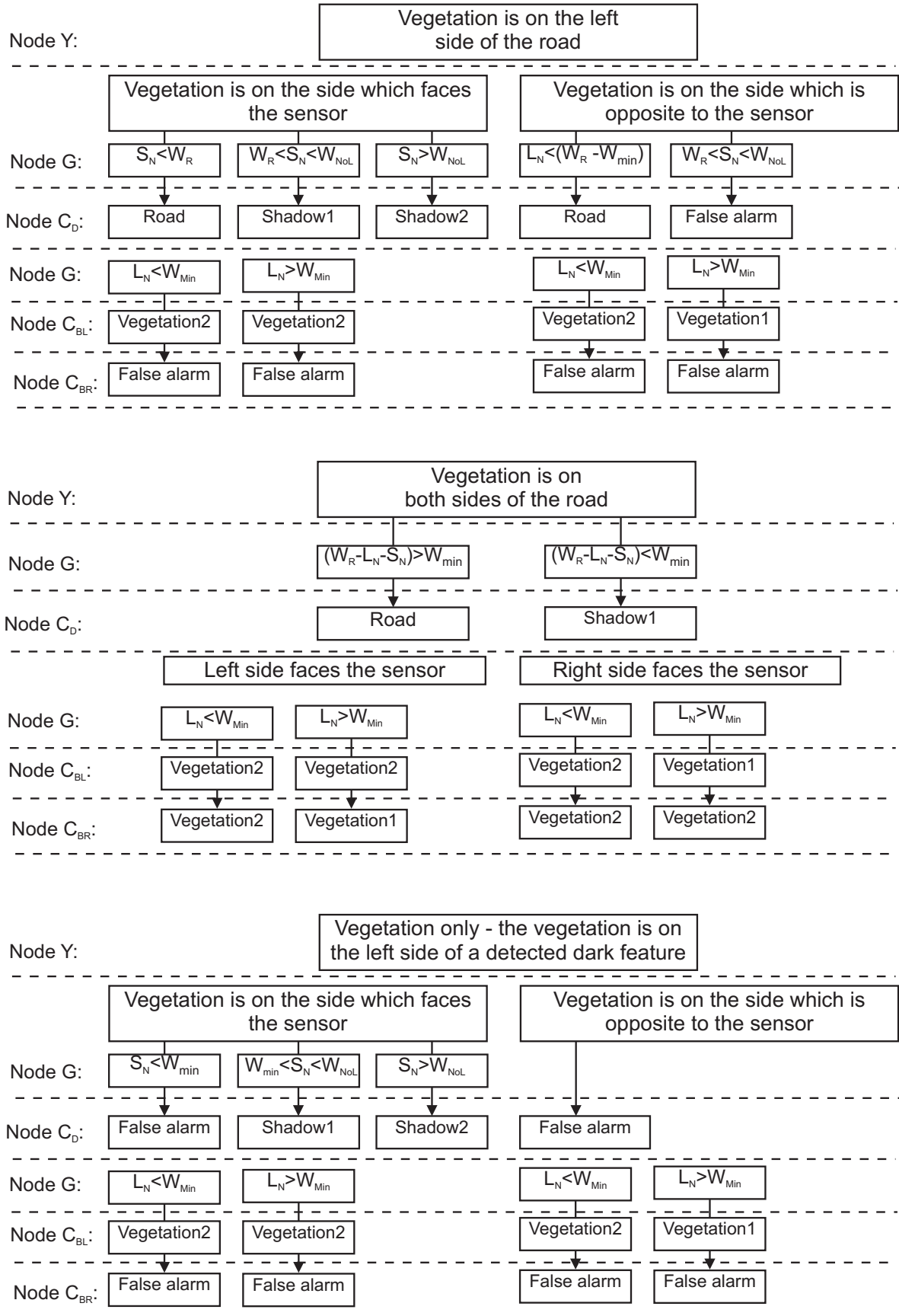


Fig. 44. The relations between some objects, their local context, and the appearance in the SAR image by different sensor geometries are shown in the figure. The appearance for all objects is strongly dependent on the sensor geometry. For each node a certain state is expected. Based on these relations, the conditional probability table $M_{C|Y,G}$ is defined.

The states defined for C_{Br} and C_{Bl} are:

- ◇ c_{b1} = the borders of the highway (crash barriers or low vegetation)
- ◇ c_{b2} = vegetation 1 (a layover region can clearly be seen)
- ◇ c_{b3} = vegetation 2 - no layover
- ◇ c_{b4} = scattering from buildings/man-made objects - with layover
- ◇ c_{b5} = scattering from buildings/man-made objects - no layover
- ◇ c_{b6} = false alarm (nothing is expected)

The definition of $M_{C_{Br}|Y,G}$ is carried out slightly different compared to $M_{D|C_D}$. The number of samples for the evaluation of the bright linear classification (Sect. 5.4.4) was unfortunately small. Instead of estimating the performance for each individual class, the overall performance was estimated. According to Tab. 8 the classifier managed to classify 96% of the bright features correctly. The numerical values for the performance of the line extractor for the individual classes were taken from Tab. 3.

Two states for vegetation and buildings/man-made objects are defined. The reason for this is that vegetation and building are more likely to be detected when layover occur. The following assumption was made:

- ◇ The probability that the line detector extracts vegetation or a building even though no layover occurs is 50%.

Bright clutter needs to be modeled just as all the other bright feature classes. Here the same problem as with the definition of dark clutter turns up. How can we estimate the performance of detecting clutter since we have no training data? As stated in the analysis of the performance of the line extractor (see Sect. 5.2.1) there is a tendency to more over-segmentation in terms of dark than in terms of bright features. We can therefore assume that less bright clutter is detected. If bright clutter is detected it has the characteristics of bright false alarms. Since bright false alarms were not included in the classifier the probability that the classifier is assigned to a particular class is supposed to be the same for all classes.

- ◇ There is a 25% chance that bright clutter will be detected.
- ◇ If bright clutter is detected, it has the appearance of a bright false alarm.
- ◇ The probability that the false alarm is classified into one of the three class: $100/3 = 33\%$

The numerical values for $M_{B_l=B_r|C_B}$ can be seen in Tab. 11.

Conditional Probabilities for Dark Features				
$p(d_i c_j)$	$C = C_{d1}$	$C = C_{d2}$	$C = C_{d3}$	$C = C_{d4}$
$D = d_1$	0.59	0.05	0.26	0.16
$D = d_2$	0.14	0.41	0.06	0.04
$D = d_3$	0.15	0.03	0.50	0.30
$D = d_4$	0.13	0.50*	0.18	0.50*

Tab. 10. Numerical values for the conditional probabilities $p(d_i|c_j)$. The table quantifies the link between node D and the hidden node C_D . The subjective probabilities are marked with a "*".

Conditional Probabilities for Bright Features						
$p(b_i c_j)$	$C = C_{b1}$	$C = C_{b2}$	$C = C_{b3}$	$C = C_{b4}$	$C = C_{b5}$	$C = C_{b6}$
$B = b_1$	0.77	0.02	0.01	0.02	0.01	0.08*
$B = b_2$	0.02	0.02	0.01	0.88	0.48	0.08*
$B = b_3$	0.02	0.90	0.48	0.02	0.01	0.08*
$B = b_4$	0.20	0.06	0.50*	0.08	0.50*	0.75*

Tab. 11. Numerical values for the conditional probabilities $p(b_i|c_j)$. The table quantifies the link between node D and the hidden nodes C_{BL} and C_{BR} . The subjective probabilities are marked with a "*".

The binary table $M_{C_l|Y,G}$ needs to consider a large number of states for G , which are all dependent on:

- ◇ The assumed shadow length S_N can be within the ranges $S_N < W_{Min}$, $S_N < W_R$, $W_R < S_N < W_{NoL}$, and $S_N > W_{NoL}$.
- ◇ The assumed layover length L_N can be within the ranges $L_N < W_{Min}$ and $L_N > W_{Min}$.

- ◇ The lengths of both layover and shadow might be within $(W_R - L_N - S_N) > W_{Min}$ and $(W_R - L_N - S_N) < W_{Min}$
- ◇ "The left side of the detected dark linear primitive D faces the sensor" or "The right side of the detected dark linear primitive D faces the sensor"

Instead of setting up such a table by the implementation, certain rules for each object are set up. The rules are defined as illustrated in Figs. 43 and 44. Buildings are treated the same as the object "vegetation only".

At this stage all conditional probabilities among the nodes are learned. The complete learning is fulfilled as the prior term is also defined. That will be discussed in the following section.

5.6 Incorporating global context information

Until now no priori information has been incorporated into our Bayesian network. Prior information represent the information that we know about the scene before the fusion begins. Global context information achieved by the textural classification (see Sect. 5.2.2) can be useful as prior information. As already stated in Sect. 5.1.2 roads have often different characteristics depending on the specific area (e.g. residential, industrial or rural areas). It is tempting to include global context into the conditional probabilities. But global context cannot be included as anything else than as prior information. It has no direct influence on the relation between the object Y and its child nodes L and X . If the characteristics of one object would be very different depending on the context area, new states must be introduced (i.e. “highway - residential” and “highway - rural”). Then, depending on the global context, the prior probability of finding these new classes would be different.

If we know the global context area our expectations of finding a road or not is changed. For instance our expectations of finding a road is very high as soon as we know that the area shows a built-up area. In addition we know beforehand that also clutter are much likely to occur in specific areas. By incorporating this information one has the option to suppress the number of false alarms in specific regions.

Priors can be learned from training data in the same way as the conditional probabilities. In this work the user specifies the priors manually. Therefore the priors represent the belief of the user to a certain degree. The primary aim of incorporating global context in this work is to suppress the frequency of line primitives falsely classified to roads in forest regions (see Fig. 45(a)). All priors were kept equal for all the other classes, except for y_{10} (clutter). The priors were defined as following:

$$\begin{aligned}\pi(y_i) &= \beta \quad \text{for } 1 \leq i \leq 9 \\ \pi(y_{10}) &= 2 \beta\end{aligned}\tag{56}$$

The advantage of including this prior information is that the impact on the classification result is noticeable only for line primitives with a relatively high rating of being clutter. That means that good road candidates are still kept after the fusion even though they are situated in an area classified as forests. The impact of prior information on the fused results on a fusion of only dark features was investigated in STILLA and HEDMAN (2010).

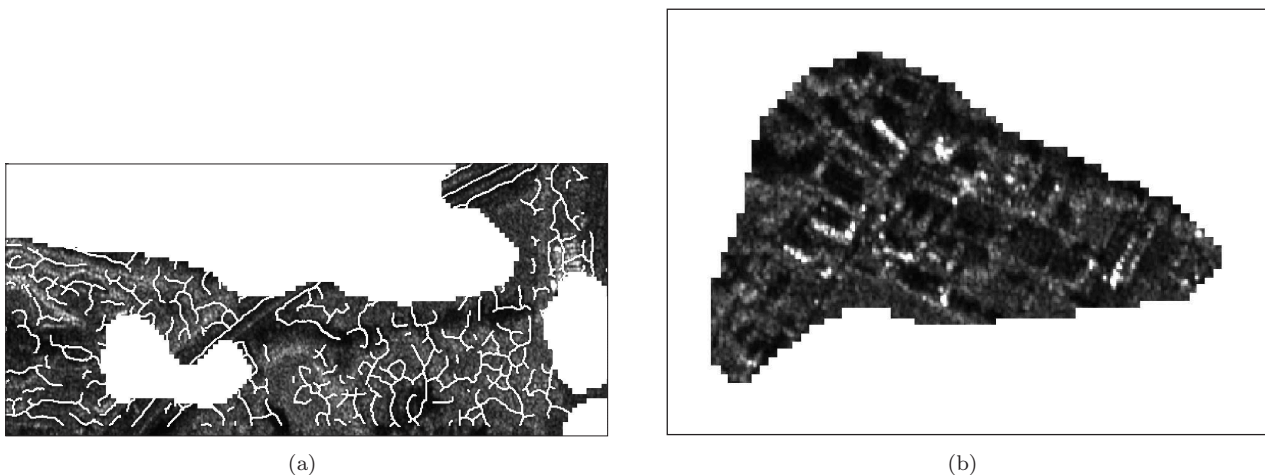


Fig. 45. Global context information is used for suppressing false alarms in forest regions and for concentrating on areas where TUM-LOREX is likely to be successful. (a) Forest regions extracted by a textural classification are highlighted. A line extraction in white show all the extracted line features. Almost all of them are only clutter. (b) Extracted built-up areas are highlighted.

Global context information can also be used for a segmentation of certain areas. The aim is then to reduce the search area and to concentrate on areas where TUM-LOREX is likely to get good results. WESSEL (2006) included a segmentation step of dark areas in TUM-LOREX for this reason. In this work built-up areas are sorted out for two reasons; (1) the path search step of TUM-LOREX is suited for rural areas and sub-urban areas ((WESSEL, 2006)) and (2) none of the Bayesian networks presented in this work are modeled for built-up areas. An object such as “road with a building nearby” is still not included as a state of Y . The modeling of roads in residential areas is particularly difficult, due to the high complexity. Despite the high resolution data,

an experienced user would have difficulties with estimating what kind of objects truly exist in the scene. The digitizing of the ground truth is also problematic in these areas (see discussion in Sect. 6). In this work extracted built-up areas are filtered out (see Fig. 45(b)).

5.7 Association

In the association process, it is determined which observations (i.e. our dark and bright linear primitives, sensor geometry, etc.) belong together and hence represent the same object in reality (i.e. the different classes y). The association requires a good co-registration of the SAR data, which can be done either automatically or manually.

One automatic co-registration approach for SAR images is based on the assumption that road intersections are unaffected by layover and shadows (DELL'ACQUA et al., 2004). By matching extracted intersections co-registration of the multi-aspect SAR data is carried out. However the approach requires an urban scene with many intersections as control points. An other approach utilizes a digital elevation model (DEM) for simulating shadow areas. Tie points are generated by matching simulated shadow areas with detected shadow structures from the SAR image (SOERGEL et al., 2004). However this requires also a detailed DEM. Since the area around Oberpfaffenhofen is rather flat, a manual co-registration was possible in this case. This was done by affine transformation. Corners of fields with different crops or smaller road intersections are usually reliable tie points. The other data set (Garching) was already geocoded and hence a co-registration was not necessary.

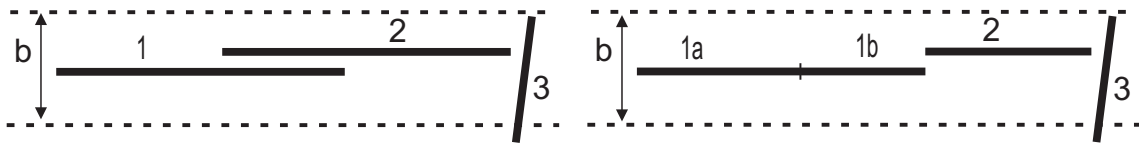


Fig. 46. Line primitive 1 is longest and is therefore selected first. All neighboring primitives which are within the buffer width b are searched for. Overlapping parts of line primitive 2 are fused. Line primitive 2 is clipped and keeps its position in the search. Line primitive 3 is not even considered due to its deviant direction with respect to line 1. The two parts of line primitive 1a and 1b get different node Y values.

The line primitives are associated to each other by a “best-first” strategy similar to the one presented in WIEDEMANN (2002). According to a certain evaluation the best evaluated line primitive is chosen first. However what kind of evaluation that should define the proper order is questionable. Before the line primitives are fused, the states L (or D and B) are already known. That means that the attributes of the line primitives are already estimated. Based on these attributes and the probability density functions (see Sect. 5.4) $\lambda(l)$ (or $\lambda(d)$ and $\lambda(b)$) are already estimated. It might be natural to choose the linear primitive with the highest probability of being road. But it is not in node L , but in node Y that the decision whether a road or not exist is made. A shadow region and a certain sensor geometry might be as well a good indicator of a road. Instead the assumption that a road network consists of long linear features is taken as a starting point. One should also keep in mind that the best evaluated linear primitives keep their length (but not necessarily their position) during the fusion.

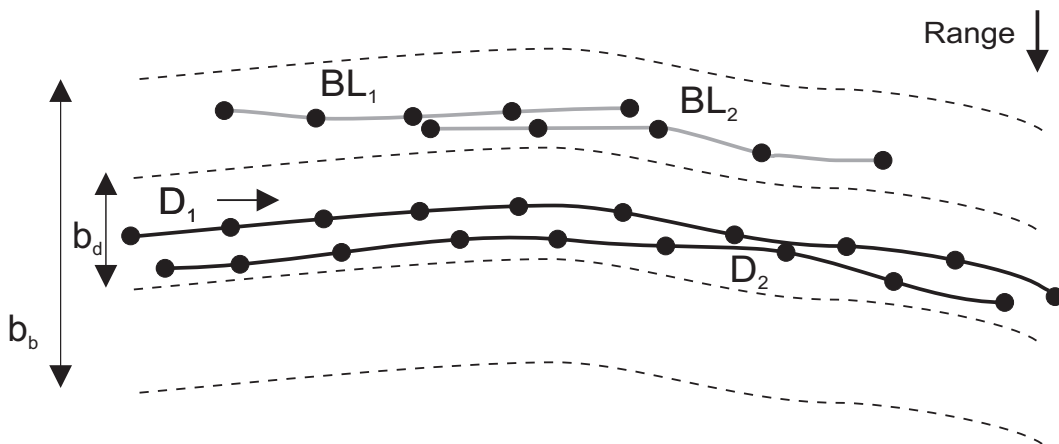


Fig. 47. The illustrated example shows what in reality could be a road with vegetation nearby. The line primitive D_1 is selected as starting primitive and becomes a direction (indicated in the figure by a small arrow). The line primitive D_2 is within the buffer width b_d . Two bright linear primitives, BL_1 and BL_2 , extracted from image 1 and image 2 are found on the left side of D_1 . In this example the left side faces the sensor (see the range direction).

The fusion is illustrated in Fig. 46. The longest line primitive is chosen first. Then, all neighboring primitives, which satisfy overlap and collinearity criteria (i.e. buffer width b and direction difference) are searched for. The check is done for each segment. All line primitives are re-sampled before the fusion so that all coordinates are separated with the same distance. Neighboring primitives that are extracted from the same image are assumed to be redundant extraction and are deleted. If only a part of the neighboring line primitive is fused, the line

primitive is clipped and the non-fused segments remain as one or more line primitives in the search. Neighboring line primitives from the second image are treated the same way but in this case information is saved for the later estimation of node Y . For each segment the index to the overlapping line primitive is stored. Lines with an all too deviant direction according to the best-evaluated line remain in the search.

If also bright linear features are included, neighboring bright features within the buffer width b_b is searched for (see Fig. 47). The buffer width b_b is larger than the buffer width for the dark segments, b_d . When the fusion also incorporates bright line extraction, all line primitives obtain a direction. Thereby it can be estimated whether the local context is on the left or on the right side. Important is also to estimate based on the known sensor geometry for each SAR image whether the left or the right side faces the sensor. Bright features extracted from both images are of importance. If the overlap and collinearity criteria are kept, the indices of the bright features are stored. All bright features remain in the search since they can be shared as local context by several dark features.

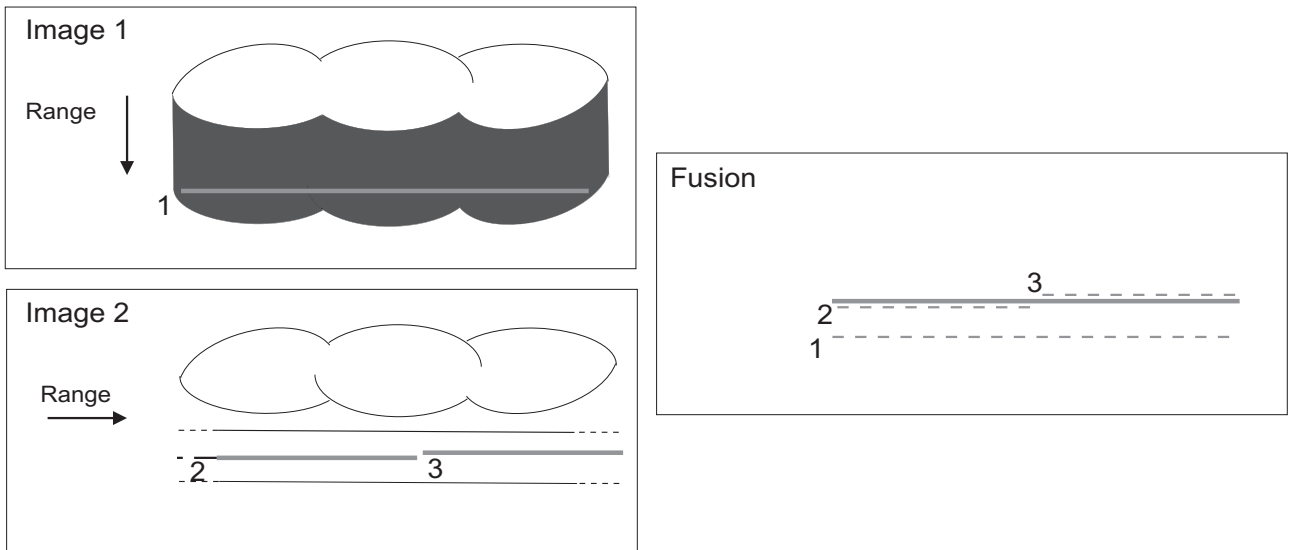


Fig. 48. The two SAR images shows a road with trees nearby but are taken from different directions. In image 1 the shadow covers the whole road. Line primitive 1 is longest and is therefore selected first. If a road really exist, then linear primitive 2 and 3 mark the correct position of the road. Line primitive 1 is moved a distance d , which is the average distance to the two line primitives.

The states of nodes G^1 and G^2 are estimated based on the sensor geometry and the direction of the longest line primitive. The sensor geometry in relation with the direction of the line primitive, is crucial for the dynamic conditional table $M_{C|Y,G}$ (see definition in Sect. 5.5.2). Incoming information from neighboring linear primitives, node L^2 , (or node D and B) is available through the stored indices. Based on that the belief in Y is calculated for each segment i according to Eq. 31 (excluding bright features) or Eq. 33 (including bright features).

The final belief in node Y for a line primitive of n segments is obtained by:

$$BEL(Y = y) = \frac{\sum_{i=1}^n BEL(Y = y)_i}{n} \quad (57)$$

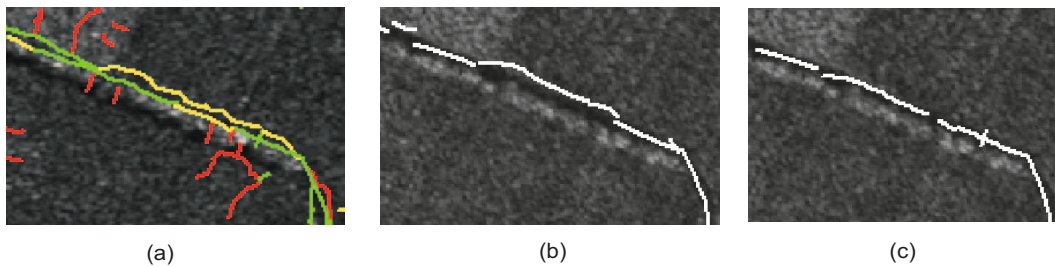


Fig. 49. The small cut out from the SAR image shows a small road with trees on the lower side of the road. Extracted line primitives from two SAR images (one illuminated from the south and one from south-east) were assessed by the “classifier” (a) green=roads, yellow=shadows, red=false alarms. In one image the shadow occludes the road while in the other the road can be seen. One of the extracted line primitives from the shadow region is very long and is kept during the fusion. Two fusions were applied, one without (b) and one with the shifting step (c).

The position of the main longest line feature may be shifted if the nodes G^1 and G^2 indicate that the neighboring primitives are closer to the original position of the road (see Fig. 48). Two criteria must be fulfilled:

- ◇ An assumed shadow width of the neighboring line primitives is smaller than the assumed shadow width of the longest line primitive ($S_n^2 < S_n^1$).
- ◇ The neighboring line primitives must be on the side which faces the sensor, since it is assumed that displacement because of shadow regions can only be on the opposite side of the sensor.

The fusion of line primitives extracted from two images are shown in Fig. 49. One can clearly see the advantage of the shifting step.

The fusion is finished when the search has gone through all linear features.

6 Results and analysis

The purpose of evaluating the results with reference data is to analyze the behavior of the fusion. The fusion shall provide a good classification for the subsequent selection of seed points for the shortest-path. Important is here to make sure that the fusion can identify the different classes correctly. For this reason an error matrix is calculated. Furthermore the fusion shall not be too severe, instead it should be rather indulgent. During the shortest-path calculation the extracted results can be further refined. The reason for this is that the step includes a selection of the “best” network, thereby avoiding detours and dead ends. Unfortunately large gaps are harder to compensate for. The quality measures are useful for this investigation. Hence the evaluation consists of two steps; 1) association of the two data sets and 2) setting up an error matrix and estimating further quality measures. The first step of the evaluation is to associate the extracted results to the reference data. The procedure is explained in Sect. 2.1.2.

The error matrix gives information about how well the fusion is able to label the output (i.e. line primitives) into the different classes. As already explained in Sect 5.4.4 the error matrix is useful since it shows the relationship between the reference classes and the extracted results. For each scene the three overall quality measures completeness, correctness and RMS are estimated. A definition of these quality measures can be found in Sect. 2.1.2. The quality measures gives us an indication about how well the overall results is. This includes both the line extraction and the fusion. The overall results are dependent on the performance of the line extraction, but also on how well the fusion can differentiate between true and false extraction. However one should keep in mind that the error matrix gives only information about the road classes. The reference data comprises only road classes. In order to get an idea about how well the remaining classification works the completeness and the correctness values were calculated before and after the classes (except clutter) were sorted out. If the completeness shows only a slight change, but the correctness varies a lot we can be certain that the identification of these classes is acceptable.

The reference data was digitized manually directly into the SAR image. Both maps and optical data were used as a further reference. In order to evaluate the fusion correctly the reference data divides the roads into a number of categories. The number of categories are matched with the outputs of the different Bayesian networks. When the bright features are included the reference data contain four classes namely; “open roads”, “highways”, “roads with vegetation on one side” and “roads with vegetation on both sides”. For an evaluation of the Bayesian network based only on dark features, the roads are divided into only two classes; “open roads” and “roads with vegetation nearby”. Highways are then included in the category open roads. Roads with buildings nearby were not included in this scene. In this work we have chosen to select reference data which reflects the “true world” meaning that parts were digitized as roads even though these were not necessarily marked as roads in a map. Hence also paved areas with a geometrical shape similar to roads (e.g. separate lanes of highways, parking lots, private roads, etc.) were categorized as one of the road classes.

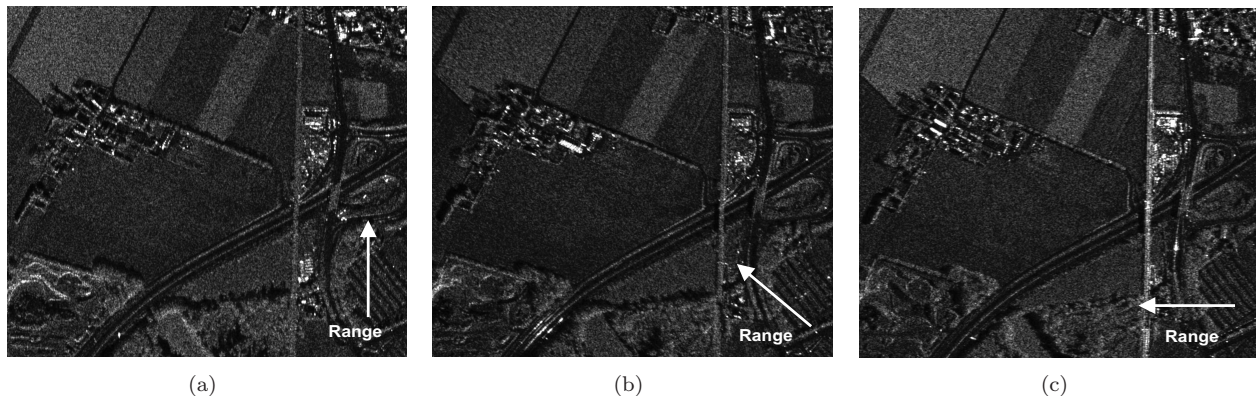


Fig. 50. The data set of Oberpfaffenhofen: (a) Oberpfaffenhofen1, (b) Oberpfaffenhofen2, (c) Oberpfaffenhofen3.

The manual digitizing was easily done for rural and sub-urban areas, but was extremely difficult for the residential areas. That was one of the reasons why built-up areas were sorted out by the texture classification described in Sect. 5.2.2. An other problem by the manual digitizing was the exact localization of very small roads in forest areas. Often only an irregular shadow structure can be seen, which is often due to the small width mixed with layover. Especially in the TerraSAR-X scene with a resolution of about 2 m, it was hard to find these irregular shadow structures, even for an experienced user. To find the exact localization of the road



Fig. 51. Manually digitized reference data (a). The ground truth is based entirely on the SAR data and optical data (b). Built-up areas are masked out (in white).

would be even harder. Since we deal with multi-aspect SAR data the localization of the road is essential for a correct evaluation. As these small roads do neither have a street name nor are included in the street map these roads were omitted by the reference. However they could be differentiated in optical data. In the future it would be preferred to digitize the reference data directly in a very high-resolution optical image instead of using directly the SAR image.

For each scene the RMS-error was estimated. But the RMS-error shall be interpreted with care, as the reference was digitized directly in the SAR image.

Data set Oberpfaffenhofen

The data set of Oberpfaffenhofen close to Munich contains three images (multilook detected image, 4 looks, ground range) taken from different directions (see Fig. 50). The ground range and azimuth pixel spacing is about 0.7 m. This dataset was acquired by the air-borne E-SAR sensor (see Sect. 3.2.3) in April, 2004. The scene is a sub-urban scene containing both residential, industrial and rural areas. Different categories of large and small roads exist; highways, primary roads, minor roads, and local streets. A sub-scene covering an area of about $840 \times 740 \text{ m}^2$ was selected for the fusion. The reference data was digitized manually based on maps and optical images (see Fig. 51).

The result of the uncertainty assessment of the dark and bright feature extraction of the respective images can be seen in Fig 52. The two different fusion approaches were tested for two combinations of images; (1) a fusion of Figs. 50(a) and 50(b) and (2) a fusion of Figs. 50(b) and 50(c). The input to the first fusion was the uncertainty assessment of the dark features only, while the input to the second fusion comprises both the dark and the bright linear features. In order to differentiate between the different image combinations, we use the denotation **Oberpfaffen1-2** and **Oberpfaffen2-3** for the fused results.

Fusion - dark features only The evaluation of the results of the fusion with only dark features can be seen in Fig. 53(a). The output of this fusion are probabilities that the fused linear primitive belong to four different classes; “ y_1 - open road”, “ y_2 - road with vegetation nearby”, “ y_3 - only vegetation”, and “ y_4 - clutter”. Only the road classes were matched with the reference. The thick lines represent the matched reference with the fused results. When the reference was not only matched but also correctly classified, the thick lines are either green (open roads) or yellow (roads with vegetation nearby). In case of an uncorrect classification the thick lines are white. Non-matched reference can be seen as white very thin lines. Some fused linear features were not matched with the reference. These “false alarms” are visualized in red. The frequency of unmatched fused results is still high even though as much as 71% (**Oberpfaffen1-2**) and 74% (**Oberpfaffen2-3**) were classified as only vegetation or as clutter and were sorted out before the evaluation.

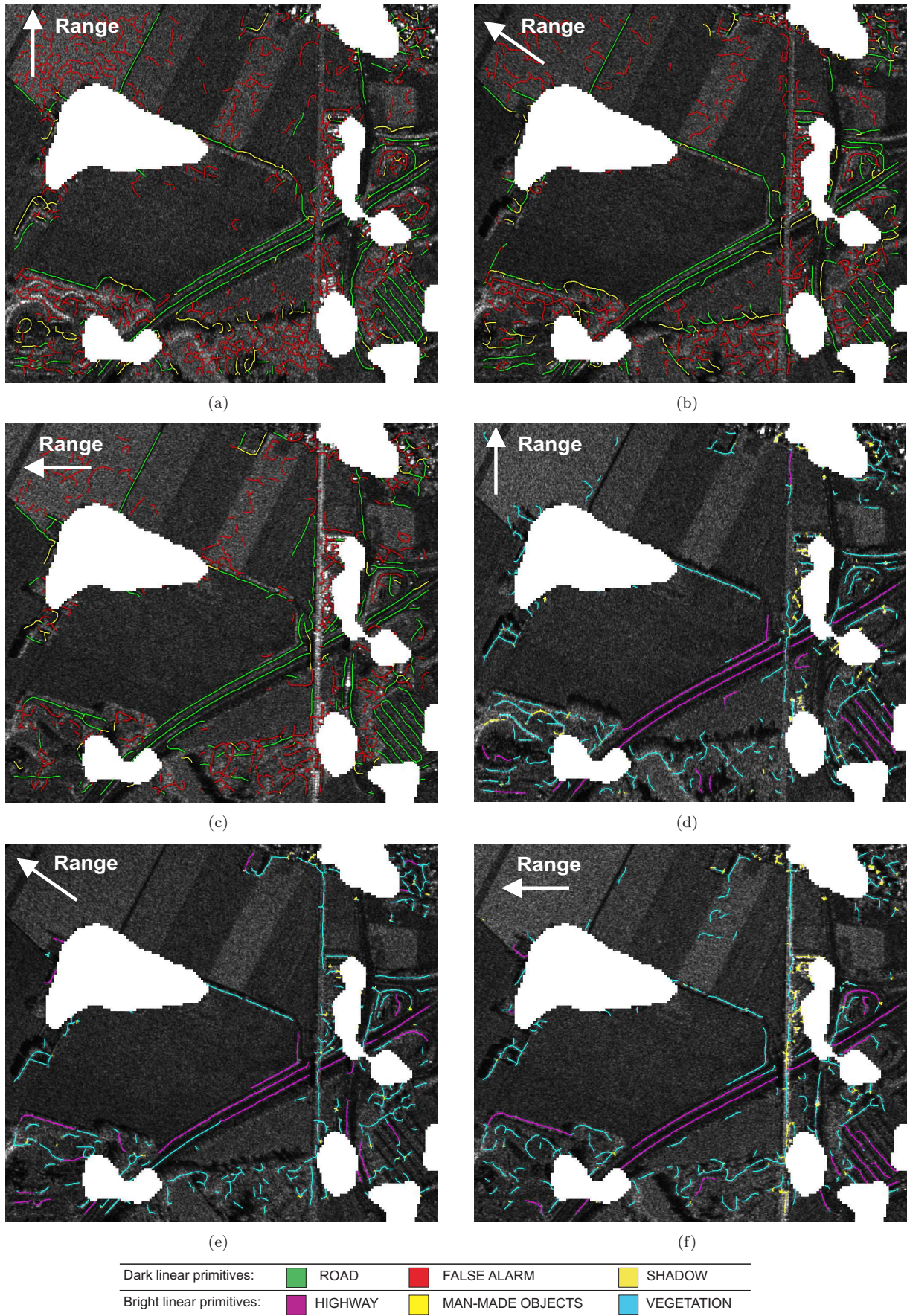


Fig. 52. Uncertainty assessment of dark linear features (a-c) and bright linear features (d-f) extracted in each of the three SAR sub-scenes (see Figs 50(a)-50(b)). The linear features and the uncertainty assessment is the input to the subsequent fusion.

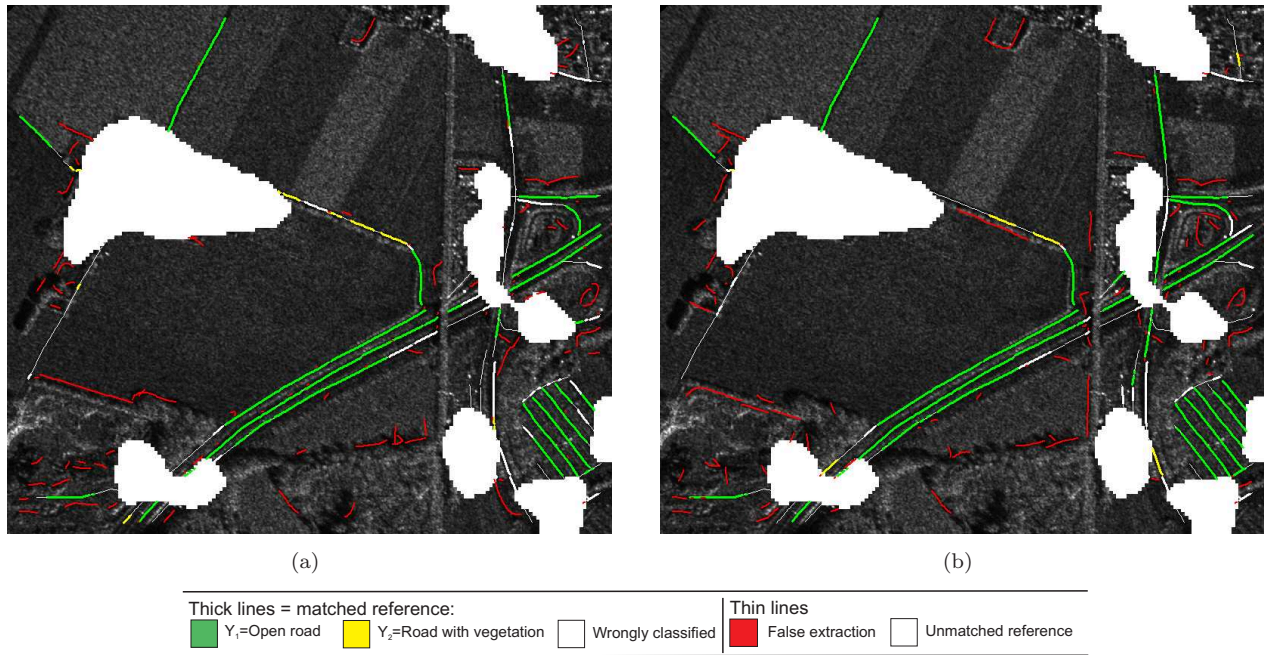


Fig. 53. Results of the dataset Oberpfaffenhofen after fusion (BN_3). Input to the fusion are the dark linear features and their uncertainty assessment. Masked built-up areas are white. (a) **Oberpfaffen1-2** shows the fusion of Figs. 52(a) and 52(b) while (b) **Oberpfaffen2-3** shows the fusion of Figs. 52(b) and 52(c).

Fusion of Oberpfaffenhofen 1 and 2						
Error Matrix						
	Y_1	Y_2	Total	User's Accuracy	Producer's Accuracy	Overall Accuracy
y_1	710	32	742	0.96	0.87	
y_2	102	98	200	0.51	0.75	
Total	812	130	942			0.86
Quality Measures						
Overall Completeness				0.70		
Overall Correctness				0.60		
RMS				4.1 m		
Fusion of Oberpfaffenhofen 2 and 3						
Error Matrix						
	Y_1	Y_2	Total	User's Accuracy	Producer's Accuracy	Overall Accuracy
y_1	773	85	858	0.90	0.92	
y_2	66	50	116	0.57	0.37	
Total	839	135	974			0.84
Quality Measures						
Overall Completeness				0.72		
Overall Correctness				0.60		
RMS				4.2 m		

Tab. 12. Error matrix for the fused linear primitives (BN_3 - only dark features) extracted from data set Oberpfaffenhofen. All fused features classified into " y_3 - only vegetation" and " y_4 - clutter" were sorted out before matching. Capital letters indicate the reference and the classification results are referred to as the lowercase letters. Y_1 means the reference class for open roads, Y_2 is the reference class for roads with vegetation nearby.

Based on the error matrix (see Tab. 12) one can draw the conclusion that the fusion is able to identify the open roads very well. Both producer's and user's accuracies are high (about 90%) for both data sets. The results for roads with vegetation nearby is not as high as for the open roads but still indeed acceptable for **Oberpfaffen1-2** (user's accuracy is 75% and producer's accuracy is 83%). Unfortunately for **Oberpfaffen2-3** the accuracies are

much lower. Interesting is that the main part of the fused linear primitives that was not matched with the reference (false extraction) were classified into roads with vegetation nearby. This is one more indicator of that the classification of this class is not as reliable as for open roads.

Both datasets showed high completeness values, 70% and 72%. The correctness is a bit lower and was 60% for both scenes. It was also tested to sort out only clutter, but then the overall completeness only increased by 4% (**Oberpfaffen1-2**) and 5% (**Oberpfaffen2-3**) while the correctness became as low as 51% (**Oberpfaffen1-2**) and as 53% (**Oberpfaffen2-3**).

Based on Fig. 53 we can draw the conclusion that the fusion is able to detect open roads very well. Still the fusion has some problems to differentiate between only vegetation and roads with vegetation. Some shadow regions close to the forest regions were wrongly assigned to one of the road classes. One explanation could be the regular shape of the forest border. Hence the extracted line features become a high assessment of being roads instead of shadows already before the fusion.

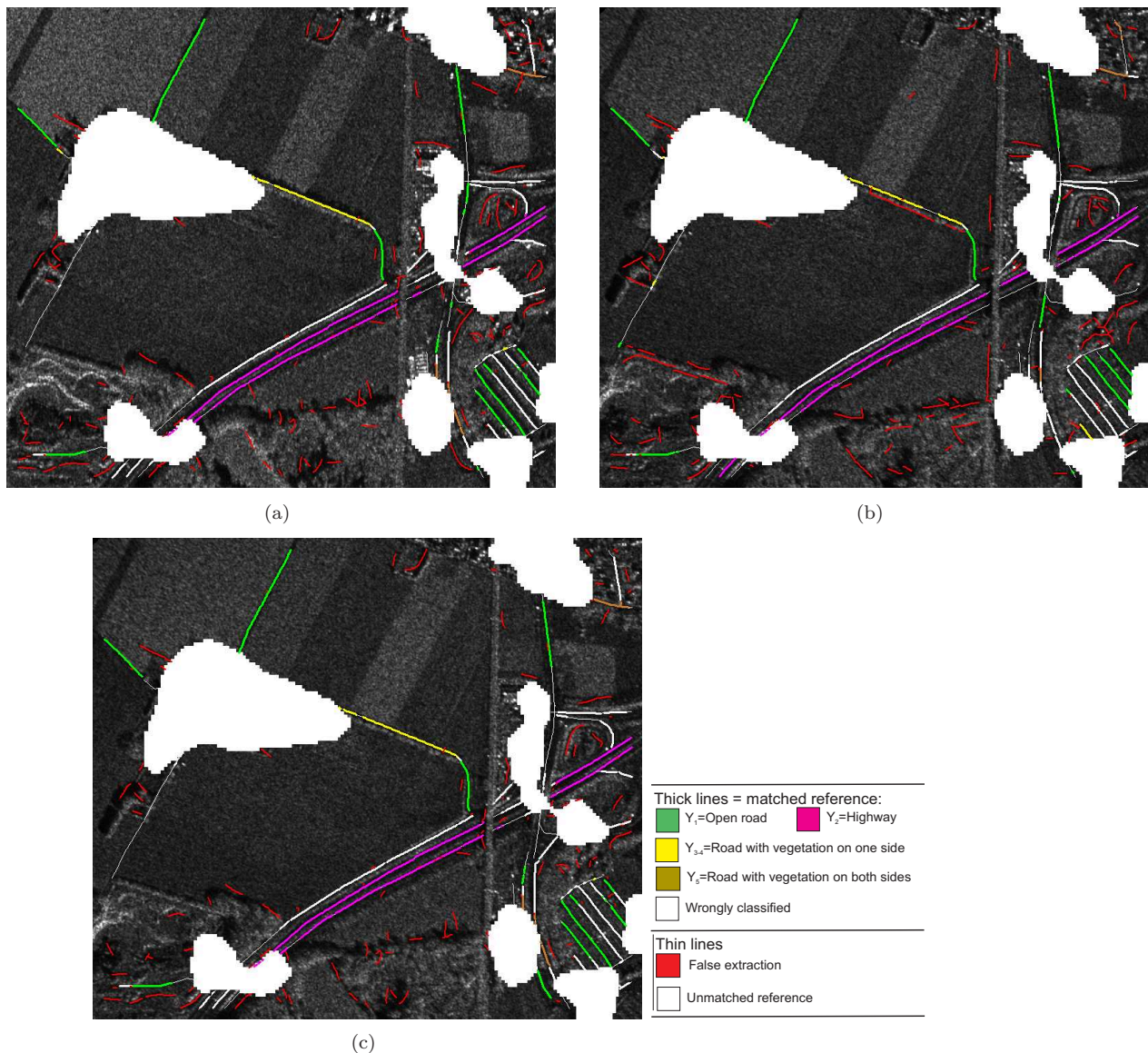


Fig. 54. The results after fusion based on the Bayesian network $BN5$ was matched with the reference. Input to the fusion are not only the dark but also the bright linear features and their uncertainty assessment. Masked built-up areas are white. (a) **Oberpfaffen1-2** shows the fusion of Figs. 52(a), 52(b), 52(d), and 52(e) while (b) **Oberpfaffen2-3** shows the fusion of Figs. 52(b), 52(c), 52(e), and 52(f). (c) **Oberpfaffen1-2** including prior information.

Fusion - bright features included The results of the fusion of both bright and dark features are visualized in Fig. 54. The fused line primitives of this fusion are classified into as many as ten different classes. Five of these are different road classes; “ y_1 - open roads”, “ y_2 - highways”, “ y_{3-4} - road with vegetation on one side of the road” and “ y_5 - road with vegetation on both sides of the road”. The remaining five are assumed to be

false alarms; “ y_{6-7} - only vegetation”, “ y_{8-9} - only buildings” and “ y_{10} - clutter”. Also in this case all false alarm classes ($y_6 - y_{10}$) were sorted out before the fused linear primitives were matched with the reference. The frequency of false alarms is even higher than for the previous fusion. But as much as 78% (**Oberpfaffenhofen1-2**) and 87% (**Oberpfaffenhofen2-3**) of the linear features were classified into the false alarm classes, indicating that a strong selection already took place.

The overall completeness is high (77% - **Oberpfaffenhofen1-2** and 73% - **Oberpfaffenhofen2-3**). If only clutter is sorted out the completeness increases a bit, but not more than 5-7%. That indicates that the fusion is indeed able to distinguish false from the true extraction.

Fusion of Oberpfaffenhofen 1 and 2								
Error Matrix (without prior)								
	Y_1	Y_2	Y_{3-4}	Y_5	Total	User's Accuracy	Producer's Accuracy	Overall Accuracy
y_1	252	24	16	33	325	0.78	0.56	
y_2	153	296	7	0	456	0.65	0.72	
y_{3-4}	30	23	59	16	128	0.46	0.58	
y_5	13	66	19	39	137	0.28	0.44	
Total	448	409	101	88	1046			0.62
Quality Measures						without prior	with prior	
Overall Completeness						0.77	0.75	
Overall Correctness						0.55	0.62	
RMS						4.0	4.0	
Fusion of Oberpfaffenhofen 2 and 3								
Error Matrix								
	Y_1	Y_2	Y_{3-4}	Y_5	Total	User's Accuracy	Producer's Accuracy	Overall Accuracy
y_1	243	43	24	27	337	0.72	0.52	
y_2	200	291	8	11	510	0.57	0.80	
y_{3-4}	21	22	57	7	107	0.53	0.61	
y_5	0	10	5	26	41	0.63	0.37	
Total	464	366	94	71	995			0.62
Quality Measures								
Overall Completeness							0.73	
Overall Correctness							0.53	
RMS							4.3 m	

Tab. 13. Error matrix for the fused linear primitives (BN_5 - dark and bright features) extracted from data set Oberpfaffenhofen. All fused features classified into “ y_{6-7} - only vegetation”, “ y_{8-9} - only buildings” and “ y_{10} - clutter” were sorted out before matching. Capital letters indicate the reference and the classification results are referred to as the lowercase letters. Y_1 means the reference class for open roads, Y_2 is the reference class for roads with vegetation nearby.

The user's and producer's accuracies are not as high as for the fusion with only dark features (see Tab. 13). But one should also keep in mind that the number of classes are now ten instead of only four. Open roads and highways are divided into two separated classes. Further roads with vegetation on one side and on both sides are differentiated. Still the user's accuracies and producer's accuracies show acceptable values, especially for open roads and highways. The results may have been even better if not a small road would be so close to the highway. Even an experienced user would think that the small road is a third lane of the highway. The fusion identifies the road in both datasets as a part of the highway. Unfortunately the road is rather long and represents a large part of the open road reference. An other interesting area is the parking lot. The parking lot is surrounded by low vegetation and therefore the bright feature extraction has similar attributes as the bright highway linear features. Unfortunately the user's and producer's accuracies for the class “ y_5 - road with vegetation on both sides of the road” show rather low values. However these values cannot be considered as reliable since the class is rarely present in the reference set. An other reason is that the class is dependent on a good detection of both dark and bright features. Shorter parts of the highway such as the highway cross are often falsely assigned to roads with vegetation nearby because of the short length of the extracted bright and dark features.

If the two Figs 54(a) and 54(b) are compared, one can notice that the two fusions classify the diagonal road in the middle differently. The fusion succeeds to identify the road as a road with vegetation nearby in the first dataset, but in the second the fusion assumes that there is a road with vegetation also below the true road. The reason for this is that the row of trees gives rise to a linear homogeneous shadow region. This region is detected by the line extraction and later on obtains a high probability of being road. Since the two dark linear features are too far away for being fused, each separately are assumed to be roads.

One way to reduce the false extraction is to introduce prior information as described in Sect. 5.6. By incorporating the knowledge that the frequency of clutter is higher in forest areas, the correctness for the scene **Oberpfaffen1-2** could be increased by as much as 15%, while the completeness was only reduced by 3%. As also stated in Sect. 5.6 the prior has an impact only on fused linear primitives with already a high assessment of being clutter. The result can be seen in Fig. 54(c).

Data set Garching

The data set Garching (see Fig. 55) contains two almost anti-parallel images (high resolution spotlight mode, multi-look ground range detected, radiometrically enhanced product) and was acquired by the space-borne sensor TerraSAR-X in March 2009 in both ascending and descending orbit. The area Garching is situated close to Munich, Germany. The scene shows a sub-urban scene with a highway dominating the scene. Compared to the data set Oberpfaffenhofen this scene covers a much larger area, about $7900 \times 3000 \text{ m}^2$. The scene shows a more complicated road network where all kind of roads exist; highways, main roads, minor roads and local streets.



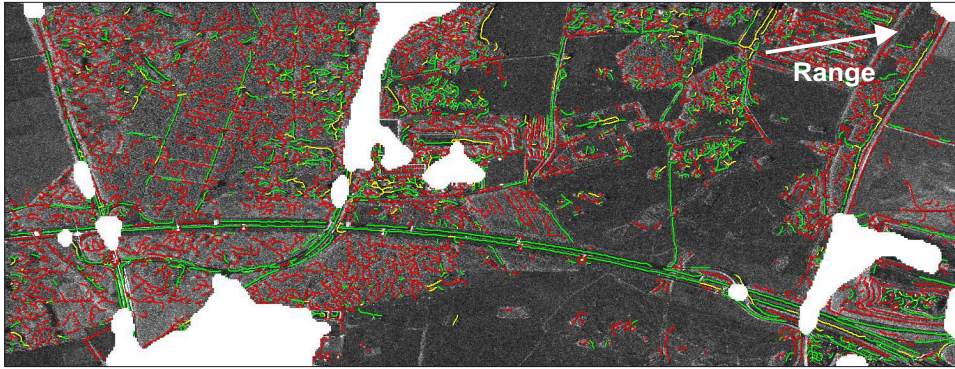
(a)



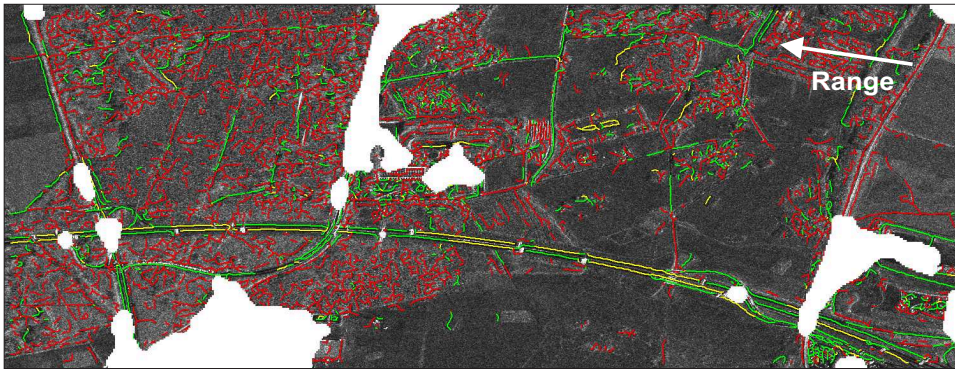
(b)

Fig. 55. The data set of Garching: Szene "Garching1" (a) was acquired in ascending orbit while Garching2 (b) was taken in descending orbit.

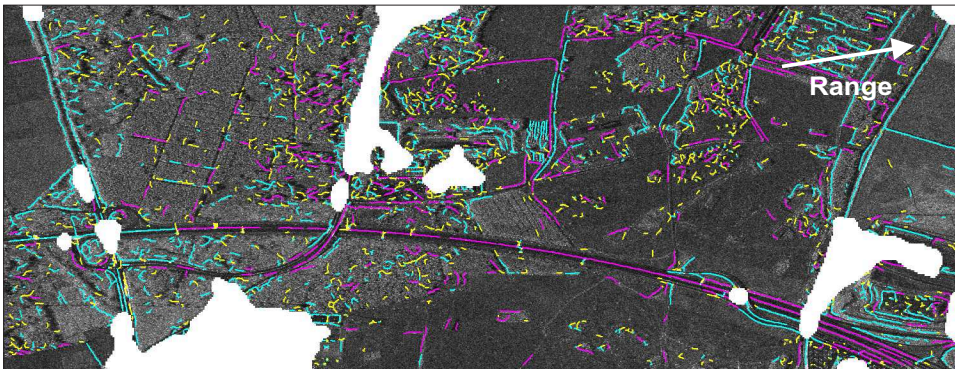
The uncertainty assessment of the dark and bright features was carried out using the same probability density functions as the ones used for E-SAR data. Only for the attribute intensity new training data had to be collected and probability density functions had to be estimated as described in Sect. 5.4. The reason is that the E-SAR training data was uncalibrated. Even though the new data set was acquired by a new sensor with lower resolution and in addition the scene is much more complex, the uncertainty assessment works fairly well (see Fig. 56). Most of the dark linear primitives seem to be correctly assigned to its state of L . But unfortunately the misclassification seems to be higher for this data set compared to the E-SAR data. Some roads are falsely classified to shadows and false alarms and vice versa. The uncertainty assessment of the bright features is able to deliver acceptable results, but unfortunately not as good as the dark linear features. Especially in forest regions linear features obtain wrongly a high assessment of belonging to either buildings or highways. The objects contained in the scene have different characteristics than the one used for collecting training data (see Fig. 25). Both bright scattering from buildings and higher vegetation (row of trees) are for instance much longer in this data set. In addition different parameters were used for the line extraction. As a result the characteristics of the bright and dark scatterer extracted from the two data sets are different.



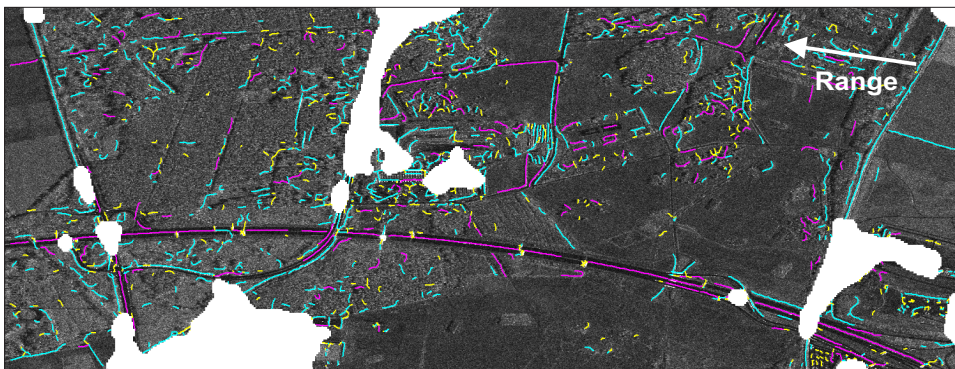
(a)



(b)



(c)



(d)

Dark linear primitives:	■ ROAD	■ FALSE ALARM	■ SHADOW
Bright linear primitives:	■ HIGHWAY	■ MAN-MADE OBJECTS	■ VEGETATION

Fig. 56. Uncertainty assessment of dark linear features (a-b) and bright linear features (c-d) extracted in each of the two SAR sub-scenes of Garching (see Figs 55(a)-55(b)). The linear features and the uncertainty assessment is the input to the subsequent fusion.

The dark and bright features including their uncertainty assessment is the input to the subsequent fusion (BN_5). The fused results matched with the reference for the data set Garching (see Fig. 57) can be seen in Fig. 58. One can draw the conclusion from the quality measures presented in Tab. 14 that the fusion - despite the different data characteristics - delivers acceptable results. The overall completeness are in the same range (74-77 %) as for the data set Oberpfaffenhofen. If only clutter is sorted out the completeness increases 12% and reaches a completeness of 86%. However then the correctness decreases as much as 30%. The correctness values are unfortunately lower (44-47%) compared to Oberpfaffenhofen. But we should keep in mind that our aim is to achieve rather higher completeness values than higher correctness values.

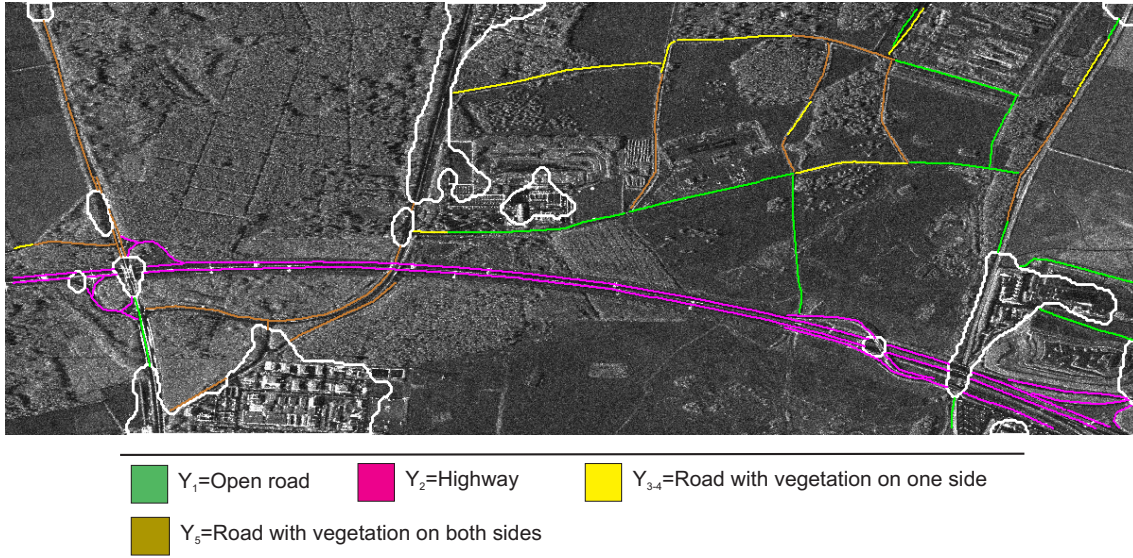


Fig. 57. Manually digitized reference for the data set Garching.

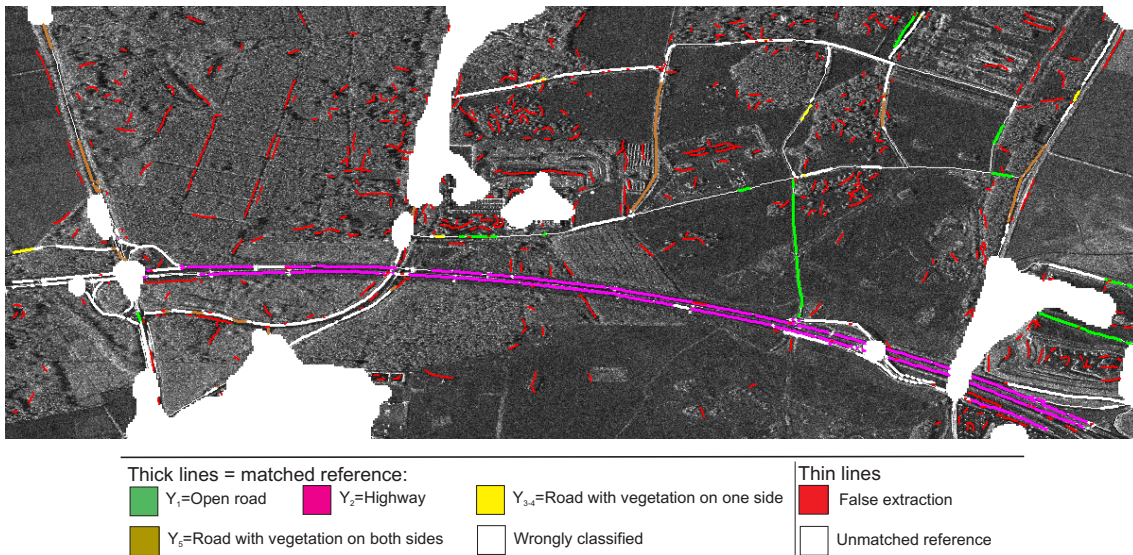


Fig. 58. **Garching1-2**: The results after fusion based on the Bayesian network BN_5 was matched with the reference. Input to the fusion are not only the dark but also the bright linear features and their uncertainty assessment (see Fig. 56). Masked built-up areas are white.

The error matrix (see Tab. 14) shows that the fusion is able to classify most highways and most open roads correctly. Both user's and producer's accuracies for these two classes are acceptable. Compared to Oberpfaffenhofen we do not longer have the problem of open roads classified into highways. Here rather the opposite occur.

Again the fusion meets problem by the classification of the class " y_{3-4} - road with vegetation one side" The reason for the rather poor classification is partly due to the mis-classification of bright features. As one can see in Figs. 56(c)-56(d) some vegetation is falsely assessed to belong to highways. Second, the reference data probably contains some errors since it was hard to estimate by means of optical data if there was vegetation on

Fusion of Garching 1 and 2								
Error Matrix (without prior)								
	Y_1	Y_2	Y_{3-4}	Y_5	Total	User's Accuracy	Producer's Accuracy	Overall Accuracy
y_1	134	119	29	59	341	0.39	0.64	
y_2	1	581	97	72	751	0.77	0.67	
y_{3-4}	45	112	25	83	265	0.09	0.14	
y_5	29	49	27	143	248	0.58	0.40	
Total	209	861	178	357	1605			0.55
Quality Measures						without prior	with prior	
Overall Completeness						0.77	0.74	
Overall Correctness						0.44	0.47	
RMS						8.8	10.8	

Tab. 14. Error matrix for the fused linear primitives (BN_5 - dark and bright features) extracted from data set Garching. All fused features classified into “ y_{6-7} - only vegetation”, “ y_{8-9} - only buildings” and “ y_{10} - clutter” were sorted out before matching. Capital letters indicate the reference and the classification results are referred to as the lowercase letters. Y_1 means the reference class for open roads, Y_2 is the reference class for roads with vegetation nearby.

both sides or not. Especially lower vegetation was hard to differentiate from the fields. These were detected in the SAR data resulting that some line features assigned to y_{3-4} in the reference data were classified into y_5 by the fusion. An other reason was also that the conditional probability table behaves similar for the states y_{3-4} as for the states “ y_{6-7} - only vegetation”. Line features with the probability $BEL(Y = y_{6-7}) > BEL(Y = y_{1-5})$ were sorted out before the matching and hence these parts are regarded as unmatched. We should keep in mind however that the classifier only gives us support by the seed point selection. For these line segments $BEL(Y = y_{3-4})$ is still high, meaning that these will most likely be involved in the subsequent shortest-path calculation.

Fortunately the classifier is able to distinguish the class “ y_5 - road with vegetation on both sides” better than for the data set Oberpfaffenhofen. The class is better represented among the reference data meaning that the evaluation of this class should be regarded as more reliable as for Oberpfaffenhofen. Due to the same reasons mentioned for y_{3-4} some linear features are wrongly assigned to be highways.

As can be seen in Fig. 58 the number of falsely extracted line primitives in forest regions is high. Most of these (63%) got a high assessment of being open roads. The reason why open roads and clutter are harder to differentiate is that these two are the only classes, which do not expect any bright feature extraction nearby. Also for this data set prior information was incorporated. Indeed the correctness was then increased but unfortunately the completeness was decreased at the same time. The fact that most of the falsely extracted line primitives were assigned to open roads makes us more certain that the conditional probabilities are not optimally estimated for the two classes open roads and clutter. But one should of course also keep in mind that the amount of clutter detected in forest regions is already very high (see the dark line extraction in Figs. 56(a) and in 56(b)).

The overall accuracy (55%) is unfortunately lower than the accuracies presented for Oberpfaffenhofen. However one should keep in mind that the fusion was primarily learned for E-SAR data and not for TerraSAR-X data.

Conclusions of results

Based on the results presented in this section we can draw the following conclusions:

- ◊ By comparing the two fusions, the fusion for both bright and dark features (BN_5) was able to deliver a slightly higher completeness. If also prior information was included the correctness increased slightly.
- ◊ The fusion was also tested on multi-aspect SAR data acquired by a different sensor than the data used for learning the fusion. Even though the new data set had both different data and scene characteristics the fusion could deliver acceptable results.
- ◊ The quality measures presented give an indication that the behavior of the fusion is rather indulgent than severe.
- ◊ The error matrices show that the fusion delivers in general an overall result for the classification, but has some difficulties by some classes. Certainly the fusion will be able to support the subsequent selection of seed points for the network generation.

7 Conclusion and discussion

Summary

In this work, we have presented a fusion approach for automatic road extraction from multi-aspect SAR images. We designed a probabilistic decision-level fusion for extracted linear features, which fully exploits multi-aspect SAR data. By means of Bayesian network theory a reasoning step could be modeled which describes the relation between the extracted road, neighboring high objects and the sensor geometry. Also global context representing prior information was incorporated. The different steps; analyzing incoming information, structuring the Bayesian networks, learning the fusion by means of training data, and the association step, were described in detail.

Two different fusions were developed and tested; one developed for dark linear features only and one incorporating both dark and bright linear features. Those two were tested and compared on multi-aspect SAR data. In addition the fusion concept was tested on data acquired from different SAR sensors.

Discussion

Designing the fusion within Bayesian network theory enables us to fully exploit multi-aspect SAR data. The advantage of using Bayesian network theory is that it offers us an optimal framework for dealing with relations. Hence the reasoning step required for the modeling of the relation between the road, neighboring objects and the sensor geometry could be implemented. Furthermore it allows us to handle as much information as feature extraction, road model, sensor geometry, and local and global context, due to its certain graph structure. As soon as the structure is defined it is straight forward to estimate the flow of incoming and outgoing information. However finding the optimal structure is the crucial and most important step and - depending on the task - can be rather complicated. The dependencies/independencies among the variables are not always obvious. One might have to try different structures before a suitable one is found. Also in this work some structures were tested before the final two proposed in this work were defined. An other disadvantage of Bayesian network is that it requires a complete probabilistic model. Hence all possible states of each variable must be defined. The more states, the more comprehensive is in general the learning. Estimating the conditional probabilities for this application required training data. The collection was unfortunately time-consuming especially when many states needed to be defined. If also parental or child nodes are correlated, the learning is even more complicated. To simplify the learning a hidden node was implemented in this work (see Sect. 5.5.2).

Despite the complexity of setting up the structure and learning, Bayesian network is the optimal framework for this work. The decisive point is that Bayesian network theory is the best suited decision-level fusion technique for dealing with relations among so much different information. In addition Bayesian network enables us to express this in a probabilistic framework.

The first fusion developed in this work concentrates on dark feature extraction, a road model and the sensor geometry. The number of variables is lower compared to the second fusion and this makes the fusion structure less complex. The implementation and the learning is relatively fast. Unfortunately this approach does not fully exploit multi-aspect SAR images. Only one occlusion effect (shadows) is included in the modeling which means that the fusion meets problems as soon as layover occlusions are present. However the second fusion includes also layover meaning that information about neighboring objects is available. Not only the number of variables needs to be increased, also the variables are partly extended with more states. Setting up the structure and the learning is now much more complicated. But the advantage is that the second fusion gives us information about different road classes and thereby delivering much more and complete information about the scene.

By testing the two fusions on the same data set it was proved that the second fusion could deliver a higher overall completeness. The same test also showed us that the accuracies of the ability of the fusion to discriminate between different road types were in general lower for the second fusion than for the first. The reason is that the first fusion contains only two road classes, while the second fusion comprises five different road classes. In addition the error matrices presented in Sect. 6 show us that most confusions occur among either highways and open roads or among road with vegetation on one side or road with vegetation on both sides. Since the first fusion combines highways and open roads into one class (open road) and has only one category for road with vegetation nearby, it is not strange that the producer's and user's accuracies are in general both higher for the first fusion. But we should not forget that the second fusion tend to falsely classify more clutter in forest regions to open roads. The number could be suppressed by incorporating prior information. But still it shows that some conditional probabilities were not optimally estimated. Most probably some parameters within the

probabilistic modeling of the reasoning step of the road, local context and sensor geometry could be optimized. The setting of the subjective probabilities may play an important role in this issue.

An other drawback of the two fusions is that a fixed height of all nearby objects and a fixed width of all roads are assumed. Of course these numbers vary highly in the real world, leading to an incorrect estimation of the impact of the global sensor geometry. Certainly this may have lead to mis-classifications among the fused results, in particular for roads with vegetation nearby.

The fusion was learned on data acquired by the E-SAR sensor. In order to check whether the learning could be transferred to other SAR data, the second fusion was tested on TerraSAR-X data. Besides adjusting the learning for a different intensity range, all other conditional probabilities remained. The results showed indeed that the fusion was applicable on images with different data and scene characteristics, even though it is recommendable to adjust some conditional probabilities for the specific SAR scene, especially if the data and scene characteristics differ too heavily.

A direct and objective comparison between the results obtained by the old fuzzy-fusion and the new statistical approach is hard to make. The reason is that the tuning of the parameters of the old system has such a high impact that the expected end results may become arbitrary "good" or "bad" depending on the time invested in the parameter setting. The previous version required the user to set a high number of parameters for different Fuzzy-functions. Nevertheless the new statistical fusion represent indeed a great improvement. It is especially developed for multi-aspect SAR image and thereby delivers more informative results compared to the old one. The use of statistics makes the fusion more compatible. The output could be used and linked to other probabilistic modules, for instance a Markov random field search similar to the one proposed by TUPIN et al. (1998). An other advantage is that the system has become more user-friendly. By using the proposed fusion - if it is properly learned - reduces the number of adjustable parameters significantly.

The applied fusion was still not completely implemented in TUM-LOREX. The remaining step is to link the output of the fusion to the last step, namely the network generation step. The output of the fusion shall support the selection of especially good candidates for roads (i.e. the seed points). The selection of the seed points is a crucial and important step for the network generation. Even though this was still not tested, the results presented in Sect. 6 are indeed an indicator of that the fusion will certainly be able to support the seed point selection.

Future work

The discussion above points out some parts of the proposed fusion, which could be optimized. One is to include the height of any nearby objects and the width of the road as variables in the Bayesian network. This would be an interesting task, since we would now be dealing with not only hypotheses but also an estimation of numerical values. These variables are most suited to be implemented in the second fusion, since it also involves the bright scattering. Second, the influence of the subjective probabilities should be tested. This can be done by varying the subjective probabilities for isolated cases and examine how the belief in different classes will change. Such an investigation would at the same time give an indication on how the clutter can be better modeled. Thereby it is expected to achieve a higher correctness. The influence of the subjective probabilities could also be checked by matching different fused results obtained by different subjective probabilities with the reference as carried out in (KIM and NEVATIA, 2003). By plotting the correctness and completeness in diagrams the optimal numerical value for the subjective probabilities could be found.

Even though the results obtained from the TerraSAR-X data set presented in Sect. 6 show that the fusion is transferable, it also gave us an indication that some additional learning could be useful. The typical attributes of the different states of variable $L(D)$, roads, shadows and false alarms, and B might differ depending on the specific scene characteristics. Therefore one might consider to incorporate a training step into TUM-LOREX. By selecting some of the extracted line primitives and assigning them to the different states, the probability density functions could be adjusted to that specific scene. Also there could be an option to adopt the performance of the line extractor. A training step would of course involve additional work by the user, but would probably not exceed much the time needed for the parameter setting of the old system.

The fusion should also preferably be tested on more than two images. Assuming that the sensor geometry differs enough so that the images can be regarded as independent, the extracted results from one or more additional images can be included using the product (compare with Eq. 28). Then the structure of the fusion would turn into an *expandable Bayesian network* similar to the concept proposed by KIM and NEVATIA (2003). The extension of this fusion to an expandable Bayesian network is easily done in theory, but would need some time for the

implementation. The complexity would increase if extracted information from images with a slightly different sensor geometry would be fused. At what point can one assume that extracted information from the two images are correlated or not? Bayesian network is able to deal with correlated information by hidden nodes (PEARL, 1988). If and how hidden nodes could be applied in this case would be a question worth looking into.

Also simulated data based on SAR data effects (BALZ and STILLA, 2009) or on SAR raw data (GUIDA et al., 2008) could improve the learning. In particular simulated data could help to improve the road and local context model, which is essential for the design of the conditional probability table.

The proposed Bayesian network fusion offers us the ability to easily integrate additional data, for instance GIS-information or remote sensing data from other sensors, such as optical data. Since the SAR data and the new information are independent, the data can be easily integrated as new variables. The learning needed for the new variables can be carried out in a similar form as the one proposed in this work. The option can be useful when for instance older optical data should be validated by recently acquired SAR data.

This work has indeed showed the potential of using Bayesian network theory for automatic object extraction from SAR data and in particular for multi-aspect SAR data. A new high-level fusion approach especially designed for SAR data has been developed. This or a similar fusion concept would certainly be suitable also to other SAR applications than automatic road extraction in the future.

References

- AMBERG, V., SPIGAI, M., COULON, M. and MARTHON, P. (2005a): From road extraction to man-made object discrimination in high resolution sar data, *4th international conference on Physics in Image and Signal Processing, PSIP'2005*, Toulouse,, Proceedings of PSIP, 163–168.
- AMBERG, V., SPIGAI, M., COULON, M. and MARTHON, P. (2005b): Improvement of road extraction in high resolution sar data by a context-based approach, *IGARSS'05, Séoul*, Proceedings of IGARSS.
- ASILO, S., PARINGIT, E., CASIWAN, C., COLLADO, W., MEHDIYEV, M., HAZARICA, M., SAMARAKKON, L. and KAMTHONKIAT, D. (2007): Fusion techniques for rice area mapping using multitemporal radarsat-1 images in pangasinan and nueva ecija, *Proceedings of the 27th Asian Conference on Remote Sensing, Kuala Lumpur, Malaysia*.
- AUCLAIR FORTIER, M., ZIOU, D., ARMENAKIS, D. and WANG, S. (1999): Automated correction and updating of road databases from high-resolution imagery, *Technical report*, Canadian Journal of Remote Sensing.
- BALZ, T. and STILLA, U. (2009): Hybrid gpu-based single- and double-bounce sar simulation, *Geoscience and Remote Sensing, IEEE Transactions on* 47(10): 3519–3529.
- BAUMGARTNER, A., ECKSTEIN, W., MAYER, H., HEIPKE, C., EBNER, H. and IX, I. (1997a): Context-supported road extraction, *In: Automatic Extraction of Man-Made Objects from Aerial and Space Images (II)*, Birkh auser Verlag Basel, 299–308.
- BAUMGARTNER, A., STEGER, C., MAYER, H. and ECKSTEIN, W. (1997b): Multi-resolution, semantic objects, and context for road extraction, *In Semantic Modeling for the Acquisition of Topographic Information from Images and Maps*, Birkhauser Verlag, 140–156.
- BENTABET, L., JODOUIN, S., ZIOU, D. and VAILLANCOURT, J. (2003): Road vectors update using sar imagery: a snake-based method, *Geoscience and Remote Sensing, IEEE Transactions on* 41(8): 1785–1803.
- BINDER, J., KOLLER, D., RUSSELL, S. and KANAZAWA, K. (1997): Adaptive probabilistic networks with hidden variables, *Mach. Learn.* 29(2-3): 213–244.
- BLOCH, I. (1996): Information combination operators for data fusion: a comparative review with classification, *Systems, Man and Cybernetics, Part A, IEEE Transactions on* 26(1): 52–67.
- BOLTER, R. (2001): *Buildings from SAR: detection and reconstruction of buildings from multiple view high resolution interferometric SAR data.*, PhD thesis, University of Graz, Austria.
- BUSCH, A. (1994): Fast recognition of lines in digital images without user-supplied parameters, Band 2357, SPIE, 91–97.
- CHAABOUNI CHOUAYAK, H. and DATCU, M. (2010): Coarse-to-fine approach for urban area interpretation using terrasar-x data, *IEEE Geoscience and Remote Sensing Letters* 7: 78–82.
- CHANUSSOT, J., MAURIS, G. and LAMBERT, P. (1999): Fuzzy fusion techniques for linear features detection in multitemporal sar images, *Geoscience and Remote Sensing, IEEE Transactions on* 37(3): 1292–1305.
- CUMMING, I. G. and WONG, F. H. (2005): *Digital Processing of Synthetic Aperture Radar Data: Algorithms and Implementation*, Artech House Inc., Boston, London.
- DEKKER, R. (2003): Texture analysis and classification of ers sar images for map updating of urban areas in the netherlands, *Geoscience and Remote Sensing, IEEE Transactions on* 41(9): 1950–1958.
- DELL'ACQUA, F. and GAMBA, P. (2001): Detection of urban structures in sar images by robust fuzzy clustering algorithms: The example of street tracking, *IEEE Transactions on Geoscience and Remote Sensing* 39(10): 2287–2297.
- DELL'ACQUA, F., GAMBA, P. and LISINI, G. (2003): Improvements to urban area characterization using multi-temporal and multiangle sar images, *Geoscience and Remote Sensing, IEEE Transactions on* 41(9): 1996–2004.
- DELL'ACQUA, F., GAMBA, P. and LISINI, G. (2004): Coregistration of multiangle fine spatial resolution sar images, *Geoscience and Remote Sensing Letters, IEEE* 1(4): 237–241.
- DELL'ACQUA, F., GAMBA, P. and LISINI, G. (2009): Rapid mapping of high resolution sar scenes, *ISPRS Journal of Photogrammetry and Remote Sensing* 64(5): 482 – 489: Theme Issue: Mapping with SAR: Techniques and Applications.
- FERRARI, S. and VAGHI, A. (2006): Demining sensor modeling and feature-level fusion by bayesian networks, *Sensors Journal, IEEE* 6(2): 471–483.
- FRITZ, T. (2007): Terrasar-x ground segment level 1b product format specification, *Technical report*, Cluster Applied Remote Sensing, German Aerospace Center.
- GAMBA, P., HELLWICH, O. and LOMBARDO, P. (2005): Editorial board, *Information Fusion* 6(4): 189–192: Fusion of Remotely Sensed Data over Urban Areas.
- GARCIA, A. L. (2000): *Numerical Methods for Physics (2nd Edition)*, Prentice-Hall, Inc., Upper Saddle River, NJ, USA: Artist-(cover), John Christiana and Designed By-(cover), Bruce Kenselaar.

- GERKE, M., BUTENUTH, M., HEIPKE, C. and WILLRICH, F. (2004): Graph-supported verification of road databases, *ISPRS Journal of Photogrammetry and Remote Sensing* 58(3-4): 152 – 165: Integration of Geodata and Imagery for Automated Refinement and Update of Spatial Databases.
- GONZALEZ, R. C. and WOODS, R. E. (2001): *Digital Image Processing*, Addison-Wesley Longman Publishing Co., Inc., Boston, MA, USA.
- GUIDA, R., IODICE, A., RICCIO, D. and STILLA, U. (2008): Model-based interpretation of high-resolution sar images of buildings, *Selected Topics in Applied Earth Observations and Remote Sensing, IEEE Journal of* 1(2): 107–119.
- HALL, D. L. (1992): *Mathematical Techniques in Multisensor Data Fusion*, Artech House, Inc., Norwood, MA, USA.
- HALL, D. L. and LLINAS, J. (2001): *Handbook of Multisensor Data Fusion*, CRC Press LLC, chapter Multisensor Data Fusion.
- HEDMAN, K., HINZ, S. and STILLA, U. (2006a): A probabilistic fusion concept for road extraction from multiple sar views, *Proc. 6th European conference on synthetic aperture radar, EUSAR 2006*.
- HEDMAN, K., HINZ, S. and STILLA, U. (2006b): A probabilistic fusion strategy applied to road extraction from multi-aspect sar data, *Symposium of ISPRS Commission III: Photogrammetric Computer Vision (PCV06). International Archives of Photogrammetry, Remote Sensing, and Spatial Information Sciences*, Band 36, 55–60.
- HEDMAN, K., HINZ, S. and STILLA, U. (2007): Road extraction from sar multi-aspect data supported by a statistical context-based fusion, *Urban Remote Sensing Joint Event: URBAN 2007 -URS 2007*, 1–6.
- HEDMAN, K., STILLA, U., LISINI, G. and GAMBA, P. (2008): Road network extraction in urban areas by means of feature-level fusion, *3. TerraSAR-X Science Team Meeting*.
- HEDMAN, K., STILLA, U., LISINI, G. and GAMBA, P. (2010): Road network extraction in vhr sar images of urban and suburban areas by means of class-aided feature-level fusion, *IEEE Transactions on Geoscience and Remote Sensing* 48(3): 1294–1296.
- HEDMAN, K., WESSEL, B. and STILLA, U. (2005a): A fusion strategy for extracted road networks from multi-aspect sar images, in U. STILLA, F. ROTTENSTEINER and F. HINZ (Herausgeber), *CMRT05 International Archives of Photogrammetry and Remote Sensing*, Band 36, 185–190.
- HEDMAN, K., WESSEL, B., STILLA, U. and SOERGEL, U. (2005b): Automatic road extraction by fusion of multiple sar views, in M. MOELLER and E. WENTZ (Herausgeber), *3th International Symposium: Remote sensing and data fusion on urban areas, URBAN 2005. International Archives of Photogrammetry and Remote Sensing*, Band 36, on CD.
- HEIPKE, C., MAYER, H., WIEDEMANN, C. and JAMET, O. (1997): Evaluation of automatic road extraction, *In: International Archives of Photogrammetry and Remote Sensing*, 47–56.
- HELLWICH, O. (1996): *Linienextraktion aus SAR-Daten mit einem Markoff-Zufallsfeld-Modell*, PhD thesis, Technische Universität München.
- HINZ, S. (2004): *Automatische Extraktion urbaner Straßennetze aus Luftbildern*, PhD thesis, Technische Universität München.
- HINZ, S. and BAUMGARTNER, A. (2003): Automatic extraction of urban road networks from multi-view aerial imagery, *ISPRS Journal of Photogrammetry and Remote Sensing* 58(1-2): 83 – 98: Algorithms and Techniques for Multi-Source Data Fusion in Urban Areas.
- HORN, R. (1996): The dlr airborne sar project e-sar, *Proceedings of International Geoscience and Remote Sensing Symposium*, 1624–1628.
- JAYNES, E. T. (2003): *Probability Theory; the logic of science*, Cambridge University Press.
- JENSEN, F. V. (1996): *An introduction to Bayesian networks*, UCL Press: ISBN 1-85728-332-5.
- JEON, B.-K., JANG, J.-H. and HONG, K.-S. (2002): Road detection in spaceborne sar images using a genetic algorithm, *Geoscience and Remote Sensing, IEEE Transactions on* 40(1): 22–29.
- JUNGHANS, M. and JENTSCH, H.-J. (2007): Qualification of traffic data by bayesian network data fusion, *Information Fusion, 2007 10th International Conference on* 1–7.
- KIM, Z. and NEVATIA, R. (2003): Expandable bayesian networks for 3d object description from multiple views and multiple mode inputs, *Pattern Analysis and Machine Intelligence, IEEE Transactions on* 25(6): 769–774.
- KIM, Z. and NEVATIA, R. (2004): Automatic description of complex buildings from multiple images, *Computer Vision and Image Understanding* 96(1): 60–95.
- LARKIN, M. (1998): Sensor fusion and classification of acoustic signals using bayesian networks, *Signals, Systems & Computers, 1998. Conference Record of the Thirty-Second Asilomar Conference on* 2: 1359–1362 vol.2.
- LEVITT, S. and AGHDASI, F. (2000): Fuzzy representation and grouping in building detection, *Image Processing, 2000. Proceedings. 2000 International Conference on*, Band 3, 324–327 vol.3.

- LILLESAND, THOMAS, M., KIEFER, RALPH, W. and CHIPMAN, W. J. (2008): *Remote Sensing and Image Interpretation*, 6 edn, John Wiley & Sons, Inc.
- LIMPERT, E., STAHEL, W. A. and ABBT, M. (2001): Log-normal distributions across the sciences: Keys and clues, *BioScience* 51(5): 341–352.
- LISINI, G., TISON, C., TUPIN, F. and GAMBA, P. (2006): Feature fusion to improve road network extraction in high-resolution sar images, *Geoscience and Remote Sensing Letters, IEEE* 3(2): 217–221.
- LOMBARDO, P., OLIVER, C., PELLIZZERI, T. and MELONI, M. (2003): A new maximum-likelihood joint segmentation technique for multitemporal sar and multiband optical images, *IEEE Transactions on Geoscience and Remote Sensing* 41(11): 2500–2518.
- MASSONNET, D. and SOUYRIS, J.-C. (2008): *Imaging with Synthetic Aperture Radar*, CRC Press, Taylor & Francis Group.
- MAYER, H., HINZ, S., BACHER, U. and BALTSAVIAS, E. (2006): A test of automatic road extraction approaches, *Symposium of ISPRS Commission III: Photogrammetric Computer Vision (PCV06). International Archives of Photogrammetry, Remote Sensing, and Spatial Information Sciences*, xx–yy.
- NEGRI, M., GAMBA, P., LISINI, G. and TUPIN, F. (2006): Junction-aware extraction and regularization of urban road networks in high-resolution sar images, *Geoscience and Remote Sensing, IEEE Transactions on* 44(10): 2962–2971.
- PEARL, J. (1988): *Probabilistic Reasoning in Intelligent Systems : Networks of Plausible Inference*, Morgan Kaufmann.
- PEARL, J. (2000): *Causality: model, reasoning, and inference*, Cambridge University Press.
- POHL, C. and VAN GENDEREN, J. L. (1998): Multisensor image fusion in remote sensing: concepts, methods and applications, *International Journal of Remote Sensing* 19(5): 823–854.
- PRICE, K. (1999): Road grid extraction and verification, *International Archives of Photogrammetry and Remote Sensing, Band XXXII, Part 3-2W5*, 101–106.
- ROTH, A., HOFFMANN, J. and ESCH, T. (2005): Terrasar-x: How can high resolution sar data support the observation of urban areas?, *ISPRS Joint Conference URBAN2005 and URS2005*.
- SHIMAZAKI, H. and SHINOMOTO, S. (2007): A method for selecting the bin size of a time histogram, *Neural Computation* 19(6): 1503–1527.
- SOERGEL, U., CADARIO, E. and THOENNESSEN, U. (2004): Geocoding and fusion of airborne high-resolution multi-aspect sar-data, *Proc. 5th European Conference on Synthetic Aperture Radars, EUSAR 2004*, 945–948.
- SOERGEL, U., MICHAELSEN, E., THIELE, A., CADARIO, E. and THOENNESSEN, U. (2009): Stereo analysis of high-resolution sar images for building height estimation in cases of orthogonal aspect directions, *ISPRS Journal of Photogrammetry and Remote Sensing* 64(5): 490 – 500: Theme Issue: Mapping with SAR: Techniques and Applications.
- SOERGEL, U., THOENNESSEN, U. and STILLA, U. (2003): Visibility analysis of man-made objects in sar images, *IEEE Geoscience and Remote Sensing Society: 2nd GRSS/ISPRS Joint Workshop on Remote Sensing and Data Fusion over Urban Areas, URBAN 2003*, 120–124.
- STEGER, C. (1998a): An unbiased detector of curvilinear structures, *Pattern Analysis and Machine Intelligence, IEEE Transactions on* 20(2): 113–125.
- STEGER, C. (1998b): *Unbiased Extraction of Curvilinear Structures from 2D and 3D images*, PhD thesis, Technische Universität München.
- STEGER, C., MAYER, H. and RADIG, B. (1997): The role of grouping for road extraction, *In: Automatic Extraction of Man-Made Objects from Aerial and Space Images (II)*, Birkh auser Verlag Basel, Verlag, 245–256.
- STEINBERG, A. N., BOWMAN, C. and WHITE, J. F. E. (1998): Revisions to the jdl data fusion model, *Proc. 3rd NATO/IROS Conf., Quebec City, Canada*.
- STILLA, U. (2007): High resolution radar imaging of urban areas, *in* D. FRITSCH (Herausgeber), *Photogrammetric Week 07*, Wichmann: Heidelberg.
- STILLA, U. and HEDMAN, K. (2010): *Feature fusion based on Bayesian network theory for automatic road extraction*, Band 15, Springer, chapter 3, 69–86.
- STILLA, U. and SOERGEL, U. (2006): *Urban Remote Sensing*, Taylor & Francis, CRC Press Inc., chapter Reconstruction of Buildings in SAR Imagery of Urban Areas, 47–68.
- STILLA, U., HINZ, S., HEDMAN, K. and WESSEL, B. (2007): *Remote Sensing of Impervious Surfaces*, Remote Sensing Application Series, CRC Press, Taylor & Francis, chapter Road extraction from SAR imagery.
- STILLA, U., SOERGEL, U. and THOENNESSEN, U. (2003): Potential and limits of insar data for building reconstruction in built-up areas, *ISPRS Journal of Photogrammetry and Remote Sensing* 58(1-2): 113 – 123: Algorithms and Techniques for Multi-Source Data Fusion in Urban Areas.

- SUN, G. and RANSON, K. (1995): A three-dimensional radar backscatter model of forest canopies, *Geoscience and Remote Sensing, IEEE Transactions on* 33(2): 372–382.
- THIELE, A., CADARIO, E., SCHULZ, K. and SOERGEL, U. (2010): Analysis of gable-roofed building signature in multiaspect insar data, *Geoscience and Remote Sensing Letters, IEEE* 7(1): 83–87.
- THIELE, A., CADARIO, E., SCHULZ, K., THONNESSEN, U. and SOERGEL, U. (2007): Building recognition from multi-aspect high-resolution insar data in urban areas, *Geoscience and Remote Sensing, IEEE Transactions on* 45(11): 3583–3593.
- TISON, C., NICOLAS, J.-M., TUPIN, F. and MAITRE, H. (2004): A new statistical model for markovian classification of urban areas in high-resolution sar images, *Geoscience and Remote Sensing, IEEE Transactions on* 42(10): 2046–2057.
- TOUZI, R. (2002): A review of speckle filtering in the context of estimation theory, *Geoscience and Remote Sensing, IEEE Transactions on* 40(11): 2392–2404.
- TOUZI, R., LOPEZ, A. and BOUSQUET, P. (1988): A statistical and geometrical edge detector for sar images, *IEEE Transactions on Geoscience and Remote Sensing* 26(6): 764–773.
- TUPIN, F. (2000): Radar cross-views for road detection in dense urban areas, *Proc. EUSAR 2000, Munich, Germany*, 617–620.
- TUPIN, F. (2010): *Radar Remote Sensing of Urban Areas*, Band 15 of *Remote Sensing and Digital Image Processing*, Springer, chapter Fusion of optical and SAR images, 133–159.
- TUPIN, F., BLOCH, I. and MAITRE, H. (1999): A first step toward automatic interpretation of sar images using evidential fusion of several structure detectors, *Geoscience and Remote Sensing, IEEE Transactions on* 37(3): 1327–1343.
- TUPIN, F., HOUSHMAND, B. and DATCU, M. (2002): Road detection in dense urban areas using sar imagery and the usefulness of multiple views, *Geoscience and Remote Sensing, IEEE Transactions on* 40(11): 2405–2414.
- TUPIN, F., MAITRE, H., MANGIN, J.-F., NICOLAS, J.-M. and PECHERSKY, E. (1998): Detection of linear features in sar images: application to road network extraction, *Geoscience and Remote Sensing, IEEE Transactions on* 36(2): 434–453.
- ULABY, F., MOORE, R. K. and FUNG, A. K. (1982): *Radar Remote Sensing and Surface Scattering and Emission Theory*, Band Band II of *Microwave Remote Sensing: Active and Passive*, Addison-Wesley Publishing Company, Reading, MA.
- WALD, L. (1998): An overview of concepts in fusion of earth data, *Future Trends in Remote Sensing, EARSeL Symposium 1997, Lyngby, Denmark*, Nummer 385-390.
- WALD, L. (1999): Some terms of reference in data fusion, *IEEE Transactions on Geoscience and Remote Sensing* 13(3): 1190–1193.
- WALD, L. (2002): *Data Fusion, Definitions and Architectures, Fusion of images of different spatial resolutions*, Les Presses de l’Ecole des Mines.
- WALTZ, E. (2001): *Handbook of Multisensor Data Fusion*, CRC Press LLC, chapter The Principles and Practice of Image and Spatial Data Fusion.
- WASKE, B. and BENEDIKTSSON, J. (2007): Fusion of support vector machines for classification of multisensor data, *IEEE Transactions on Geoscience and Remote Sensing* 45(12): 3858–3866.
- WASKE, B. and VAN DER LINDEN, S. (2008): Classifying multilevel imagery from sar and optical sensors by decision fusion, *IEEE Transactions on Geoscience and Remote Sensing* 46(5): 1457–1466.
- WEIDNER, U. and CENTENO, J. A. S. (2009): Pansharpening - simple approaches and their evaluation, *Photogrammetrie - Fernerkundung - Geoinformation* 2009(4): 317–327.
- WESSEL, B. (2004): Road network extraction from sar imagery supported by context information, *XXth ISPRS Congress, Istanbul, International Archives of Photogrammetry and Remote Sensing*.
- WESSEL, B. (2006): *Automatische Extraktion von Straßen aus SAR-Bilddaten*, PhD thesis, Technische Universität München.
- WESSEL, B. and HINZ, S. (2004): Context-supported road extraction from sar imagery: transition from rural to built-up areas, *Proceedings of EUSAR '04, Ulm*.
- WESSEL, B. and WIEDEMANN, C. (2005): Analysis of automatic road extraction results from airborne sar imagery, *Proceedings of the ISPRS Conference Photogrammetric Image Analysis*, Band 34, 105–110.
- WIEDEMANN, C. (2002): *Extraktion von Straßennetzen aus optischen Satellitenbilddaten*, PhD thesis, Technische Universität München.
- WIEDEMANN, C. and EBNER, H. (2000): Automatic completion and evaluation of road networks, *In: International Archives of Photogrammetry and Remote Sensing*, 979–986.
- WIEDEMANN, C. and HINZ, S. (1999): Automatic extraction and evaluation of road networks from satellite imagery, *International Archives of Photogrammetry and Remote Sensing*, 95–100.

-
- ZHANG, J. (2010): Multi-source remote sensing data fusion: status and trends, *International Journal of Image and Data Fusion* 1(1): 5–24.
- ZIOU, D. (2000): Optimal line detector, *Pattern Recognition, International Conference on* 3: 3534.

Acknowledgements

My sincere thanks go to my two doctoral advisers Prof. Dr.-Ing. Stefan Hinz and Prof. Dr.-Ing. Uwe Stilla. Thanks to Prof. Stilla for giving me the opportunity to start my Thesis at Photogrammetry and Remote Sensing, Technische Universität München (TUM). He was also the one who gave me the first inputs to this topic. Despite heavy workload and time pressure he took his time for fruitful discussions. I am also glad that he continued to support me even though I changed my place of work to the Institute of Astronomical and Physical Geodesy in 2006. Thanks to Prof. Hinz for giving me useful guidance and for supporting me to get out of dead-ends at times. His inputs and ideas, both for small and big things, were very helpful for this work. Without his knowledge and experience in this topic I would never have gotten this far. Thanks also for the intensive support and useful comments in the very end.

Many thanks also to Prof. Dr.-Ing. Hans-Peter Bähr for his willingness to support my work with such a short notice.

I am also grateful to Dr.-Ing. Birgit Wessel for her advising during the first year. She was the one who introduced the work with automatic road extraction from SAR. Without her and her knowledge in SAR and road extraction it would have taken a long time before I got familiar with this topic.

A special thanks goes to Prof. Gamba and Dr. Gianni Lisini for supporting me during my research stay at Università di Pavia, Pavia, Italy. Thanks to them I learned a lot about their research in the field of automatic road extraction and SAR data. Also thanks to Prof. Riccio and to my dear friend Dr. Raffaella Guida for the time at Università Federico II di Napoli, in Naples, Italy.

My next thanks go to all my former colleagues at the Institute of Photogrammetry and Cartography, TUM. Thanks to Stefan Gernhardt for supporting me with the SAR data and thanks to Stefan Auer for helping me with the reference data. Also a special thank to Christine Elmauer for everything she did. I am especially grateful to my colleagues Andreas Laika, Jens Leitloff and Diana Weihing. Their support in both personal and professional issues made me enjoying my time at TUM.

I would also like to express my gratitude to all my colleagues at the Institute of Astronomical and Physical Geodesy (IAPG), TUM. First of all to Prof. Dr.-Ing. Reiner Rummel for giving me such freedom for organizing my work so that I could find time for doing research. His support was very valuable to me. Next I would like to thank Prof. Dr.-Ing. Florian Seitz for the same reason. Due to his support and understanding during the busiest period I was able to finish in such a short time. Also special thanks to Mary Fletcher for her understanding.

Last but not least I would like to thank my dear family and friends. No matter living in Sweden or in Germany or somewhere else in the world, all of them have always been there for me. A special thanks to my mom, who has taught me to strive hard for my goals. Many thanks to my dear Martin for his understanding for all my busy working weekends and late nights. I hope that I some day can make up for it.

Curriculum Vitae

Name: Karin Helena Margareta Hedman

Place of Birth: Karlstad, Sweden

Date of Birth: June, 04, 1979

Educational background:

1995 — 1998 A-levels (school leaving exams) at Sundsta-Älvkullegymnasiet, Karlstad, Sweden

1999 — 2004 Master of Science in Space Engineering, Lulea University of Technology, Sweden

2001 Exchange studies at Nanyang Technological University, Singapore

Professional experience:

2004 — 2006 Scientific collaborator at Department of Photogrammetry and Remote Sensing, Technische Universität München

Since 2006 Scientific collaborator at Institute of Astronomical and Physical Geodesy, Technische Universität München
Program coordinator and student academic advisor for the international Master's program "Earth Oriented Space Science and Technology" (ESPACE)